FINAL REPORT

U.S. Department of Energy

Permanganate Treatment of DNAPLs in Reactive Barriers and Source Zone Flooding Schemes

Principal Investigator and Institution:
Dr. Franklin W. Schwartz
Department of Geological Sciences
The Ohio State University
Columbus, OH

Collaborator and Institution
Dr. Hubao Zhang
Duke Engineering & Service, Inc.
Albuquerque, NM

Project Number: 54585
Grant Number: DE-FG07-96ER14735

Grant Project Officers:
Contract Specialist; Kara Twitchell,
Technical Program Officer; George J. Schneider

Project Duration: 9/15/96-9/14/00

December, 2000

TABLE OF CONTENTS

EXECUTIVE SUMMARY 3
RESEARCH OBJECTIVES 4
METHODS AND RESULTS 4
Chemicals 4
Chemical Analyses 5
Task 1. Fundamental Experiments; Kinetic Reaction Rates 6
Task 2. Mechanisms for TCE Oxidation by Permanganate 8
Task 3. Efficiency Problems Related to Permanganate Oxidation Schemes 11
Task 4. Oxidation of DNAPL with a Phase-Transfer-Catalyst 12
Task 5. Computer Simulations 15
RELEVANCE, IMPACT AND TECHNOLOGY TRANSFER 19
PROJECT PRODUCTIVITY 20
PERSONNEL SUPPORTED 20
PUBLICATIONS 20
INTERACTIONS 21
FUTURE WORK 22
LITERATURE CITED 23
APPENDICES 23

EXECUTIVE SUMMARY

Permanganate is a simple and common chemical, which has proven useful in oxidizing common chlorinated solvents. Due to the nature of oxidation, the byproducts and products are much less harmful than those from reduction-type remedial schemes, and the degradation process is rapid. The main goal of this project is to understand oxidative destruction of chlorinated solvents using potassium permanganate. The study has provided a theoretical basis for evaluating the feasibility of in-situ applications, to couple kinetic reaction with transport models, and to develop an appropriate field test for further assessing the approach.

Many studies have been performed to demonstrate the potential of potassium permanganate as an effective remediating reagent for recalcitrant chlorinated solvents. Most of these experiments can be considered as a proof-of-concept level studies. However, our study was designed to provide a detailed process-level understanding of the oxidative destruction of the organic contaminant emphasizing on reaction pathways and kinetics. Dr. Eugene Yan has finished his doctoral dissertation and published three peer-reviewed articles in major scientific journals. One of his major accomplishments was to determine kinetic reaction rates for several chlorinated ethylenes including PCE, TCE and three isomers of DCE in different conditions of pH and ionic strength. He also undertook experimental and modeling studies to establish complete reaction pathways as well as to identify final products involved with the oxidation of chlorinated compounds with permanganate.

In order to apply the remediation scheme to field condition, several parameters need to be understood and estimated. The limitation of permanganate-based schemes for remediation includes potential releases of toxic heavy metals in the oxidation process and unwanted blocking of flow conduits by product precipitation. X. David Li, a Ph. D student, is currently examining those limitations. His 2-D flow tank experiments with visual image processing clearly demonstrate the precipitation of manganese dioxide and the presence of CO_2 bubbles reduced the permeability requiring greater injection pressure to maintain the flow injection. His work also has verify the impact of the strong oxidant on natural organic matter and other oxidizable mineral components. These results suggest that applications of the oxidation scheme to environmentally sensitive areas with large concentrations of heavy metals, associated with natural organic matter, could be of concern.

We are also interested in enhancing the reaction rates between permanganate and chlorinated solvents. Our efforts, mainly by Drs. Min-Ho Koo and Yongkoo Seol, were initially concentrated on increasing oxidation rates by facilitating oxidation reactions in the nonaqueous phase. Phase transfer catalysts have shown promise in transfering the reactive regent, here MnO_4^- into the nonaqueous phase liquid. Rates of TCE, PCE destruction were found to increase due to reactions in the DNAPL phase. It was also found that some NAPLs, such as TCA, have an improved capability of transferring the reactant to provide a proper reaction environment. Other NAPLs, such as PCE, can become more reactive to the transferred reactants in the nonaquatic environment. A remarkable rise in the MnO_4^- consumption rate with TCA and PCE mixtures proves that the phase transfer catalysts have the ability to increase oxidation rate of DNAPLs either in pure phase or mixtures and that there is significant potential for testing the catalyzed scheme under field conditions. Secondly, as an attempt to enhance the oxidation of DNAPL, we are trying to exploit cosolvency effects, utilizing various alcohol-water mixtures to increase DNAPL solubilization. Preliminary results of cosolvency experiments indicate the

enhancement in the transfer of nonaqueous phase TCE to TBA-water solution and the rate of TCE degradation in aqueous phase.

Our research iinvolves the collaborative efforts of a team from the Ohio State University and Duke Engineering & Service. Researchers at the Ohio State University are primarily responsible for the experimental work, while Dr. Hubao Zhang at Duke Engineering & Service undertakes the numerical modeling. Dr. Zhang's efforts resulted in a new computer code (ISCO3D) which is capable of simulating the coupled processes of NAPL dissolution, chemical reactions, and solute mass transport in an in-situ oxidation scheme. The code is also capable of simulating key reactions between the aquifer material and permanganate, and the kinetic sorption of chemicals. It has been optimized for computational efficiency. The code fills the gap between the laboratory studies and field operations by providing a numerical model capable of assisting with the design of systems and the interpretation of field observations.

The results of all these efforts have been recently presented in a 69 page comprehensive report entitled *"Permanganate Treatment of DNAPLs in Reactive Barriers and Source Zones".* Additionally, We have made disk copies for broad distribution and we have launched our web site (http://www.geology.ohio-state.edu/~hydro) for public access to our research results. Beyond these efforts, we also have published or submitted 11 journal/conference articles, which are listed in a separate section in the publication section of this report. We have contributed talks and poster sessions at various DOE workshops (Chicago, Oak Ridge, Augusta, Oakland, Atlanta) and presented about 7 talks to AGU, GSA, NGWA, and Old Dominion University. Draft manuscripts were made available to other researchers and consultants interested in oxidation schemes for DNAPL clean ups.

RESEARCH OBJECTIVES

The goals of this study are (1) to elucidate the basic mechanisms by which potassium permanganate oxidize common chlorinated solvents, various constituents in aqueous solution, and porous-medium solids, and (2) to assess the potential for chemical oxidation by potassium permanganate to serve as a remedial scheme involving either source zone flooding or reactive barriers. The specific objectives of this study are (1) to describe through batch experiments the kinetics and mechanisms by which potassium permanganate oxidized dissolved tetrachloroethene (PCE), trichloroethene (TCE), and dichloroethene (DCE), (2) to examine using column studies the nature and kinetics of reactions between potassium permanganate, residual DNAPLs (PCE, TCE, and DCE) and porous medium solids, (3) to represent the process understanding in flow and transport models that demonstrate the potential applicability of the approach, and (4) to apply the resulting computer code in the development of appropriate field tests for assessing the approach.

METHODS AND RESULTS

Chemicals

The chlorinated ethylenes, PCE (C_2Cl_4, 99+%), TCE (C_2HCl_3, 99.5+%), cis-DCE ($C_2H_2Cl_2$ 97%), trans-DCE ($C_2H_2Cl_2$ 97%), and 1, 1-DCE ($C_2H_2Cl_2$, 99%) were obtained from Aldrich Chemical Co.(Milwaukee, WI) and used as received. Radiolabeled [1,2-^{14}C] TCE (3.1 mCi/mmol) was purchased from Sigma Chemical Co. (St. Louis, MO).

Potassium permanganate stock solution was prepared by dissolving $KMnO_4$ crystals in Milli-Q water or phosphate-buffered Milli-Q water. The stock solution was stored in brown glass bottles and used freshly. The reducing agents, thiosulfate and hydrazine hydrate (95+%), are both research grade and were prepared as a stock solution (6 mg/mL) for quenching the reaction in some kinetic experiments. A total organic carbon (TOC) stock solution (1000 mg C/L) for use in the TOC analysis was prepared by dissolving 0.2125 g of dried, reagent grade potassium hydrogen phthalate in 100 mL of Milli-Q water. Carboxylic acids were obtained from Fluke (Buchs, Switzerland) with purity 99+% and used as received.

Three phase transfer catalysts (PTCs), tetra-n-ethylammonium bromide (TEA, $(C_2H_5)_4NBr$, 99.9 %), tetra-n-butylammonium bromide (TBA, $(CH_3(CH_2)_3)_4NBr$, 99.9 %), and pentyltriphenylphosphonium bromide (PTPP, $CH_3(CH_2)_4P(C_6H_5)_3Br$, 99.8 %) were obtained from Aldrich Chem. Co. The catalysts were selected on the basis of their extraction constants (K_E) and molecular structures (Table 3). Due to the lack of available solubility data for TCE, estimated extraction constants for methylene chloride were used to guide the selection of PTCs. The concentration of selected PTCs in all experiments was kept below the aqueous phase solubility in order to avoid aggregation and precipitation of catalyst-permanganate salts.

Chemical Analyses

Analysis of chlorinated ethylenes was conducted with a gas chromatograph from Fisons Instruments (GC 8060) equipped with a Ni^{63} electron capture detector and a DB-5 capillary column (J&W Scientific, Rancho Cordova, CA), 30 m 0.32 mm I.D, with a film thickness of 1.0 µm. Helium was used as the carrier gas and nitrogen as the make-up gas. The gas chromatograph was calibrated daily with a minimum four calibration standards, and duplicate measurements were made for each sample or standard.

Aqueous concentration of $KMnO_4$ was analyzed using a Varian Cary 1 UV-visible spectrophotometer at wavelengths ranging from 400 to 700 nm. In this range of wavelength, permanganate (MnO_4^-) and hypomanganate (MnO_4^{3-}) ions have a maximum of absorbance at 525/546 nm and 667 nm, respectively, while manganate (MnO_4^{2-}) has two absorbance peaks at 439 and 606 nm (Stewart, 1965). These species are almost transparent to radiation at 418 nm. The absorbance at 418 nm is a measure of the concentration of either cyclic hypomanganate ester (Lee and Brownridge, 1973; Wiberg *et al.*, 1973) or a soluble form of colloidal manganese dioxide (Mata-Perez and Perez-Benito, 1985; Simandi and Jaky, 1976).

Initially, the activity of Cl^- was measured using an Orion ion selective electrode (ISE) with a glass body (Model 9617). The ISE was calibrated using a standard solution of NaCl in the range from 0.1 to 10^{-5} M. Because of low sensitivity of the ISE to the trace amount of Cl^-, ranging from 10^{-4} - 10^{-5} M, additional samples were measured by a Buchler Digital Chloridometer, using a coulometric titration of chloride ions (Cotlove, 1958). Before the titration, a 0.1-mL aliquot of reducing reagent stock solution (6 mg/mL), hydrazine hydrate, was added to a 0.9-mL sample taken from the reaction vessel to quench the reaction in the sample solution. To prepare for the titration, the total 1-mL sample aliquot was added to a test vial containing 3-mL of an acid reagent comprised of 0.4 N HNO_3 and 40% glacial acetic acid. Finally, four drops of gelatin reagent were added to the test vial. The samples in the test vials were titrated at either the LOW or HIGH switch position in order to provide the proper concentration range from 3.3×10^{-3} to 33.3 mM.

TOC was analyzed using a Shimadzu TOC-5000 TOC Analyzer. The four standards for calibration were prepared by diluting the TOC stock solution to a concentration in the range of 10 - 60 mg C/L. All standards and samples were acidified with concentrated HCl and sparged with CO_2 free air. Samples of contaminated ground water and landfill leachate with high TOC concentration were diluted as needed in order for concentrations to fall within the calibrated range of the TOC analyzer. Standards and samples were analyzed in triplicate and the values of TOC were accepted when the standard deviation was less than 2%.

The organic acids were analyzed on a Waters high performance liquid chromatography (HPLC) fitted with a Bio-Rad Aminex HPX-87H column (300 × 7.8 mm I.D.).

Task 1. Fundamental Experiments; Kinetic Reaction Rates

The oxidative treatment of chlorinated ethylenes in ground water using permanganate was investigated in a series of batch kinetic tests using water-jacketed reaction vessel (Figure 1).

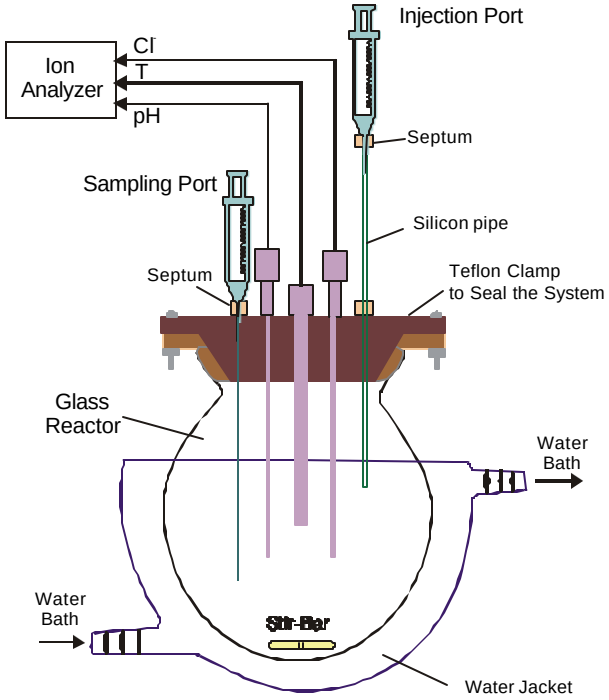

Figure 1. Schemetic diagram of a reactor. In kinetic experiments, each sample aliquot was withdrawn from the sampling port by a syringe when the same volume of solution as the aliquots was injected via the injection port. Zero headspace was maintained at all times.

Five chlorinated ethylenes including tetrachloroethylene (PCE), trichloroethylene (TCE), and three isomers of dichloroethylenes (DCEs) were examined. The degradation process was rapid with pseudo-first-order rate constants ranging from 4.5×10^{-5} to 0.03 s^{-1} at MnO_4^- =1 mM (Table 1). The rate increased with a decreasing number of chlorine substituents on the ethylene. The higher reactivity of trans-DCE ($k_{obs}=30\times10^{-3}$ s^{-1} at MnO_4^-=1 mM) as compared to cis-DCE ($k_{obs}=0.9\times10^{-3}$ s^{-1} at MnO_4^-=1 mM) is thought to be caused by a significant steric effect due to the formation of a large cyclic activated complex. TCE oxidation as a second-order reaction was confirmed and the rate constant, $k=0.67\pm0.03$ M^{-1} s^{-1}, is independent of pH over the range of 4-8

Table 1. Rate constants and half lives for the oxidative degradation of chlorinated ethylenes by permanganate (1 mM).

Chlorinated Ethylenes	k_{obs} (10^{-4} s^{-1})	Determination coef. of regression (r^2)	$T_{1/2}$ (min)
PCE	0.45±0.03	0.924	256.7
TCE	6.5±0.1	0.997	17.8
cis-DCE	9.2±0.5	0.976	12.6
trans-DCE	300±20	0.991	0.4
1,1-DCE	23.8±1.3	0.980	4.9

(Figure 2). The activity of both Cl^- and hydrogen ions was monitored over time and suggests essentially complete dechlorination, making the degradation products less harmful than the parent compounds. Competition for MnO_4^- from other organic compounds in ground water or highly contaminated ground water was also evaluated in experiments.

A simple and quick approach was demonstrated to estimate permanganate consumption by other organic compounds for field applications and to predict the TCE degradation rate in a system involving multiple contaminants. The modeling results suggest that the effect of autocatalysis by MnO_2 on TCE degradation is significant when the system contains high concentration levels of MnO_4^- and TOC.

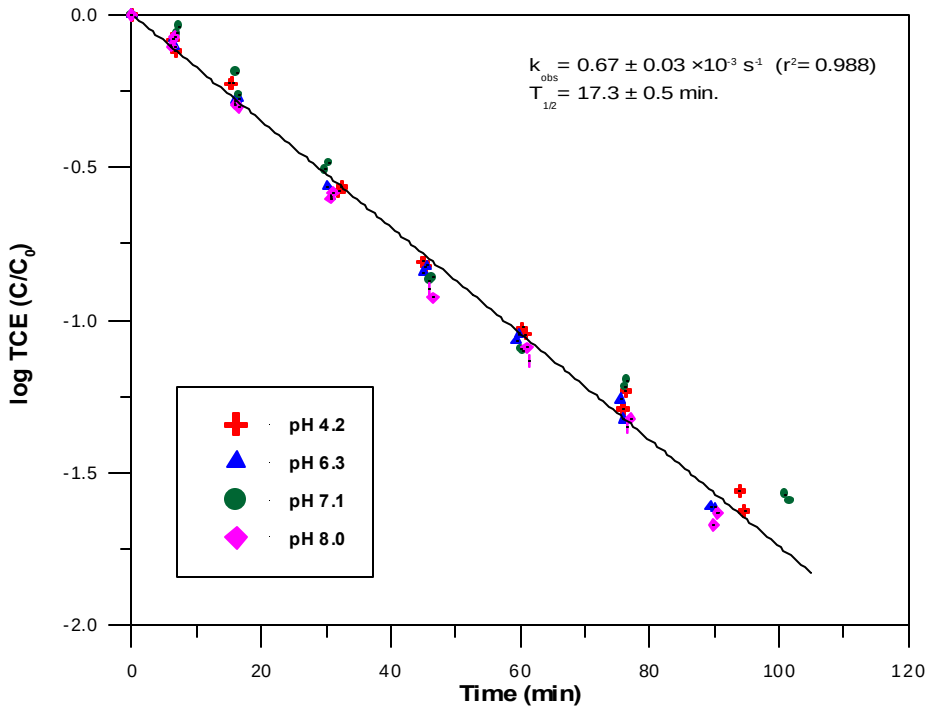

Figure 2. Pseudo-first-order plot of TCE transformation in 1 mM MnO_4^- over the pH range of 4-8. Rate constant $k_{obs} = 0.67 \pm 0.03 \times 10^{-3}$ s^{-1} and half life $T_{1/2} = 17.3 \pm 0.5$ minutes.

Task 2. Mechanisms for TCE Oxidation by Permanganate

The oxidation of trichloroethylene (TCE) by permanganate was studied via a series of kinetic experiments. The goal in product identification and parameterization of the oxidation kinetics was to assess the utility of this reaction as the basis for the in-situ remediation of ground water contaminated by chlorinated ethenes. TCE oxidation mainly involves the formation and decomposition of an organometallic compound (hypomanganate ester) to form carboxylic acids, and eventually, oxidation to the final product, CO_2 (Figure 3). The initial and final reactions in

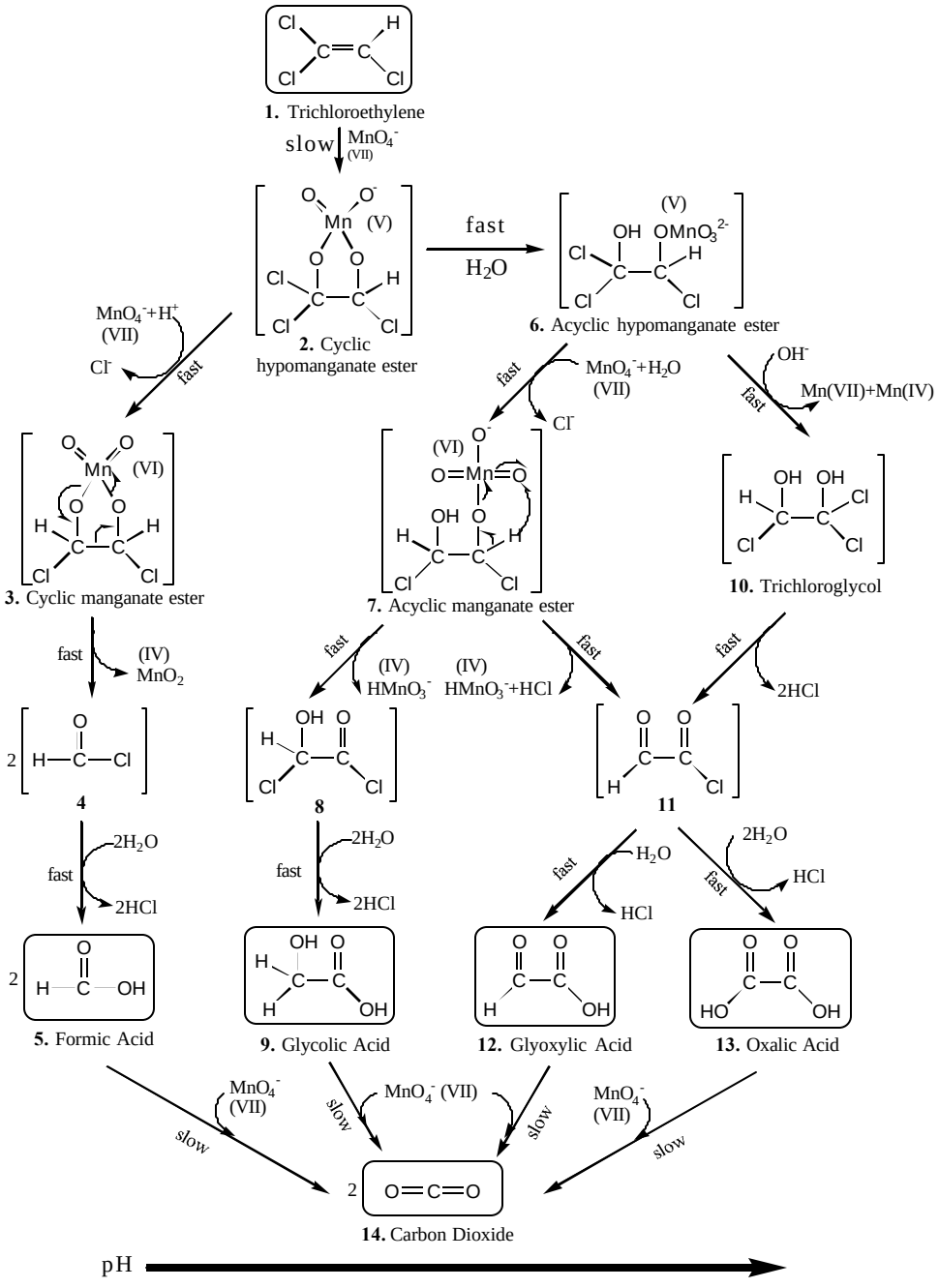

Figure 3. Proposed TCE oxidation pathways. Shadowed boxes are products identified in this study.

the TCE oxidation are subject to rate-limiting steps, which control the destruction rate of TCE and formation rate of the final product. The fast reactions involved in the second step determine the nature of products. Four carboxylic acids, including formic, oxalic, glyoxylic and glycolic acids, and CO_2 were identified and quantified in kinetic measurements. The distribution of products is highly dependent upon experimental conditions, particularly pH (Figure 4). Based on our understanding of various processes involved with TCE oxidation, a kinetic model (Table 2) was

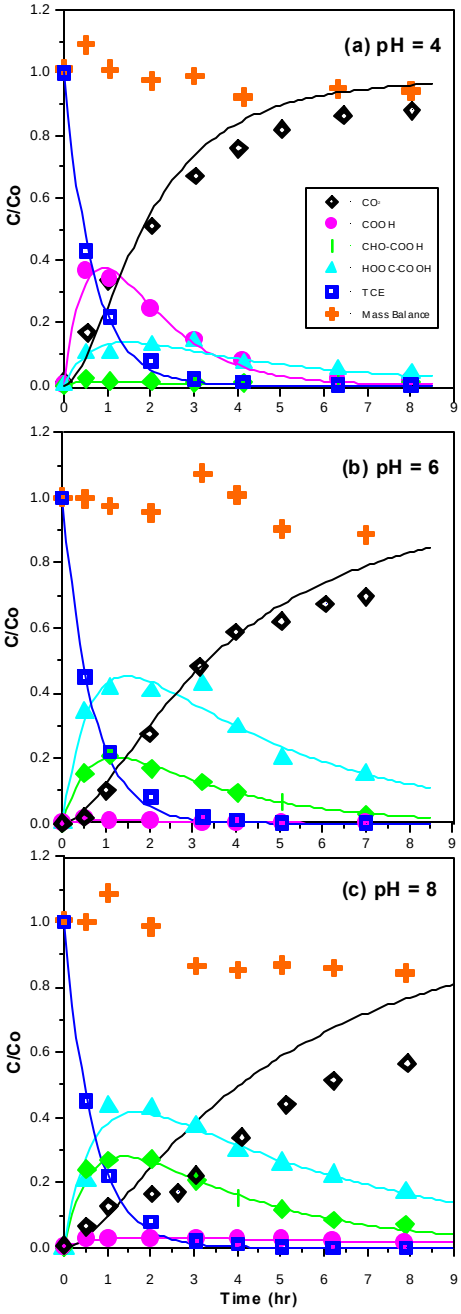

Figure 4. Product distribution with time in TCE oxidation at pH 4 (a), pH 6 (b) and pH 8 (c). Lines for TCE and carboxylic acids represent best fits using eqs 16-17, whereas the line for CO_2 is calculated using rate constants from the previous curve fitting.

developed and the model parameters (seven rate constants) were estimated (Table 3). The kinetic model proposed in this study successfully simulates observed experimental data.

Table 2. Listing of kinetic equations.

Equation	No
$\frac{d[HCOOH]_t}{dt} = -k_{3ap}[HCOOH]_t[MnO_4^-]$	2.7
$\frac{d[OHC-COOH]_t}{dt} = -k_{3bp}[OHC-COOH]_t[MnO_4^-]$	2.8
$\frac{d[HOOC-COOH]_t}{dt} = -k_{3cp}[HOOC-COOH]_t[MnO_4^-]$	2.9
$\frac{d[C_2HCl_3]}{dt} = -k_1[C_2HCl_3] \qquad k_1 = k_{1p}[MnO_4^-]$	2.10
$\frac{d[CHME]}{dt} = k_1[C_2HCl_3] - k_2[CHME] \qquad k_2 = k_{2a} + k_{2b} + k_{2c}$	2.11
$\frac{d[HCOOH]_t}{dt} = 2k_{2a}[CHME] - k_{3a}[HCOOH]_t \quad k_{3a} = k_{3ap}[MnO_4^-]$	2.12
$\frac{d[HCO-COOH]_t}{dt} = k_{2b}[CHME] - k_{3b}[OHC-COOH]_t \; k_{3b} = k_{3bp}[MnO_4^-]$	2.13
$\frac{d[HOOC-COOH]_t}{dt} = k_{2c}[CHME] - k_{3c}[HOOC-COOH]_t k_{3c} = k_{3cp}[MnO_4^-]$	2.14
$\frac{d[CO_2]}{dt} = k_{3a}[COOH]_t + 2k_{3b}[OHC-COOH]_t + 2k_{3c}[HOOC-COOH]_t$	2.15
$\frac{d[HCOOH]_t}{dt} = -(k_{3ap1}[HCOOH] + k_{3ap2}[HCOO^-])[MnO_4^-]$ $= -\left(\frac{k_{3ap1}[H^+] + k_{3ap2}K_a}{[H^+] + K_a}\right)[HCOOH]_t[MnO_4^-]$	2.25
$\frac{d[HOC-COOH]_t}{dt} = -(k_{3bp1}[HOC-COOH] + k_{3bp2}[HOC-COO^-])[MnO_4^-]$ $= -\left(\frac{k_{3bp1}[H^+] + k_{3bp2}K_a}{[H^+] + K_b}\right)[HOC-COOH]_t[MnO_4^-]$	2.26
$\frac{d[HOOC-COOH]_t}{dt} = -(k_{3cp1}[HOOC-COOH] + k_{3cp2}[HOOC-COO^-] + k_{3cp3}[^-OOC-COO^-])[MnO_4^-]$ $= -\left(\frac{k_{3cp1}[H^+]^2 + k_{3cp2}K_{c1}[H^+] + k_{3cp3}K_{c1}K_{c2}}{K_{c1}K_{c2} + K_{c1}[H^+] + [H^+]^2}\right)[HOOC-COOH]_t[MnO_4^-]$	2.27

subscript t for each acid denotes the total concentration; k_1, k_{3a}, k_{3b}, and k_{3c} are pseudo-first-order rate constants; k_{2a}, k_{2b}, and k_{2c} are first-order rate constants; k_{3ap}, k_{3bp}, and k_{3cp} are second-order rate constants; k_{3ap1}, k_{3ap2}, k_{3bp1}, k_{3bp2}, k_{3cp1}, k_{3cp2}, and k_{3cp3} are rate constants.

Table 3. Rate constants obtained for TCE transformation pathways using equations, 16-17. Estimation was based on experiments conducted with an initial concentration of 0.63 mM MnO_4^-. $k_2 > 10^2\ k_1$.

pH	k_1 $10^{-4}\ s^{-1}$	k_{2a}/k_2	k_{3a} $10^{-4}\ s^{-1}$	r^2	k_{2b}/k_2	k_{3b} $10^{-4}\ s^{-1}$	r^2	k_{2c}/k_2	k_{3c} $10^{-4}\ s^{-1}$	r^2
4	4.30	0.77	2.19	0.98	0.03	2.34	0.98	0.20	0.70	0.95
6	4.11	0.02	1.53	0.91	0.32	1.05	0.99	0.63	0.64	0.95
8	4.11	0.04	0.47	0.97	0.42	0.80	0.99	0.55	0.46	0.95

Task 3. Efficiency Problems Related to Permanganate Oxidation Schemes

This study investigates problems that potentially could impact a permanganate oxidation scheme, such as competitive permanganate utilization in reactions with aquifer materials, MnO_2 precipitation around zones of high DNAPL saturation, and permeability-related flow bypassing. A series of batch experiments were conducted to examine whether typical aquifer materials (glacial deposits, alluvium and carbonate-rich sand) reacted with permanganate.

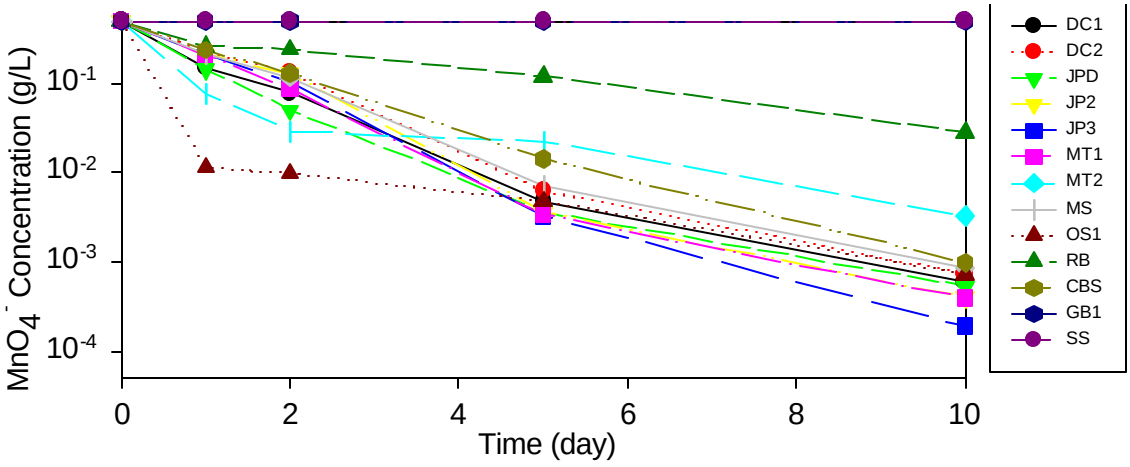

Figure 5. Utilization of MnO_4^- through oxidation of various aquifer materials.

The results show a dramatic consumption of the oxidant and a significant change in the concentrations of some chemical species, which may be of environmental concern (Figure 5). 1-D column (Figure 6) and 2-D flow tank (Figure 7) experiments have been conducted to examine mass removal rates and related flushing efficiencies. The results indicate that mass removal rates are also greatly influenced by the MnO_2 precipitation and flow bypassing. It is anticipated that in actual field settings, the issue of flushing efficiency needs to be considered in the design.

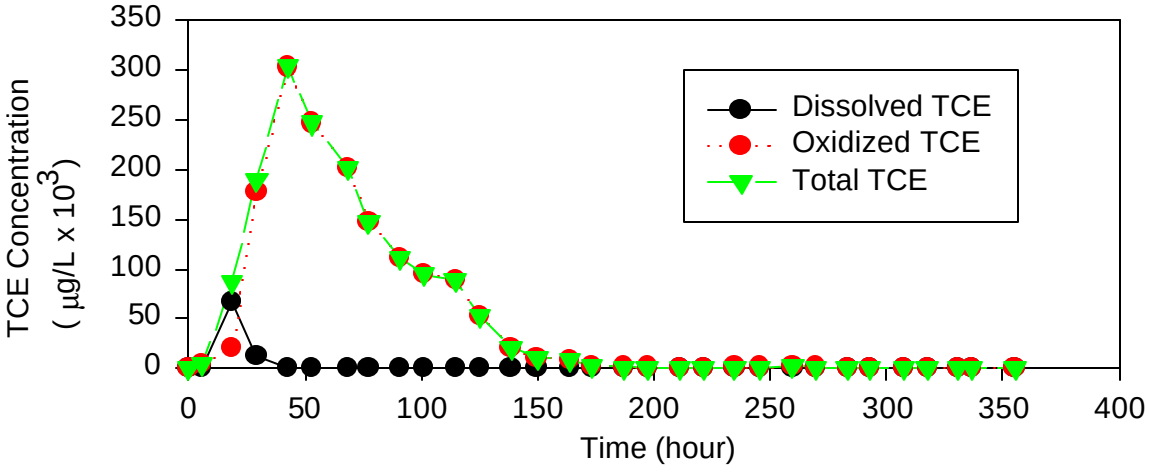

Figure 6. TCE concentration with time in the effluent of the 1 – D column and calculated removal based on Cl^- stoichiometry.

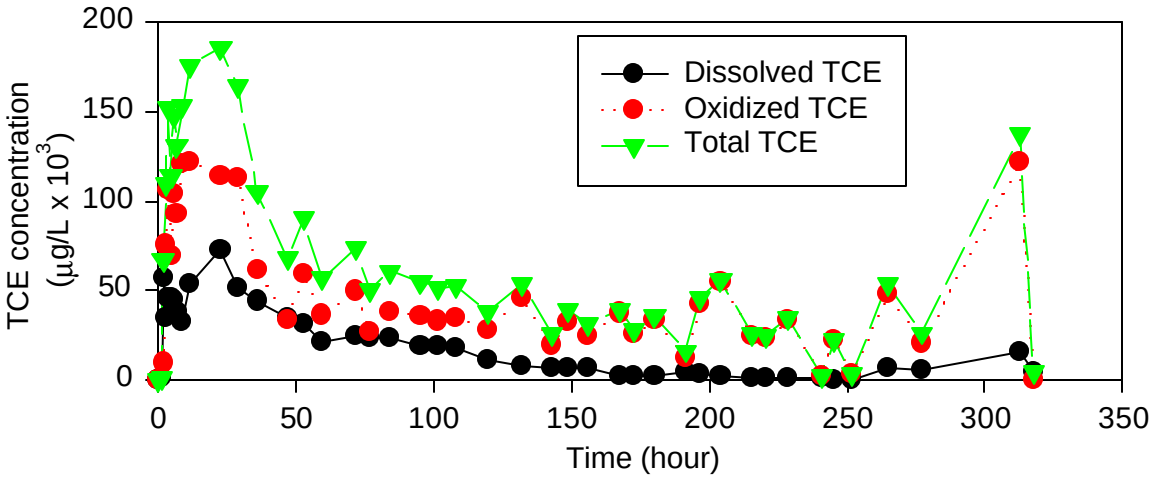

Figure 7. Effluent TCE concentration change with time in the 2 – D column experiment.

Task 4. Oxidation of DNAPL with a Phase-Transfer-Catalyst

The use of potassium permanganate to oxidize chlorinated solvents has been demonstrated as an effective process for treating nonaqueous phase liquids in ground-water systems. This study evaluates the effectiveness of phase-transfer-catalysts (PTCs) in enhancing the degradation rate. PTCs work by transferring permanganate ion into the nonaqueous phase where it initiates oxidative decomposition (Figure 8). We studied the oxidation of

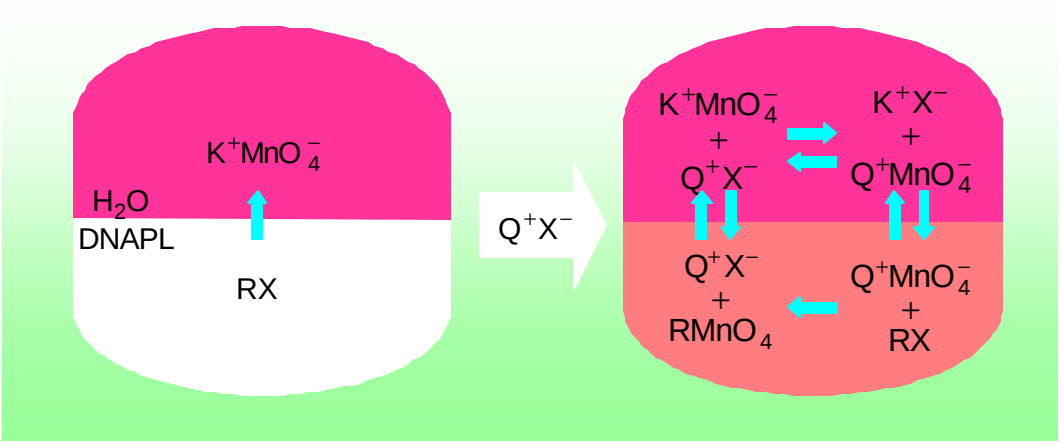

Figure 8. Schematic diagram for phase transfer catalyst facilitated permanganate oxidation of nonaqueous phase TCE. RX is organic reactant (e.g. TCE) with leaving group X^- (e.g. Cl). Q^+ is the catalytic cation.

Table 4. Chemical properties of selected PTC- MnO_4^- ion pairs.

Name/PTCs	Abbr.	FW[a]	S_w[b]	S_o[b]	logK_E[c]
tetraethylammonium	TEA	165.71	7.30×10^{-4}	0.235	1.64
tetrabutylammonium	TBA	277.92	2.10×10^{-4}	0.417	4.98
pentyltriphenylphosphonium	PTPP	413.35	2.40×10^{-4}	1.460	7.40

FW; formula weight (g/mole), S_w; solubility (M) in water, S_o; solubility (M) in methylene chloride, a; formula weight of bromide salts only, b; Karaman, *et al.*, (1984), c; calculated with Eq. (8)

trichloroethylene (TCE) by potassium permanganate, conducting kinetic batch experiments in conjunction with three PTCs that varied in terms of their extraction constants and molecular structures (Table 4). Using the same batch technique, we examined whether PTCs could enhance the aqueous solubility of TCE. Solubilization could also increase oxidation rates in the aqueous phase. Rates of TCE oxidation in solutions containing the PTCs and a blank were estimated

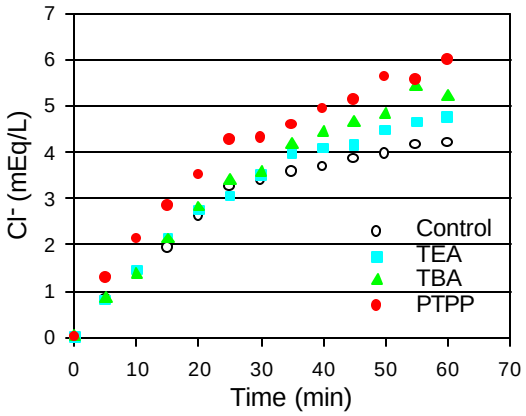

Figure 9. Concentration of chloride ion released from permanganate oxidation of TCE with different PTCs.

separately by measuring chloride concentration and UV/Vis absorbance in the aqueous phase. The enhanced rate of TCE destruction by the PTCs was reflected by an increase in the rate of consumption of permanganate ion and production of chloride ion (Figure 9 and 10). There was

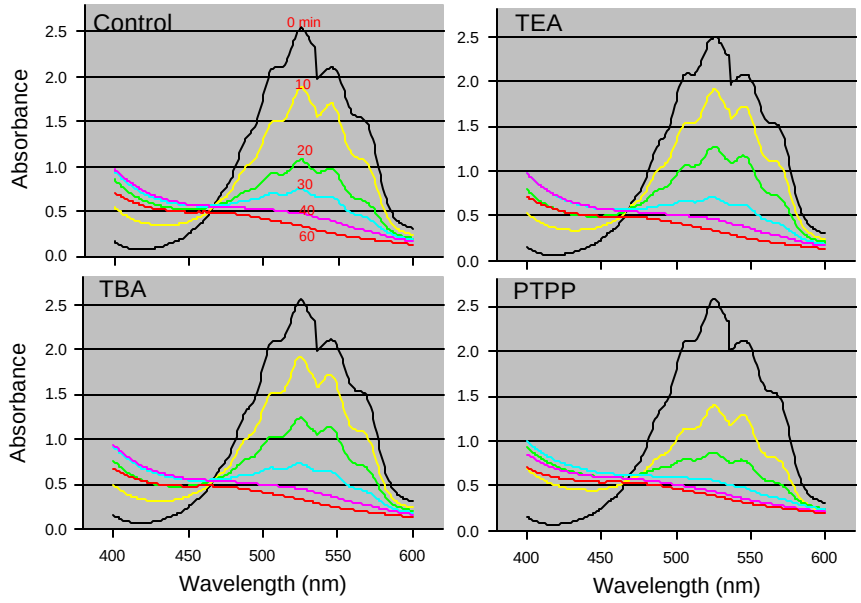

Figure 10. UV-Vis spectra of aqueous phase in permanganate oxidation of TCE facilitated with different PTCs. Numbers on graphs indicate the reaction time (min.)

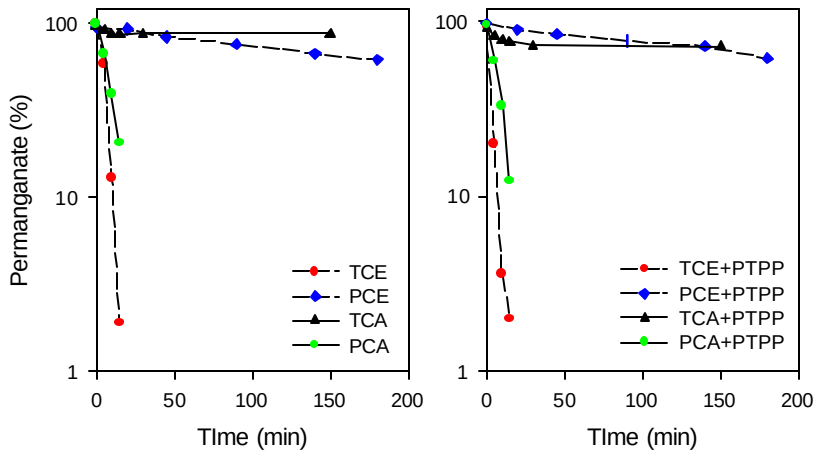

Figure 11. Degradation of selected chlorinated DNAPLs with and without PTPP, as represented by MnO_4^- consumption with time

no tendency for the PTCs, however, to solubilize TCE in the aqueous phase. Therefore, the PTCs increased the rate of TCE decomposition by catalyzing permanganate oxidation in the organic phase. This study suggests that there is significant potential for testing this scheme under field conditions.

Another experimental study examined the influence of pentyltriphenylphosphonium bromide (PTPP) as a PTC on the rate of permanganate (MnO_4^-) oxidation of DNAPLs in pure phases and mixtures. Kinetic batch experiments with trichloroethylene (TCE), 1,1,2-trichloroethane (TCA), tetrachloroethylene (PCE), 1,1,2,2-tetrachloroethane (TECA), and their mixtures (1:1, v/v) were performed in test tubes to assess reaction rates. The disappearance of MnO_4^- was quantified by capturing digital images of the tubes. This rapid photographic

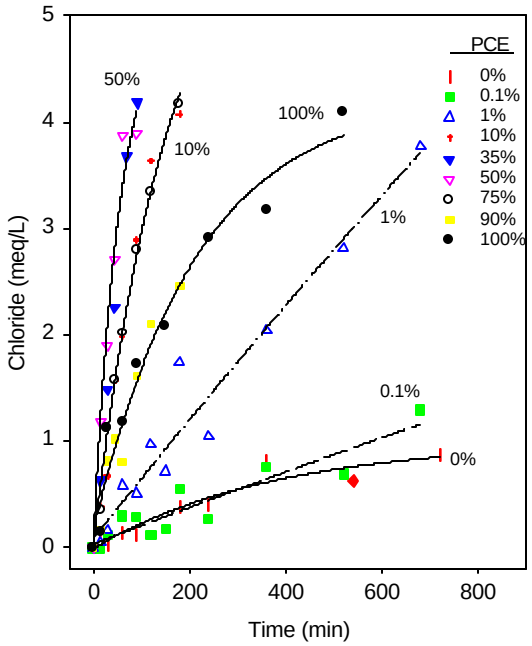

Figure 12. Chloride releases from oxidation of PCE/TCA catalyzed by PTPP. The volumetric percentage of PCE in the mixture varied from 0 to 100 %.

monitoring approach was validated by comparison with an UV-Vis spectrometer method. The PCE/TCA mixture was selected to examine the impact of relative contents of a component in the binary mixture on the MnO_4^- disappearance. The comparative rates of MnO_4^- consumption for pure phases were TCE > TECA > PCE > TCA (Figure 11). PTPP increased MnO_4^- consumption rates, especially for TCE and TECA as pure phases. The consumption rates of mixtures without PTPP were lower than those including the pure phases. However, due to their high extraction capability for PTPP-MnO_4^- ion pairs, TCA and TECA appeared to increase the MnO_4^- consumption significantly when they were mixed with TCE or PCE. The increase in consumption rates with PTPP was most remarkable with the mixture of PCE and TCA. Chloride concentration showed faster increases for the mixtures with relative PCE contents ranging about 5 to 90%, maximum at about 50% PCE, than for pure phases of PCE and TCA when the PTC-assisted the reactions (Figure 12). The PTC appears to be promising in its ability to increase oxidation rates of DNAPL mixtures.

Task 5. Computer Simulations

Several laboratory and field studies have demonstrated the potential viability of oxidation schemes using MnO_4^- for the in-situ treatment of DNAPL source areas, which are contaminated by chlorinated ethylenes (PCE, TCE and DCE). Chemically, the chlorinated ethylenes are oxidized to CO_2, Cl^-, and MnO_2. The goal of this study was to develop a theoretical framework for the chemical and physical processes involved. To this end, a computer model was developed to simulate the coupled processes of NAPL dissolution, chemical reactions, and solute mass transport in the in-situ chemical oxidization scheme. The model incorporates a kinetic description of reactions between the MnO_4^- and the chlorinated ethylenes and the rate of dissolution of the NAPL. A Strang operator-splitting method, which coupled the different physical and chemical processes and an exponentially-expressed solution of the kinetic equations, led to a significant speed up in the solution process. The products in reactions were calculated based on the stoichiometry of the reaction;

PCE; $$C_2Cl_4 + 2MnO_4^- \Rightarrow 4Cl^- + 2CO_2 + 2MnO_2(s) \quad (3)$$

TCE; $$C_2HCl_3 + 2MnO_4^- \Rightarrow 3Cl^- + 2CO_2 + H^+ + 2MnO_2(s) \quad (4)$$

DCE; $$C_2HCl_2 + 2MnO_4^- \Rightarrow 2Cl^- + 2CO_2 + 2H^+ + 2MnO_2(s) \quad (5)$$

Natural organic carbon; $$C + MnO_4^- \Rightarrow CO_2 + MnO_2(s) \quad (6)$$

We demonstrated the capabilities of this code using already published results of column, test cell, and field experiments. The first simulation attempted to reproduce column flushing experiments by Schnarr et al. (1998), using aquifer materials from the Canadian Forces Base Borden. Figure 13 shows the simulation domain and basic data for the five column experiments.

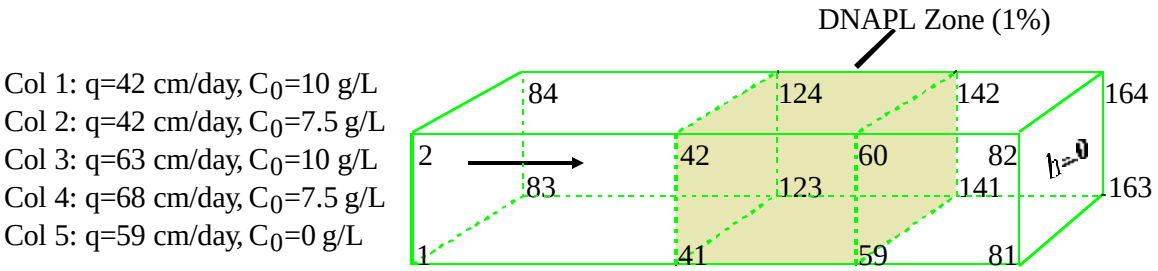

$\Delta x = 0.01$ m, $\Delta y = \Delta z = 0.045$ m, $\alpha_L = 0.02$ m, $n = 0.41$

Figure 13. Model setup for the simulation of MnO_4^- oxidation of PCE in column experiments.

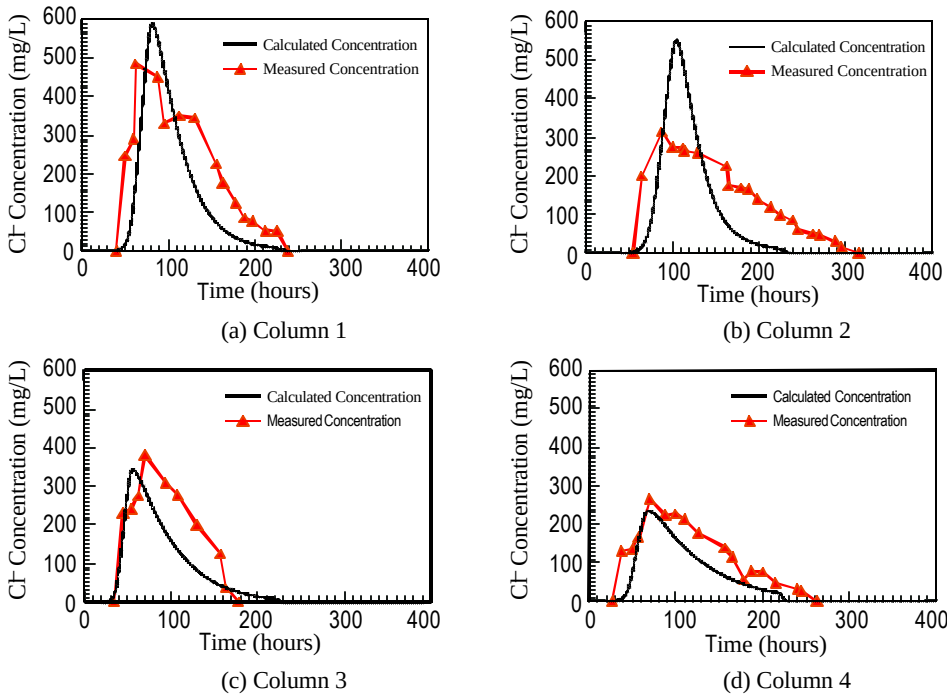

Figure 14. Simulated breakthrough curves for Cl- for column experiments 1 through 4.

The domain is discretized by 40 rectangular blocks with $\Delta x = 0.01$ m, and $\Delta y = \Delta z = 0.045$m. To maintain a Peclet number of 2, a longitudinal dispersivity of 0.02 m was specified in the model. The measured porosity of 0.41 was assigned uniformly. A constant-head boundary condition was assumed at the end of column. The basic characteristics of the breakthrough curves of Cl- were simulated reasonably well (Figure 14) although there were differences between the measured and the calculated breakthrough curves.

The second set of simulations sought to match the Cl- mass production rate in a field test designed as a proof-of-concept of source-zone flooding by MnO_4^- (Schnarr et al., 1998).The

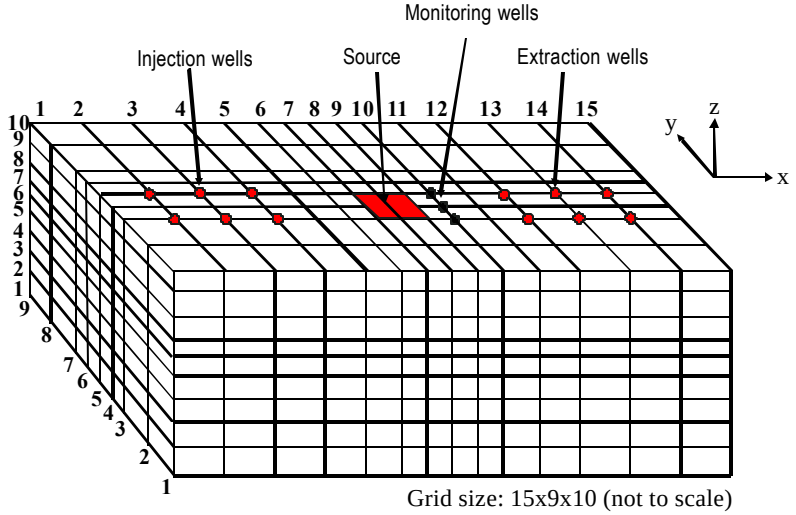

Figure 15. A three-dimensional model of the injection and extraction system in the Borden test cell

demonstration is based on a field-scale experiment at CFB Borden that demonstrated the potential of MnO_4^- flooding for removing pure-phase PCE (Schnarr et al., 1998). The model conceptualization of the field experiment cell is shown in Figure 15. Simulated mass removal rate in terms of Cl^- was compared with measurements (Figure 16). The two results exhibit a relatively close match after trial and error adjustment of reaction parameters. Interestingly, the mass removal rate could not be simulated without accounting for MnO_4^- oxidation of the aquifer materials. Thus, for both column and field cell experiments, simulations indicated that a major factor affecting the transport of the MnO_4^- front is the quantity of reactive materials existing in an aquifer.

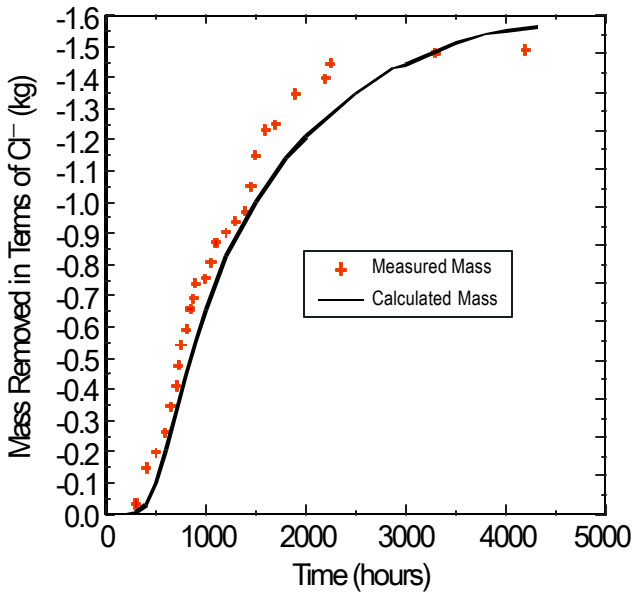

Figure 16. Simulated and measured mass removal rates in terms of Cl^- for the Borden test cell.

The third set of simulations was based on a similar field-demonstration of $KMnO_4$ flooding at a DOE facility (West et al, 1997). A field-scale experiment of MnO_4^- oxidation of TCE was performed at the Department of Energy Portsmouth Gaseous Diffusion Plant (PORTS) in Ohio by researchers from Oak Ridge National Laboratory (ORNL) (West et al., 1997). There are four major geological units of interest at the test area at Portsmouth (X701-B). The upper unit, the Minford silt and clay, has an average thickness of 7.5 m. The zone targeted for treatment is the Gallia sand and gravel with an average thickness of 1.5 m. Deeper units include the 4 m thick Sunbury shale, and the 15 m thick Berea Sandstone. The field test involved injecting MnO_4^- in one horizontal well and extracting fluid in other horizontal well about 27 m up-gradient of the injection well (Figure 17). In the experiment, there was preferential flow of the MnO_4^- near the ends of the injection well. There was difficulty in the experiment in maintaining a constant injection/withdrawal rate of 10 gpm for both the injection and extraction wells. The injection rate was reduced to 6 gpm. MnO_4^- was also added through a vertical well at the center of the treatment zone to improve the efficiency of flooding. A two-dimensional model of 51x51 nodes was constructed to represent the treatment zone and its vicinity (Figure 18). The simulation grid was designed with relatively small node spacings inside the test region (Δx = 1m, and Δy = 2 m) and relatively large spacings outside (maximum Δx = 6 m, and maximum Δy = 7.5 m). The thickness of the simulation domain is the same as the Gallia formation (Δz = 1.5 m).

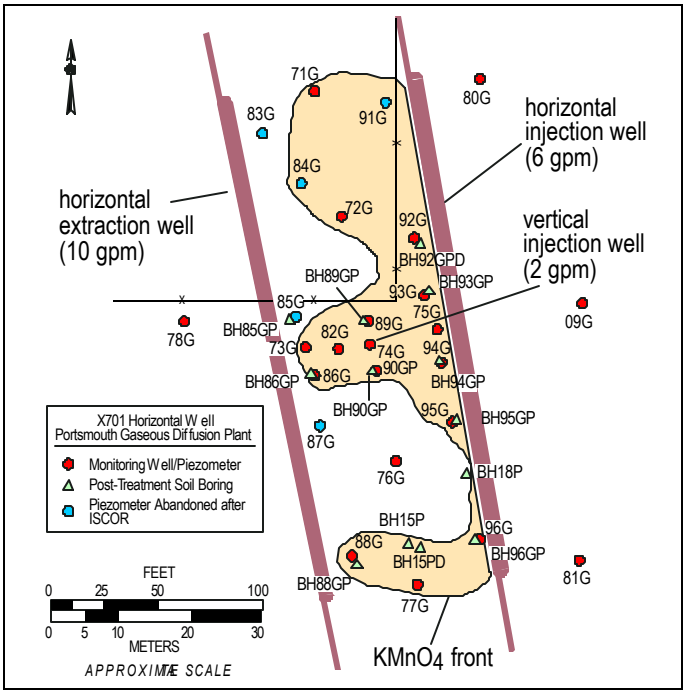

Figure 17. A field-scale experiment of permanganate oxidation of TCE at the Department of Energy Portsmouth Gaseous Diffusion Plant (PORTS)

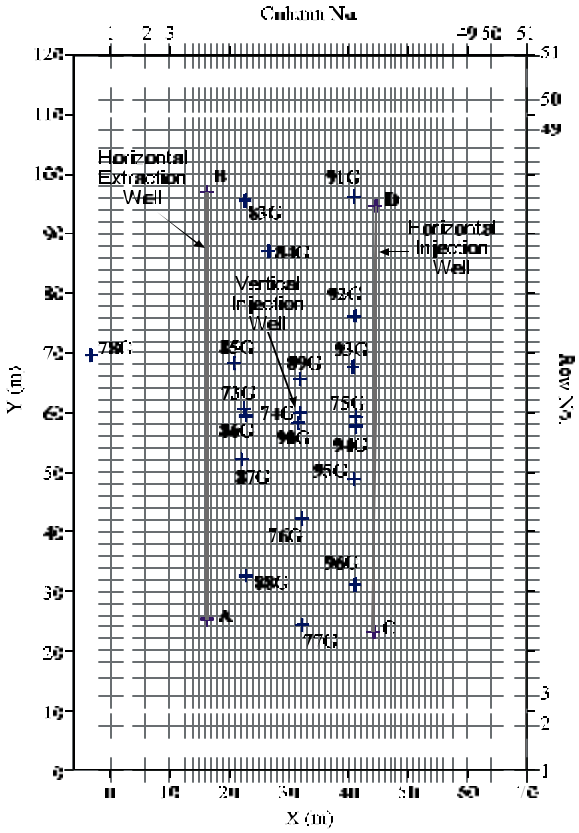

Figure 18. A two-dimensional model of 51x51 nodes representing the treatment zone and vicinity at the PORTS experiment site.

The simulation indicates that dissolved TCE concentrations were significantly reduced, where the MnO_4^- was delivered, as compared to the initial TCE concentration (Figure 19a). At time = 7 days, the contour line of 0.005 mg/L TCE (drinking water standard) is located near the horizontal injection well (Figure 19b). After 32 days, the zone of 0.005 mg/L or less TCE concentration expanded outward significantly (Figure 19c). After this time (e.g., 120 days; Figure 19d), there is relatively little enlargement of the treated zone because the zone flooded by MnO_4^- didn't expand very much. Generally, the simulated results matched well with experimental measurements. The computer model provides a useful tool for assisting the design and the prediction of the oxidization processes under field conditions.

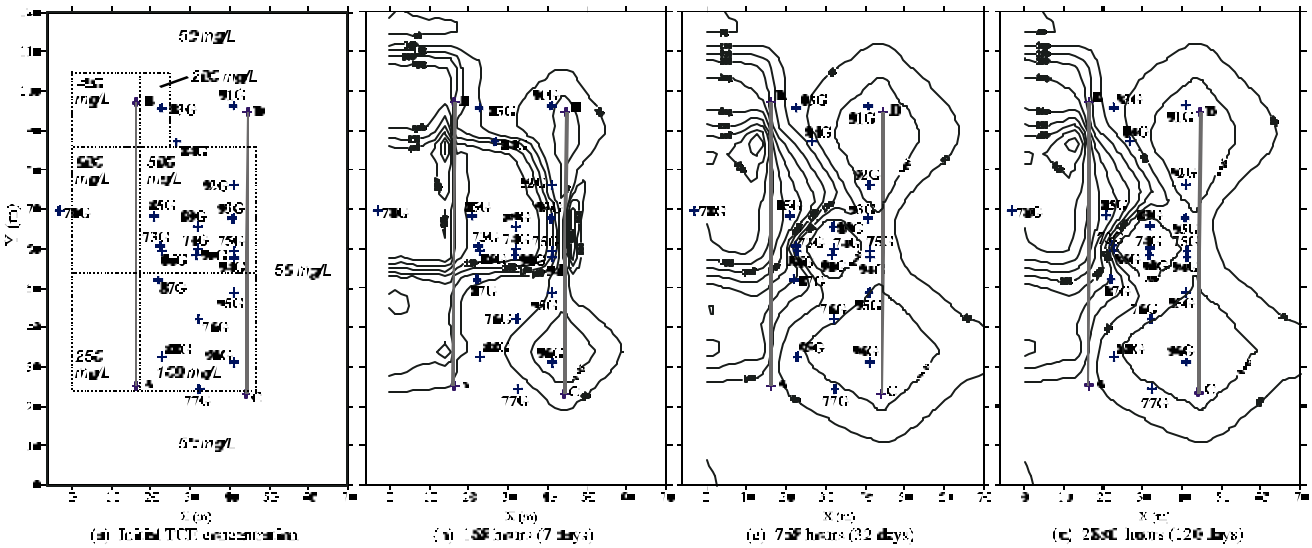

Figure 19. Simulated TCE distribution. (a) Time = 7 days; (b) Time = 32 days; (c) Time = 120 days.

RELEVANCE, IMPACT AND TECHNOLOGY TRANSFER

There are many research performed previously to test potassium permanganate as a strong oxidant for many contaminant. With this project, we have extensively contributed to the basic understanding of rates and reaction pathways involved with MnO_4^- as an oxidant. These studies support proof-of-concept research showing that MnO_4^- is able to destroy chlorinated ethylenes rapidly and efficiently.

Fundamentally, the approach has merit in field applications. Most applications involve flooding the zone of contamination using injection/withdrawal wells. This technology is being deployed in field demonstration and industrial application in the hopes of achieving large mass removals. The project achievements made to particularly develop new compute code make significant impact on the field application of this remediation scheme since the code is cable of simulating key reactions between the aquifer materials and permanganate and the kinetic sorption of chemicals. The code eventually is expected to provide a numerical tool to design field operation system and interpret the field observations.

The new compute program and extensive knowledge on these remediation approach will help regulatory agencies, consulting institutions, and field practicing organizations to

significantly reduce future costs, schedules, and risks. However, we believe that there are still some hurdles that we must overcome before the results of this project can be successfully employed into field operation. The major aspects we are currently focusing on include the delivery of oxidants into zones of contamination and the enhancement in reaction speed. Further findings on those areas will certainly improve the efficacy of the remediation technology and minimize the adverse impact on environment.

PROJECT PRODUCTIVITY

The project has accomplished all the proposed goals for the grant period. Our accomplishments have been documented in 11 scientific journal/conference articles and numerous participations at various DOE workshops and national conferences such as AGU, GSA, NGWA, Battelle DNAPL conferences throughout the period. The project has also provided support for 3 students and 2 post-docs and training in areas of experimental design and performance, sophisticated chemical analysis, and numerical and computer modeling skills.

PERSONNEL SUPPORTED

Faculty; Dr. Franklin W. Schwartz, Ohio Eminent Scholar in Hydrogeology.
Co-Investigator; Dr. Hubao Zhang (Duke Engineering & Services)

Post-Docs; Dr. Yongkoo Seol
Dr. Min-Ho Koo (Kong-Ju National University, Korea)

Graduate Students; Dr. Y. Eugene Yan (Argonne National Laboratory),
X. David Li
Yao-Chuen Fang

PUBLICATIONS

a. Published in peer-reviewed journals and books

Yan, Y.E. and F.W. Schwartz, 1999. Oxidative degradation and kinetics of chlorinated ethylenes by potassium permanganate. Journal of Contaminant Hydrology, 37(3-4), p343-365 .

Yan, Y.E. and F.W. Schwartz, 2000, Kinetics and mechanisms for TCE oxidation by permanganate, Environmental Science and Technology, V.34, p2535-2541.

Seol, Y. and F.W. Schwartz, 2000. Phase-transfer-catalysis applied to the oxidation of nonaqueous phase trichloroethylene by potassium permanganate, Journal of Contaminant Hydrology, V.44, No.2, p185-201

Zhang, H. and F.W. Schwartz, 2000. Simulating the in situ oxidative treatment of chlorinated ethylenes by potassium permanganate. Water Resources Research, V. 36, No.10, p3031-3042

b. Published in unreviewed publications

Yan, Y.E. 1998. Abiotic remediation of ground water contaminated by chlorinated solvents, Ph.D. Thesis, The Ohio State University, Columbus, OH.

Yan, Y.E. and F.W. Schwartz, 1998. Oxidation of chlorinated solvents by permanganate. Physical, Chemical and Thermal Technologies, The First International Conference on Remediation of Chlorinated and Recalcitrant Compounds. May 18-21, 1998, Monterey, CA., Battelle Press, Columbus, 1(6); 403-408.

Seol, Y. and F.W. Schwartz, 2000. Phase-transfer-catalysis on the oxidation of trichloroethylene by permanganate, in Chemical oxidation and reactive barriers, The Second International Conference on Remediation of Chlorinated and Recalcitrant Compounds. May 22-25, 2000, Monterey, CA., 2(6); 17-24

Zhang, H. and F.W. Schwartz, 2000. Simulation of oxidative treatment of chlorinated compounds by permanganate, in Chemical oxidation and reactive barriers, The Second International Conference on Remediation of Chlorinated and Recalcitrant Compounds. May 22-25, 2000, Monterey, CA., 2(6); 1-8

Li, X. and F.W. Schwartz, 2000. Efficiency problems related to permanganate oxidation schemes, in Chemical oxidation and reactive barriers, The Second International Conference on Remediation of Chlorinated and Recalcitrant Compounds. May 22-25, 2000, Monterey, CA., 2(6); 41-48

Ibaraki, M. and F.W. Schwartz, 2000. On source-zone flooding for treating DNAPL sites, in Treating dense nonaqueous phase liquids (DNAPLs), The Second International Conference on Remediation of Chlorinated and Recalcitrant Compounds. May 22-25, 2000, Monterey, CA., 2(2); 125-132

c. Accepted/submitted for publication

Seol, Y., S. Lee, and F.W. Schwartz, 2000. Oxidation of binary DNAPL mixtures using potassium permanganate with a phase-transfer-catalyst, Ground Water Monitoring and Remediation, Accepted.

Seol, Y., Zhang, H. and F.W. Schwartz, 2000. Heterogeneity and in-situ advanced oxidation for DNAPL, A Review, Environmental and Engineering Geosciences, Submitted.

INTERACTIONS

Participation/Presentation at meeting, workshops, and conferences

Yan, Y.E. and F.W. Schwartz, 1998. Oxidation of chlorinated solvents by permanganate, The First International Conference on Remediation of Chlorinated and Recalcitrant Compounds. May 18-21, 1998, Monterey

Seol, Y. and F.W. Schwartz, 2000. Phase-transfer-catalysis on the oxidation of trichloroethylene by permanganate, The Second International Conference on Remediation of Chlorinated and Recalcitrant Compounds. May 22-25, 2000, Monterey, CA.

Zhang, H. and F.W. Schwartz, 2000. Simulation of oxidative treatment of chlorinated compounds by permanganate, The Second International Conference on Remediation of Chlorinated and Recalcitrant Compounds. May 22-25, 2000, Monterey, CA.

Li, X. and F.W. Schwartz, 2000. Efficiency problems related to permanganate oxidation schemes, The Second International Conference on Remediation of Chlorinated and Recalcitrant Compounds. May 22-25, 2000, Monterey, CA.

Ibaraki, M. and F.W. Schwartz, 2000. On source-zone flooding for treating DNAPL sites, The Second International Conference on Remediation of Chlorinated and Recalcitrant Compounds. May 22-25, 2000, Monterey, CA., 2(2); 125-132

Seol, Y., F. W. Schwartz, and E.Y. Yan, 2001, Kinetics of permanganate oxidation of chlorinated ethylenes, Groundwater Quality 2001, 3rd International Conference, June 17-21, 2001 University of Sheffield, UK

Seol, Y. and F. W. Schwartz, 2000. Evaluation of alcohol cosolvency and phase-transfer catalysis to enhance the reaction rates between potassium permanganate and chlorinated solvents, American Geophysical Union. Fall Meeting 2000, San Francisco, CA. Dec. 14-19

Seol, Y. and F. W. Schwartz, 1999, Phase-transfer-catalysis enhanced potassium permanganate oxidation of trichloroethylene, Abstract, Geological Society of America, Denver, CO, Oct. 25-29

Seol, Y., F. W. Schwartz, M. Ibaraki, X. Li, E. Yan, and H. Zhang, 1999, Permanganate oxidation in DNAPL source remediation, US Department of Energy, Oak Ridge Operation, Environmental Science Management Program Workshop, Oak Ridge, TN, Oct. 22

FUTURE WORK

In spite of apparently quite positive results, problems with the permanganate oxidative scheme remain. Our studies and one at Sandia National Laboratory have shown that the typical approach for delivering $KMnO_4$ - using injection and withdrawal wells to circulate many pore volumes of a $KMnO_4$ solution through a zone of DNAPL contamination - may not likely achieve the expected, high destruction rates. The main problems are that the combination of natural medium heterogeneity and formation plugging due to the formation of MnO_2 commonly diverts flow around the zones of highest contamination. The $KMnO_4$ solution ends up being circulated without contacting the zones of greatest contamination. This problem is essential one of delivery - well systems might not be capable of effectively getting the $KMnO_4$ to the zones of significant NAPL saturation.

We are currently planning to conduct basic research on a new delivery scheme that involves mixing the appropriate quantity of $KMnO_4$ as a solid into the zone of DNAPL contamination. This scheme actually takes advantage of the tendency for reaction products to reduce the permeability of the treatment zone, which will control the dissolution of the solid and keep the MnO_4^- in contact with the DNAPL. What needs to be determined, however, is how various solid forms of $KMnO_4$ behave in porous media and dissolve under the combined influence of fluid flow and MnO_2 precipitation.

The goals of this future study are to (1) to elucidate the dissolution/reaction processes accompanying the amendment of media containing chlorinated solvents with $KMnO_4$ and (2) to assess the potential for solid $KMnO_4$ amendments as a scheme to clean up source zones. We will try to describe through column experiments how solid forms of potassium permanganate

($KMnO_4$) behave in saturated media with and without TCE and PCE, to undertake flow tank studies that examine the hydraulic impact of reaction products (especially MnO_2) on the flux of water through the zone of contamination, and to represent the process understanding in flow and transport models that demonstrate the potential applicability of the approach.

LITERATURE CITED

Cotlove, E., 1958. An instrument and method for automatic, rapid, accurate and sensitive titration of chloride in biologic samples. Journal of Laboratory and Clinical Medicine, 51:461-468.

Karaman, H., Barton, R.J., Robertson, B.E. and Lee, D.G., 1984. Preparation and properties of quaternary ammonium and phosphonium permanganates. J. Org. Chem, 49: 4509-4516.

Lee, D. G. and Brownridge, J. R., 1973. The oxidation of cinnamic acid by permanganate ion. Spectrophotometric detection of an intermediate. Journal of American Chemical Society, 95: 3034-3035.

Mata-PJrez, F. and PJrez-Benito, J. F., 1985. Identification of the product from the reduction of permanganate ion by trimethylamine in aqueous phosphate buffers. Canadian Journal of Chemistry, 63:988-992.

Schnarr, M., Truax, C., Farquhar, G., Hood, E., Gonullu, T., and Stickney, B., 1998. Laboratory and controlled field experiments using potassium permanganate to remediate trichloroethylene and perchloroethylene DNAPLs in porous media. Journal of Contaminant Hydrology, 29:205-224.

Simandi, I. and Jaky, M., 1976. Nature of the detectable intermediate in the permanganate oxidation of trans-cinnamic acid. J. Am. Chem. Soc., 98: 1995-1997.

West, O. R., S. R. Cline, W. L. Holden, F. G. Gardner, B. M. Schlosser, J. E. Thate, D. A. Pickering, T. C. Houk, A full-scale demonstration of in situ chemical oxidation through recirculation at the X-701B site, Oak Ridge National Laboratory, Oak Ridge, TN, ORNL/TM-13556, 101 p., 1997.

Wiberg, K. B., Deutsch, C. J., and Rocek, J., 1973. Permanganate oxidation of crotonic acid. Spectrometric detection of an intermediate. Journal of American Chemical Society, 95: 3034-3035.

APPENDICES

Appendix 1. Manuscript of published article entitled “Oxidative degradation of chlorinated ethylenes by potassium permanganate” by Y. E. Yan and F. W. Schwartz.

Appendix 2. Manuscript of published article entitled “Kinetics and mechanisms for TCE oxidation by permanganate” by Y. E. Yan and F. W. Schwartz.

Appendix 3. Manuscript of published article entitled “Phase-transfer-catalyst applied to the oxidation of nonaqueous phase TCE by potassium permanganate” by Y. Seol and F. W. Schwartz.

Appendix 4. Manuscript of published article entitled “Oxidation of binary DNAPL mixtures using potassium permanganate with a phase transfer catalyst” by Y. Seol and F. W. Schwartz.

Appendix 5. Manuscript of published article entitled “Efficiency problems related to permanganate oxidation schemes” by X. D. Li and F. W. Schwartz.

Appendix 6. Manuscript of published article entitled “Simulating the in-situ oxidative treatment of chlorinated ethylenes by potassium permanganate” by H. Zhang and F. W. Schwartz.

Appendix 1. Manuscript of published article entitled:

OXIDATIVE DEGRADATION OF CHLORINATED ETHYLENES BY POTASSIUM PERMANGANATE

Y. Eugene Yan[1] and Frank W. Schwartz[2]
Department of Geological Sciences
The Ohio State University
Columbus, OH 43210

ABSTRACT

The oxidative treatment of chlorinated ethylenes in ground water using permanganate was investigated in a series of batch kinetic tests. Five chlorinated ethylenes including tetrachloroethylene (PCE), trichloroethylene (TCE), and three isomers of dichloroethylenes (DCEs) were examined. The degradation process was rapid with pseudo-first-order rate constants ranging from 4.5×10^{-5} to 0.03 s^{-1} at MnO_4^- =1 mM. The rate increased with a decreasing number of chlorine substituents on the ethylene. The higher reactivity of trans-DCE ($k_{obs}=30\times10^{-3}$ s^{-1} at MnO_4^-=1 mM) as compared to cis-DCE ($k_{obs}=0.9\times10^{-3}$ s^{-1} at MnO_4^-=1 mM) is thought to be caused by a significant steric effect due to the formation of a large cyclic activated complex. TCE oxidation as a second-order reaction was confirmed and the rate constant, $k=0.67\pm0.03$ M^{-1} s^{-1}, is independent of pH over the range of 4-8. The activity of both Cl^- and hydrogen ions was monitored over time and suggests essentially complete dechlorination, making the degradation products less harmful than the parent compounds. Competition for MnO_4^- from other organic compounds in ground water or highly contaminated ground water was also evaluated in experiments. A simple and quick approach was demonstrated to estimate permanganate consumption by other organic compounds for field applications and to predict the TCE degradation rate in a system involving multiple contaminants. The modeling results suggest that the effect of autocatalysis by MnO_2 on TCE degradation is significant when the system contains high concentration levels of MnO_4^- and TOC.

Keyword: chlorinated ethylenes, permanganate, oxidation, ground water, remediation.

[1] Corresponding author. Fax: 614-292-7688. E-mail: yan@geology.ohio-state.edu

[2] Fax: 614-292-7688. E-mail: frank@geology.ohio-state.edu

INTRODUCTION

Chemical approaches for the remediation of ground water contaminated by chlorinated solvents commonly utilize reduction or oxidation schemes to transform organic contaminants. To date, most work has concentrated on reductive dechlorination, which occurs with hydrolysis (Jeffers et al., 1989) and surface reactions involving pyrite, sulfide, biotite or vermiculite (Kriegman-King and Reinhard, 1992 and 1994) and zero-valent iron (Gillham and O'Hannesin, 1994; Matheson and Tratnyek, 1994). In particular, remedial schemes developed around zero-valent iron have shown considerable promise due to the relatively short half lives of the reactions.

There has been much less recent work on oxidation processes, even though experience has shown oxidative degradation to be fast with half lives of degradation for chlorinated organic compounds of the order of several minutes in a O_3/H_2O_2 system (Glaze and Kang, 1988). An apparent limitation with this reaction is that the key reactive intermediate hydroxyl radical, generated in this advanced oxidation process (AOP), strongly reacts with common inorganic species in ground water such as carbonate and bicarbonate (HoignJ and Bader, 1983).

Not all oxidants suffer from this limitation. Permanganate, as a metal-oxo reagent (Gardner and Mayer, 1995), does not apparently rely on generating a hydroxyl radical to oxidize halogenated ethylenes as AOPs do. Experience spanning more than a century in laboratory-scale organic synthesis indicates that metal-oxo reagents can attack a double carbon-carbon bond (Stewart, 1964) powerfully through direct oxygen transfer (Wiberg and Saegebarth, 1957). This feature of metal-oxo reagents facilitates the degradation of chlorinated ethylenes with little scavenging of carbonate or bicarbonate.

Both laboratory and field experiments have demonstrated the ability of potassium permanganate to oxidize common chlorinated ethylenes like trichloroethylene (TCE) and tetrachloroethylene (PCE). In a series of batch experiments with both water (Vella and Veronda, 1992) and soil (Gates et al., 1995), both TCE in water and TCE and PCE in soil were oxidized by permanganate. Compared to Fenton's reagent (a mixture of hydrogen peroxide and ferrous ion), permanganate was less dependent on pH and had a higher efficiency in water or soil treatment. Schnarr et al. (1998) observed in column tests that more than 90% of the TCE and PCE was degraded after flushing with several pore volumes of aqueous permanganate. Most of these experiments can be considered as a proof-of-concept that demonstrates the efficacy of the remedial concept with less emphasis on reaction pathways and kinetics.

Our investigations provide a detailed process-level understanding of the oxidative destruction of chlorinated ethylenes by permanganate. The specific objectives are (1) to examine reaction order, degradation rate and kinetic behavior of chlorinated ethylenes in reactions with permanganate, (2) to demonstrate the extent of dechlorination, and (3) to assess the effects of pH and other organic compounds in subsurface environment on the TCE degradation rate. Further work is underway to elucidate the detailed reaction pathways based on product analysis.

CHEMICAL BACKGROUND

There has been little direct process-oriented work on the oxidation of chlorinated ethylenes by permanganate. However, the body of work on alkene (C=C) oxidation in chemical synthesis provides a general understanding of the oxidation of chlorinated ethylenes. Figure 1 depicts a reaction scheme for the oxidation of ethylene in a neutral to weak acidic condition. The oxidation reaction begins with the formation of a cyclic hypomanganate ester (**1**) (Wiberg and

Saegebarth, 1957; Wiberg et al., 1973; Lee and Brownridge, 1973). The cyclic ester then undergoes oxidative decomposition in a neutral to weak acidic medium through hydrolysis, with fission of the Mn-O bonds to form a glycol aldehyde (Wiberg and Saegebarth, 1957). The glycol aldehyde could be further oxidized to glyoxylic acid and oxalic acid (**2**) (Arndt, 1981; Szammer and J<ky, 1992). Another possible reaction pathway has the ester directly cleaved by permanganate to form two formic acids (**3**) (Wiberg and Saegebarth, 1957). All the carboxylic products could be further oxidized to carbon dioxide under certain conditions (Stewart, 1965).

The kinetics and mechanism of the reaction are affected when halogens substitute for hydrogen on ethylene. Burdon and Tatlow (1958) observed a faster oxidation reaction (a few seconds) with fluorinated alkene, as compared to hydrocarbon alkene, using permanganate in acetone during the synthesis of carboxylic acids. They thought that an electron-withdrawing group such as fluorine on the alkene facilitates the nucleophilic attack by permanganate ions. Lee (1982) also pointed out that the oxidation of hydrocarbons could sometimes be facilitated by prior halogenation of the oxidation site. However, Freeman (1975) considered the permanganate ion as an electrophile in the reaction. In his overview of activated complexes in addition reactions, he suggested that the attack of permanganate ion on carbon double bond, as an electrophilic addition, resulted in the formation of a five-member cyclic activated complex in the transition state. A chlorine as an electron-withdrawing substituent induces a deficiency of electrons at the carbon double bond of the substituted ethylene. Based on the concept of electrophilicity, a decrease of electron availability at the carbon double bond should decrease the rate of the electrophilic addition reaction.

Although only a few studies are available on the oxidation of halogenated ethylenes, we postulatethe following reaction,

$$\alpha\ C_2Cl_nH_{4-n} + \beta\ MnO_4^- \rightarrow \gamma\ CA + \delta\ MnO_2 + \zeta\ Cl^- \quad (1)$$

where α, β, γ, δ, and ζ are stoichiometric coefficients, $C_2Cl_nH_{4-n}$ represents various chlorinated ethylenes, including PCE, TCE and dichloroethylenes (DCEs), and CA is a group of intermediate products. These intermediate products could be either chlorinated or hydrocarbon carboxylic acids, which might be further oxidized to carbon dioxide under certain conditions as follows,

$$\gamma\ CA \xrightarrow{MnO_4^-} \eta CO_2 \quad (2)$$

In oxidation by permanganate, pH is considered as a primary variable because it strongly influences the redox potential in a system. Table 1 lists the redox reactions, the corresponding potentials of various couples of manganese ions, andpH ranges in which each redox reaction predominates, based on Stewart's overview (1965) on oxidation by permanganate. Table 1 suggests that pH determines the number of electrons and couples of manganese ions involved in the over-all reaction. In general, the over-all redox potential of the system increases with decreasing pH. With organic substrates, however, mechanistic factors are of major importance, whereas the over-all free energy change of the oxidant, determined by its potential, is of minor importance. For the chlorinated ethylenes, a lack of knowledge about the reaction mechanism makes it unclear whether pH will affect the degradation rates of chlorinated ethylenes.

MATERIALS AND METHODS

Materials

The chlorinated ethylenes, PCE (C_2Cl_4, 99+%), TCE (C_2HCl_3, 99.5+%), cis-DCE ($C_2H_2Cl_2$ 97%), trans-DCE ($C_2H_2Cl_2$ 97%), and 1, 1-DCE ($C_2H_2Cl_2$, 99%) were obtained from

Aldrich Chemical Co.(Milwaukee, WI) and used as received. A high purity pentane of GC grade (Burdick & Jackson) from Baxter Diagnostics Inc. (McGaw Park, IL) was used as a liquid-liquid extraction solvent for analysis of chlorinated ethylenes. Potassium permanganate stock solution of 1-10 mg/mL was prepared by dissolving $KMnO_4$ crystals in Milli-Q water or phosphate-buffered Milli-Q water. The stock solution was stored in brown glass bottles and used freshly. The reducing agents, thiosulfate and hydrazine hydrate (95+%), are both research grade and were prepared as a stock solution (6 mg/mL) for quenching the reaction in some kinetic experiments. A total organic carbon (TOC) stock solution (1000 mg C/L) for use in the TOC analysis was prepared by dissolving 0.2125 g of dried, reagent grade potassium hydrogen phthalate in 100 mL of Milli-Q water.

Experiments were performed using solutions prepared by dissolving the various chlorinated ethylenes in Milli-Q water (Millipore Corp., Bedford, MA), phosphate-buffered Milli-Q water, ground water, and contaminated ground water, respectively. Contaminated ground water was synthesized as a mixture of ground water and landfill leachate at various ratios. Ground water was collected from the uppermost perched aquifer below the CECOS/BFI landfill site in Cincinnati, Ohio, and landfill leachate was obtained from the same site. These waters were filtered by 0.2 μm filters to provide a homogeneous reaction solution but were not acidified. Apparently, most of metals in solution were oxidized when they were exposed to the atmosphere. For example, no ferrous iron was detected by phenanthroline colorimetric method. Thus, the effect of metal on oxidation of TCE by permanganate was not evaluated in this investigation.

Kinetic Experiments

Most of kinetic experiments were conducted in a sealed and water-jacketed spherical glass reaction vessel (Figure 2) where a zero headspace was maintained at all times. To test impact of subsurface environment on the reaction, experiment conditions were adjusted with pH ranging from four to eight. One experiment was run without a pH buffer to monitor the change in acidity of the solution. Other experiments were run with aqueous solutions prepared from phosphate-buffered Milli-Q water, ground water or contaminated ground water, and with initial concentrations of TCE ranging from two mg/L (1.52×10^{-5} M) to 10 mg/L (7.61×10^{-5} M). The test solution of contaminated ground water was a mixture of ground water with 2% or 20 % landfill leachate.

The rate at which the chlorinated-ethylene is degraded can be simply measured when the other reactant, permanganate, is held essentially constant through experiment. To maintain a constant concentration of $KMnO_4$, a more than ten-fold excess concentration of $KMnO_4$ was employed in each experiment. The activity of Cl^-, pH, temperature and the concentration of chlorinated ethylenes were monitored with time.

In addition to the above experiments, a set of experiments was designed to examine the consumption rate of $KMnO_4$ by organic compounds other than the chlorinated ethylenes. The organic compounds in ground water and contaminated ground water were characterized by TOC. In this set of experiments, $KMnO_4$ (20 mg/L) was isolated by using solutions containing various percentages of landfill leachate with excess concentration of TOC varying from 302 to 506 mg/L. The concentration of $KMnO_4$ was monitored through the experiment.

Chemical Analyses

(a) Analysis of chlorinated ethylenes. A sample ranging from 20-:L to 2-mL was collected at a fixed time interval from the reaction vessel using a syringe. The sample was diluted as necessary with Milli-Q water in 10-mL to 1-L volumetric glass flasks, depending on the concentration of the chlorinated ethylenes. A 10-mL sample after dilution was transferred to an extraction vial containing 4 mL of pentane. The vial was shaken for one minute and then equilibrated for 10 minutes. The extractant was analyzed for the particular chlorinated ethylene using a Fisons Instruments 8060 gas chromatograph equipped with a Ni^{63} electron capture detector and a DB-5 capillary column (J&W Scientific, Rancho Cordova, CA), 30 m H 0.32 mm I.D, with a film thickness of 1.0 µm. Helium was used as the carrier gas and nitrogen as the make-up gas. The gas chromatograph was calibrated daily with a minimum four calibration standards, and duplicate measurements were made for each sample or standard. If the standard deviation of measurements was greater than 10 %, another measurement would be made.

(b) Analysis of $KMnO_4$ and its product. A 1.5-mL sample was collected and transferred into a quartz cuvette with 1 cm pathline and analyzed using a Varian Cary 1 UV-visible spectrophotometer at wavelengths ranging from 400 to 700 nm. In this range of wavelength, permanganate (MnO_4^-) and hypomanganate (MnO_4^{3-}) ions have a maximum of absorbance at 525/546 nm and 667 nm, respectively, while manganate (MnO_4^{2-}) has two absorbance peaks at 439 and 606 nm (Stewart, 1965). These species are almost transparent to radiation at 418 nm. The absorbance at 418 nm is a measure of either a cyclic hypomanganate ester (Wiberg et al., 1973; Lee and Brownridge, 1973) or a soluble form of colloidal MnO_2 (Sim<ndi and J<ky, 1976; Mata-PJrez and PJrez-Benito, 1985). These interpretations have been controversial for a long time.

(c) Measurement of Cl⁻. Initially, the activity of Cl⁻ in the reaction vessel was measured using an Orion ion selective electrode (ISE) with a glass body (Model 9617). The ISE was calibrated using a standard solution of NaCl in the range from 0.1 to 10^{-5} M. Because of low sensitivity of the ISE to the trace amount of Cl⁻, ranging from 10^{-4} - 10^{-5} M, additional samples were measured by a Buchler Digital Chloridometer, using a coulometric titration of chloride ions (Cotlove, 1958). Before the titration, a 0.1-mL aliquot of reducing reagent stock solution (6 mg/mL), hydrazine hydrate, was added to a 0.9-mL sample taken from the reaction vessel to quench the reaction in the sample solution. To prepare for the titration, the total 1-mL sample aliquot was added to a test vial containing 3-mL of an acid reagent comprised of 0.4 N HNO_3 and 40% glacial acetic acid. Finally, four drops of gelatin reagent were added to the test vial. The samples in the test vials were titrated at either the LOW or HIGH switch position in order to provide the proper concentration range from 3.3×10^{-3} to 33.3 mM.

(d) TOC analysis. TOC was analyzed using a Shimadzu TOC-5000 TOC Analyzer. The four standards for calibration were prepared by diluting the TOC stock solution to a concentration in the range of 10 - 60 mg C/L. All standards and samples were acidified with concentrated HCl and sparged with CO_2 free air. Samples of contaminated ground water and landfill leachate with high TOC concentration were diluted as needed in order for concentrations to fall within the calibrated range of the TOC analyzer. Standards and samples were analyzed in triplicate and the values of TOC were accepted when the standard deviation was less than 2%.

RESULTS AND DISCUSSIONS

Reaction Order

Based on the Eq. 1, the degradation of chlorinated ethylenes can be described with the following general rate equation

$$r = -\frac{1}{a}\frac{d[C_2Cl_nH_{4-n}]}{dt} = k[C_2Cl_nH_{4-n}]^a[MnO_4^-]^b \quad (3)$$

When the concentration of $[MnO_4^-]$ is in excess, Eq. 3 can be simplified as Eqs. 4 and 5.

$$r = k_{obs}[C_2Cl_nH_{4-n}]^a \quad (4)$$

$$k_{obs} = k[MnO_4^-]^b \quad (5)$$

where r is a reaction rate, k is a rate constant, and k_{obs} is a pseudo-order rate constant because $[MnO_4^-]$ is effectively constant during the course of the experiment. By varying the values of $[C_2Cl_nH_{4-n}]$ and measuring reaction rate, the order α with respect to $[C_2Cl_nH_{4-n}]$ can be simply determined by a log-log form of Eq. 4:

$$\log r = \log k_{obs} + a \log [C_2Cl_nH_{4-n}] \quad (6)$$

In a similar way but varying initial concentration of $[MnO_4^-]_0$ and measuring k_{obs}, the order β with respect to $[MnO_4^-]$ can be obtained by a log-log form of Eq. 5:

$$\log k_{obs} = \log k + b \log [MnO_4^-]_0 \quad (7)$$

To avoid complications from subsequent reactions or catalysis, an initial rate method (Casado et al.1986) was used here and Eq. 6 can be expressed as:

$$\log r_0 = \log k_{obs} + a \log [C_2Cl_nH_{4-n}]_0 \quad (8)$$

The two sets of kinetic experiments were designed to estimate α and β values for TCE oxidation. The first set of eight experiments was conducted with initial TCE concentrations varying from 0.031 to 0.083 mM. The initial permanganate concentration was fixed at 1 mM for all experiments. The initial reaction rates were estimated as the tangent to the TCE concentration-time curve. As shown in Figure 3, the slope $\alpha = 1.01 \pm 0.02$ was calculated (based on Eq. 8) through a linear regression of the logarithm of initial rates versus the logarithm of initial TCE concentration (r^2=0.998). The reaction order with respect to TCE is unity and k_{obs} is a pseudo-first-order rate constant.

In the second set of five duplicate experiments, the initial concentration of TCE was fixed at 0.078 mM and TCE was reacted with excess MnO_4^- ranging from 0.37 to 1.2 mM. The pseudo-first-order rate constant k_{obs} for each experiment was obtained based on an integrated form of equation 4 at $\alpha = 1$. Thus, a slope of $\beta = 1.05 \pm 0.03$ was determined from a plot of the logarithm of k_{obs} versus the logarithm of MnO_4^- at initial concentration (Figure 4). The reaction order with respect to MnO_4^- is also unity.

Hence, the results from both Figures 3 and 4 demonstrate that the initial reaction between TCE and MnO_4^- is a second-order reaction with α=1 and β=1. The second-order rate constant k of $0.66 \pm 0.01 M^{-1}s^{-1}$ can be estimated as shown in Figure 4.

Degradation of chlorinated ethylenes

Five chlorinated ethylenes were investigated through kinetic experiments using 1 mM MnO_4^-. As before, to maintain MnO_4^- in excess, the concentration of chlorinated ethylenes was at least 10 times less than MnO_4^-. Figure 5 depicts the degradation behavior of the chlorinated

ethylenes. Apparently, the disappearance of chlorinated ethylenes can be simply characterized by a pseudo-first-order model. The pseudo-first-order rate constants were calculated from the results in Figure 5. Values range from 0.45 to 300×10^{-4} s^{-1} and are listed in Table 2. The degradation is rapid for most of compounds with half lives generally less than 20 minutes. PCE is the exception with a half life of 257 minutes or about four hours.

Figure 5 illustrates that the degradation rate is inversely proportional to the number of chlorines as substituents on ethylenes. The fact that chlorine as a substituent slows down the reaction is consistent with the idea of electrophilic addition proposed by Freeman (1975). The high deficiency of electrons in the carbon double bond, induced by four chlorine substituents in PCE, reduces the rate of electrophilic attack. Therefore, PCE degradation is slow and its rate constant is small compared to the others.

Trans isomers are generally more stable than the corresponding cis isomers in alkenes. However, Figure 5 shows a higher reactivity of trans-DCE as compared to the degradation rate for cis-DCE. The ratio of k_{cis} to k_{trans} is only 0.03. It indicates that a significant steric effect was evident in the reaction. The steric interaction of cis substituents is caused by the change in bond angles in the addition reaction involving the large cyclic activated complexes, such as five- and six-membered cyclic complexes (Freeman, 1975). Apparently, a significant steric effect involving cis-DCE is consistent with the formation of the five-membered cyclic hypomanganate ester, which was originally proposed by Wagner (1895) and later supported by Wiberg and Saegebarth's (1957) experimental data.

Dechlorination

The oxidation of chlorinated ethylenes likely starts with a MnO_4^- attack on the C=C double bond to form a cyclic complex, similar to the oxidation of ethylenes. However, it is unclear whether dechlorination proceeds by hydrolysis or further oxidation during the decomposition of the cyclic complex. If chlorines remain in intermediate products after the cleavage of C=C bond, the most likely compounds would be chlorinated organic acids such as formyl chloride, oxalyl chloride and phosgene. Otherwise, all chloride ions would be released to the solution.

It is known that most of chlorinated organic compounds are much more toxic than the corresponding hydrocarbon compounds due to the existence of chlorine substituents. In treating chlorinated ethylenes, the ideal by-products and final products in the reaction are carboxylic acids and CO_2 without any chlorine substituent. To evaluate the extent of dechlorination of chlorinated ethylenes in more detail, the degradation of TCE was examined by monitoring Cl^- ions through a kinetic experiment. Stoichiometry indicates that the dechlorination of 1 M TCE (C_2HCl_3) releases 3 M Cl^- ions, or

$$C_2HCl_3 \rightarrow \gamma CA + 3Cl^- \qquad (9)$$

where CA is a group of carboxylic acids without chlorine substituents and γ is a group of stoichiometric coefficients, γ_1, γ_2, ……, γ_n, for n potential carboxylic acids, respectively. When excess MnO_4^- is used for the oxidation of TCE, the degradation of TCE and the formation of chloride ions can be described by

$$\frac{[C_2HCl_3]}{[C_2HCl_3]_0} = e^{-k_{obs}t} \quad (a) \qquad \frac{[Cl^-]}{3[C_2HCl_3]_0} = 1 - e^{-k_{obs}t} \quad (b) \qquad (10)$$

where k_{obs} is the pseudo-first-order rate constant confirmed previously.

A kinetic experiment was conducted using 0.06 mM TCE with more than 15 fold excess of MnO_4^- (1 mM). The measurement of chloride concentration in the experiment was triplicated

and the standard deviation is shown by error bars in Figure 6. About three times the concentration of Cl^- ions as compared to transformed TCE was observed over time (Figure 6). As shown in Figure 6, the total chlorine mass is accounted as both chlorine substituents in untransformed TCE and chlorides liberated from transformed TCE. This result indicates that the amount of chlorine substituents remaining in intermediate products is negligible.

The pseudo-first-order rate constant $k_{obs}=7.0\pm0.5\times10^{-4}$ s^{-1} was obtained from a best fit to the data points of TCE concentrations using Eq. 10(a). Based on a k_{obs} of 7.0×10^{-4} s^{-1}, both the degradation of TCE and the formation of Cl^- with time, as predicted from Eq. 10 (see lines in Figure 6), coincided very well with the observations. The kinetic results from this experiment suggest that the complete dechlorination be achieved rapidly during the decomposition of the cyclic complex after TCE is transformed.

Change in Acidity and pH dependence

The formation of carboxylic acids has been proposed to accompany the rapid decomposition of the cyclic complex. To examine the change in acidity of the solution due to the production of carboxylic acids, an experiment with a high concentration of TCE (0.76 mM) reacting with 3.8 mM MnO_4^- was conducted without the pH buffer. A drop in pH to 2-3 was observed within several minutes. Stewart (1965) pointed out that pH of the solution would be close to the pK of an acid produced in the reaction using permanganate. The carboxylic acids that likely formed would be oxalic acids, formic acids and so on. Oxalic acid has a $pK_1=1.23$ and a $pK_2=4.19$, and formic acid has a pK=3.75. A more detailed analysis of these carboxylic acids is now underway.

The effect of pH on the TCE degradation rate was studied over the pH range of 4-8 at constant concentration of MnO_4^- (1 mM). The pseudo-first-order rate constants (k_{obs}) obtained from four duplicate experiments are within $0.63\text{-}0.69\times10^{-3}$ s^{-1} with standard deviation up to $\pm 0.04\times10^{-3}$ s^{-1}. Apparently, they do not show strong pH dependence in the pH range 4-8. A TCE degradation rate, independent of pH, is in agreement with the suggestion that neither hydrogen nor hydroxyl ions significantly facilitate the attack by permanganate on C=C in TCE in an initial transformation step, where a cyclic complex forms. It is possible that pH affects the reaction afterwards. In a later step, when hydrolysis and further oxidation proceed, it is well known that the decomposition of the complex is highly pH dependent and that both permanganate and hydroxyl ions compete for reaction with a common cyclic intermediate (Wiberg and Saegebarth, 1957). A typical example is diol formation in a basic solution and ketol formation in a neutral solution.

To obtain the TCE disappearance rate over the pH range 4-8, $\log [TCE]/[TCE]_0$ is plotted versus time for all data points from eight kinetic experiments at four pH levels with 1 mM MnO_4^- (Figure 7). A linear regression with a determination coefficient of 0.988 gives a rate constant $k_{obs}=0.67\pm0.03\times10^{-3}$ s^{-1}. A second-order rate constant, thus, can be simply estimated as $k=0.67\pm0.03$ M^{-1} s^{-1} by dividing 1 mM MnO_4^-. TCE degradation by permanganate is rapid with a half life about 17 minutes.

Permanganate Decomposition and Products

Figure 9 shows the spectra of the reacting solution over time. The absorbance at both 525 and 546 nm at the beginning of the reaction (see a solid bold line in Figure 8) is representative of the initial concentration of MnO_4^- (0.23 mM). The reduction in absorbance

with time in a first-order fashion indicates a decreasing concentration of MnO_4^-. A slight decrease in absorbances at 606 and 667 nm suggests that MnO_4^{2-} and MnO_4^{3-} apparently do not form as reaction products. At a wavelength 418 nm, the spectrum of the initial solution has the lowest absorbance and MnO_4^- is almost transparent to the source light. The increase of absorbance at 418 nm with time indicates the formation of a decomposition product of MnO_4^-. Based on independent observations when crotonic and cinnamic acid were oxidized by MnO_4^-, respectively, both Wiberg et al. (1973) and Lee and Brownridge (1973) interpreted a similar spectrum (a dashed line in Figure 8) as indicative of cyclic hypomanganate ester. However, Sim<ndi and J<ky (1976) and Freeman et al. (1981) using an iodometric technique believed that it was a manganate (IV) with the +4 oxidation state.

In our spectrophotometric examination, all final spectra representing a decomposition product of MnO_4^- in TCE oxidation show a linear relationship between the logarithm of the absorbance and the logarithm of the wavelength. A typical plot of log A versus log λ has been reproduced in Figure 9. The linear relationship with the slope of -4.22±0.05 appears to be a reflection of Rayleigh's law, which can be written as in Eq. 11,

$$A = \frac{C}{\lambda^4} \quad (a) \qquad \log A = \log C - 4 \log \lambda \quad (b) \tag{11}$$

where A is the absorbance, λ the wavelength, and C a constant depending on the polarizability, cell path length, mass and concentration of the colloidal particles. As a consequence of Rayleigh's law, the lost energy is due to light scattering by a product present in the form of colloidal particles. Figure 9, thus, confirms the suggestion that the product is actually soluble colloidal manganese dioxide.

Permanganate Consumption in Contaminated Ground Water

Permanganate is a powerful and reactive oxidant that would likely oxidize other organic compounds existing in ground water or contaminated ground water. The presence of these compounds would reduce the rate of TCE oxidation because of competition for the permanganate. To compare TCE loss rate in various solutions containing different quantities of other compounds, experiments were designed using 2 mg/L (0.015mM) TCE reacting with 20 mg/L (0.13 mM) MnO_4^- in the Milli-Q water, ground water (TOC < 2 mg/L), and contaminated ground water (TOC = 10 mg/L), respectively. The contaminated ground water was synthesized by mixing ground water with 2% landfill leachate. Figure 10 depicts the reduction of TCE degradation rate due to the consumption of permanganate by other compounds in the solution. Based on the ratio of second-order rate constant in ground water (k_{GW}=0.61 M^{-1} s^{-1}) to that in Milli-Q water (k_{MQ}=0.68 M^{-1} s^{-1}), the TCE degradation rate in ground water was slightly decreased by 10%, compared to that in Milli-Q water. In the ground water contaminated by 2% landfill leachate, the second-order rate constant (k_{CGW}) is 0.44 M^{-1} s^{-1}. The rate was reduced to 65 % of that observed in Milli-Q water.

Although chlorinated ethylenes are the most frequently detected ground-water contaminants at hazardous waste sites, they are often found with other organic compounds. Accounting for the effects of competition in multi-contaminant solutions is complicated by the fact that many different organic compounds could be involved and many of which may not be identifiable. As a first-step in dealing with the issue of complex aqueous solutions, we provide results of several experiments involving ground water and contaminated ground water, where the

relative abundance of these other organic compounds is represented by total organic carbon (TOC).

Clearly, using TOC to represent other reactive compounds assumes that all compounds present in solution would react with permanganate, which is able to oxidize most organic contaminants characterized by carbon-carbon double bonds (e.g. most alcohol, ketones, organic acids, phenolic compounds, and humic substances). Apparently, the competition of TOC for permanganate varies from site to site. However, the simplified kinetic-reaction model, which accounts for the general effect of other organic compounds in the reaction, would be a quick approach to evaluate the site-specific consumption of permanganate by TOC for a field application.

Here, we describe a simple and quick evaluation method for estimating site-specific consumption of permanganate and for predicting TCE degradation in a multi-organic compounds system. The approach is based on a series of experiments in an aqueous reaction system contaminated by landfill leachate from a sanitary landfill at age less than 10 years. The majority of organic compounds in this type of leachate is short chain volatile fatty acids (Lu et al., 1985) and level of TOC mainly reflects the quantity of short chain organic acids present in the system.

Experiments were designed using 20 mg/L (0.13 mM) MnO_4^- reacting with excess TOC prepared from landfill leachate at five different concentrations from 302 to 506 mg/L. MnO_4^-, as a monitoring species, was measured over time. The MnO_4^- disappearance rate is the greatest at the beginning of the 30-minute reaction period. A simple pseudo-first-order kinetic equation fits the initial 6 data points well during the first 10% of reaction time in a plot of logarithm of MnO_4^- versus time, which provides a slope indicating a maximum rate constant for permanganate decomposition.. Figure 11 is a plot of the derived decomposition rate constant against TOC concentration. The rate constant (k_{obs}) depends almost linearly on TOC concentration. The over-all kinetic behavior of TOC reacting with MnO_4^- for this specific site is close to second-order. It indicates that the majority of organic compounds represented by TOC at this site react with MnO_4^- in second-order kinetics, which is reasonable for most reactions involving short chain organic acids based on previous studies in organic chemistry (Aendt, 1981 and Freeman, 1975). To simplify the evaluation of MnO_4^- decomposition by TOC, a second order kinetic equation was used and the second order rate constant $k_{TOC\text{-}MnVII} = 3.40\times10^{-6}$ L/mg s^{-1} was obtained from the slope of a linear fitting line in Figure 11. Assuming that a single compound is utilizing MnO_4^- at the same reaction rate as all reacting organic compounds, reflected by TOC, the effective molecular weight of the compound will be equivalent to a composite molecular weight for all reacting compounds. This assumption provides a a way of assessing the general impact on MnO_4^- utilization and of estimating an effective consumption rate of MnO_4^- by a broad spectrum of organic compounds. In this case, if the composite weight is between 50 and 300 g , the maximum rate constant for MnO_4^- decomposition by TOC is in the range from 0.17 to1.02 M^{-1} s^{-1}.. This rate constant is similar to that observed for TCE.

To predict the TCE degradation in the system involving TOC, TCE and MnO_4^-, the rate equations are simplified based on the over-all kinetic behavior of TOC in the contaminated ground water we tested,

$$\frac{d[TCE]}{dt} = -k_{TCE-MnVII}[TCE][MnO_4^-], \qquad [TCE](t=0) = [TCE]_0$$

$$\frac{d[TOC]}{dt} = -k_{TOC-MnVII}[TOC][MnO_4^-], \qquad [TOC](t=0) = [TOC]_0 \qquad (12)$$

$$\frac{d[MnO_4^-]}{dt} = -(k_{TCE-MnVII}[TCE] + k_{TOC-MnVII}[TOC])[MnO_4^-], \quad [MnO_4^-](t=0) = [MnO_4^-]_0$$

The equations can be generalized as follows

$$\frac{dy_i}{dt} = f_i(t, y_1, y_2, y_3), \qquad y_i(t=0) = y_{i0}, \qquad i = 1, 2, \text{ and } 3. \qquad (13)$$

where y_1, y_2, and y_3 represent TCE, TOC and MnO_4^-, respectively. Second order rate constants derived from previous experiments were used ($k_{TCE\text{-}MnVII} = 0.67\ M^{-1}s^{-1}$ and $k_{TOC\text{-}MnVII} = 3.40\times10^{-6}$ L/mg s^{-1}). Equation 13 was solved numerically using the Runge-Kutta method with adaptive step-size control. In this case, the molar concentration of TOC is unknown without a composite molecular weight for TOC. However, it can be find from experimental data by solving an inverse problem.

Three experiments were conducted in a highly contaminated ground water containing 101 mg/L TOC. TCE at a fixed initial concentration of 2 mg/L reacted with three different concentrations of MnO_4^- (20, 80, and 120 mg/L). The data points in Figure 12 illustrate the TCE degradation at various concentrations of MnO_4^-. To model the experimental data using Eq. 13, an initial composite weight of 50 g was assigned to compute TCE degradation with time and the residual between predicted TCE and observed TCE. The automatic adjustment of the composite weight with a fixed step was made until a minimum residual was calculated. A composite molecular weight, 176 g, for TOC was obtained based on the first experimental data (20 mg/L MnO_4^-). The simulated results with a composite weight of 176 g match the observed rate of TCE degradation very well. In the second experiment, where 80 mg/L MnO_4^- was used, the simulated TCE-time curve is consistent with that observed in the first hour but deviates at later time. The same behavior was evident in the third experiment in which a relatively high concentration of MnO_4^- (120 mg/L) was used. However, the later-time deviation in the third experiment is much larger than that in the second. The observed TCE loss with time in the third experiment is close to the calculated result for Milli-Q water without TOC (the dashed line in Figure 12). Apparently, reduction in the TCE degradation rate due to the presence of other organic compounds was much less than expected with a high concentration of MnO_4^- .These results do not necessarily imply that some of the MnO_4^- was not being used in competing reactions with TOC. We believe that there was an actual increase in the TCE degradation rate. In effect, the increase in TCE degradation rate masked the effect of competition with TOC. The increased TCE loss rate could be caused by the large amount of colloidal MnO_2 produced in the reaction with the high concentrations of TOC and MnO_4^-. In the third experiment, the calculations indicate that 91 mg/L (0.58 mM) MnO_4^- was lost and converted to MnO_2. Meanwhile, 2.15 mg/L (0.016 mM) TCE and 99 mg/L of the other organic compounds represented by TOC were transformed. The MnO_2 has been reported to catalyze reactions between MnO_4^- and many organic compounds (PJrez-Benito et al., 1987; PJrez-Benito and Arias, 1991).

The approach used in this study provides a way for estimating site-specific permanganate consumption by other organic compounds in field applications. This same procedure can be

extended to evaluate permanganate removal by organic matter, mainly humic and fulvic acids, after being transportedaway from the treatment zone. To predict the TCE degradation rate in the system involving multiple matrixes, the rate constant $k_{TOC\text{-}MnVII}$ in equation 12 can be expanded to a sum of rate constants of permanganate utilization by TOC from various matrixes. In a system with high concentrations of MnO_4^- and TOC, an additional component need to be added into the modeling to account for the autocatalysis of MnO_2. A further study is now underway to examine autocatalysis of MnO_2 on TCE degradation rates.

CONCLUSIONS

This study shows that chlorinated ethylenes can be rapidly degraded by permanganate in aqueous solution. The half lives of TCE, cis-1,2-DCE, trans-1,2-DCE and 1,1-DCE with 1 mM MnO_4^- range from 0.4-18 minutes. The half life of PCE, however, is much longer, about four hours. In PCE degradation, the attack of permanganate ion, as an electrophile, is slowed by the deficiency of electrons in the carbon-carbon double bond induced by four chlorines in PCE. The ratio of k_{cis} to k_{trans} (0.03) represents a much higher reactivity of trans-DCE than that of cis-DCE. The significant steric effect of cis substituents on reaction rate supports the postulate that a five-membered cyclic complex is formed during the transition state and leads to an intermediate product, the cyclic hypomanganate ester.

Extensive kinetic studies of TCE oxidation by permanganate suggest that TCE degradation is a second-order reaction. The reaction can be reasonably described through major known reactants and products:

$$C_2HCl_3 + MnO_4^- \xrightarrow{k_1} I \xrightarrow{k_2} \gamma CA + MnO_2 + 3Cl^- \qquad (14)$$

where I is a cyclic complex, CA is carboxylic acids, and γ is their stoichiometric coefficients. In the first reaction step, the permanganate attack, as an electrophilic addition, on the C=C bond in TCE, leads to the formation of a cyclic complex. k_1 at this step is a second-order rate constant. The fact that the rate constant k_1 is independent of pH over the range 4-8 indicates that this attack is not affected by either hydrogen or hydroxyl ions. In the second step, however, the decomposition of I may involve hydrogen or hydroxyl ions as suggested by numerous studies on the oxidation of other organic compounds by permanganate in chemical synthesis. The reaction in the second step proceeds rapidly and k_2 is an unknown-order rate constant. A dechlorination of the complex (I) over time was observed in the kinetic experiments. The results show that Cl^- ions are completely liberated from I immediately after its formation. Because the rate constant k_2 is much greater than k_1, the liberation of Cl^- ions in the kinetic experiment is in excellent agreement with the calculation based on a second-order reaction model using k_1. Therefore, the reaction rate in Eq. 14 can be approximated by the rate-limiting step (the first step) using the second-order rate constant k_1. Over the pH range 4-8, a k_1 value of 0.67 ± 0.03 M^{-1} s^{-1} at 21^o C was calculated based on eight experiments.

The essentially complete dechlorination and possible formation of organic acids suggest that the degradation products of chlorinated ethylenes are much less harmful than parent compounds and miscible with water. In an in situ scheme-based permanganate flushing, those products would be readily removed from ground water as flushing proceeds. Research is continuing to identify the carboxylic acids and to elucidate the pathways of formation and further oxidation of acids.

In TCE oxidation, spectrophotometric evidence shows that permanganate is reduced to form soluble colloidal manganese dioxide. The consumption of permanganate in ground water with

low TOC is limited. Ground water contaminated by landfill leachates, however, will consume permanganate depending on the TOC level. A simple and quick approach was used to estimate permanganate consumption by TOC. TCE degradation in a system involving TCE, TOC, and MnO_4^- was modeled with a system of ordinary deferential equations (Eq. 13) and solved using the Runge-Kutta method. The simulated results are consistent with the observations at early time but deviate from those at later time, especially in the experiment with a relatively high concentration of permanganate. A greater TCE degradation rate than expected at later time might be caused by autocatalysis on the surface of colloidal MnO_2 produced in the reaction. Competition of TOC for permanganate would be offset by the presence of a large quantity of MnO_2, which promotes the reaction between TCE and permanganate.

ACKNOWLEDGMENTS

We thank Dr. Y. P. Chin for use of his laboratory in conducting several of these experiments, and Dr. S. Traina for discussion and helpful suggestions over the course of the study. This material is based upon work supported by BFI/CECOS and the Department of Energy under Grant No. DE-FG07-96ER14735.

REFERENCES

Arndt, D., 1981. Manganese compounds as oxidizing agents in organic chemistry. Open Court Publishing Company, La Salle, Illinois.

Burdon, J. and Tatlow, J. C., 1958. The reactions of highly fluorinated organic compounds. X. The oxidation of fluoro-olefins by potassium permanganate in acetone. Journal of Applied Chemistry, 8:293-296.

Casado, J., Lopez-Quintela, M. A. and Lorenzo-Barral, F. M., 1986. The initial rate method in chemical kinetics. Journal of Chemical Education, 63:450-452.

Cotlove, E., 1958. An instrument and method for automatic, rapid, accurate and sensitive titration of chloride in biologic samples. Journal of Laboratory and Clinical Medicine, 51:461-468.

Gardner, K. A. and Mayer, J. M., 1995. Understanding C-H bond oxidations: H• and H⁻ transfer in the oxidation of toluene by permanganate. Science, 269:1849-1851.

Gates, D. D, Siegrist, R. L. and Cline, S. R., 1995. Chemical oxidation of volatile and semivolatile organic compounds in soil. Proceedings of 88th annual meeting and exhibition, San Antonio, Texas.

Gillham, R. W. and O'Hannesin, S. F., 1994. Enhanced degradation of halogenated aliphatics by zero-valent iron. Ground Water, 32:958-967.

Glaze, W. H. and Kang, J. K., 1988. Advanced oxidation processes for treating groundwater contaminated with TCE and PCE: laboratory studies. Journal AWWA, 80:57-63.

HoignJ, J. and Bader, H., 1983. Rate constants of reaction of ozone with organic and inorganic compounds in water, I. Non-dissociating organic compounds. Water Research, 17:173-183.

Jeffers, P. M., Woytowitch, L. M., and Wolfe, N. L., 1989. Homogeneous hydrolysis rate constants for selected chlorinated methanes, ethanes and propanes. Environmental Science and Technology, 23:965-969.

Freeman, F., 1975. Possible criteria for distinguishing between cyclic and acyclic activated complexes and among cyclic activated complexes in addition reactions. Chemical

reviews, 75:439-491.
Freeman, F., Fuselier, C.O., Armstead, C.R., Dalton, C.E., Davidson, P.A., Karchefski, E.M., krochman, D.E., Johnson, M.N., and Jones, N.K., 1981. Permanganate ion oxidation. 13. Soluble manganese (IV) species in the oxidation of 2,4(1H,3H)-pyrimidinediones (Uracils). Journal of American Chemical Society, 103:1154-1159.
Kriegman-King, M. R. and Reinhard, M., 1992. Transformation of carbon tetrachloride in the presence of sulfide, biotite, and vermiculite. Environmental Science and Technology, 26:2198-2206.
Kriegman-King, M. R. and Reinhard, M., 1994. Transformation of carbon tetrachloride by pyrite in aqueous solution. Environmental Science and Technology, 28:692-700.
Lee, D. G. and Brownridge, J. R., 1973. The oxidation of cinnamic acid by permanganate ion. Spectrophotometric detection of an intermediate. Journal of American Chemical Society, 95: 3034-3035.
Lee, D. G., 1982. Phase transfer assisted permanganate oxidations. In Oxidation in organic chemistry, W. S. Trahanovsky, ed., Academic Press, New York, Part D, Charpter 2, pp 147-206.
Lu, J. C. S., Eichenberger, B., and Stearns, R. J., 1985. Leachate from municipal landfills: production and management. Noyes Publications, Park Ridge, New Jersey, pp 108-187.
Mata-PJrez, F. and PJrez-Benito, J. F., 1985. Identification of the product from the reduction of permanganate ion by trimethylamine in aqueous phosphate buffers. Canadian Journal of Chemistry, 63:988-992.
Matheson, L. J., and Tratnyek, P. G., 1994. Reductive dehalogenation of chlorinated methanes by iron metal. Environmental Science and Technology, 28:2045-2053.
PJrez-Benito, J. F., Mata-PJrez, F., and Brillas, E., 1987. Permanganate oxidation of glycine: kinetics, catalytic effect, and mechanisms. Canadian Journal of Chemistry, 65:2329-2337.
PJrez-Benito J. F. and Arias, C., 1991. A kinetic study of the permanganate oxidation of triethylamine. Catalysis by soluble colloids. International Journal of Chemical Kinetics, 23:717-732.
Schnarr, M., Truax, C., Farquhar, G., Hood, E., Gonullu, T., and Stickney, B., 1998. Laboratory and controlled field experiments using potassium permanganate to remediate trichloroethylene and perchloroethylene DNAPLs in porous media. Journal of Contaminant Hydrology, 29:205-224.
Sim<ndi, L. I. and J<ky, M., 1976. Nature of the detectable intermediate in the permanganate oxidation of trans-cinnamic acid. Journal of American Chemical Society, 98: 1995-1997.
Stewart, R., 1964. Oxidation mechanisms. Benjamin, New York, pp 58-76.
Stewart, R., 1965. Oxidation by permanganate. In Oxidation in organic chemistry, Wiberg, K. B.,ed., Academic Press, New York, Part A, Charpter 1, pp 1-68.
Szammer, J and J<ky, M., 1992. Oxidation by permanganate in strong alkaline medium. Oxidation of ethane-1,2-diol, glycol aldehyde, glycollic acid, and glyoxylic acid. International Journal of chemical kinetics, 24:145-154.
Vella, P. A. and Veronda, B., 1992. Oxidation of trichloroethylene: comparison of potassium permanganate and Fenton's reagent. In Chemical oxidation technologies for the nineties, Eckenfelder, W. W., ed., Technomic publishing, Lancaster, Basel.
Wagner, G., 1895. History of oxidation reaction of unsaturated compounds. Journal of Russian

Physical-Chemical Society, 27:219-236.
Wiberg, K. B., Deutsch, C. J., and Rocek, J., 1973. Permanganate oxidation of crotonic acid. Spectrometric detection of an intermediate. Journal of American Chemical Society, 95: 3034-3035.
Wiberg, K. B. and Saegebarth, K. A., 1957. The mechanisms of permanganate oxidation. IV. Hydroxylation of olefins and related reactions. Journal of American Chemical Society, 79: 2822-2824.

Table 1. Redox reactions and their potentials of various couples of manganese ions.

Half-cell reactions (Mn)	E^0 (volts)	pH ranges in which the half-cell reaction predominates
$MnO_4^- + e^- = MnO_4^{2-}$	+0.56	> 12
$MnO_4^- + 3e^- + 2H_2O = MnO_2 + 4OH^-$	+0.59	pH high
$MnO_4^- + 3e^- + 4H^+ = MnO_2 + 2H_2O$	+1.70	3.5 – 12 ❮ pH low
$MnO_4^- + 5e^- + 8H^+ = Mn^{2+} + 4H_2O$	+1.51	<3.5

Table 2. Rate constants and half lives for the oxidative degradation of chlorinated ethylenes by permanganate (1 mM).

Chlorinated Ethylenes	k_{obs} (10^{-4} s^{-1})	Determination coef. of regression (r^2)	$T_{1/2}$ (min)
PCE	0.45±0.03	0.924	256.7
TCE	6.5±0.1	0.997	17.8
cis-DCE	9.2±0.5	0.976	12.6
trans-DCE	300±20	0.991	0.4
1,1-DCE	23.8±1.3	0.980	4.9

Figure 1. Reaction scheme. The oxidation of ethylene in a neutral to weak acidic condition.

Figure 2. Schematic diagram of a reactor. In kinetic experiments, each sample aliquot was withdrawn from the sampling port by a syringe when the same volume of solution as the aliquot was injected via the injection port. Zero headspace was maintained at all times.

Figure 3. Plot of initial rates versus initial concentration for eight kinetic experiments. TCE ranging from 0.031 to 0.083 mM was oxidized by 1 mM MnO_4^- at pH 7.1. A slope $\alpha = 1.01 \pm 0.02$ confirms a first order reaction with respect to TCE.

Figure 4. Plot of pseudo-order rate constant k_{obs} versus initial concentration of permanganate. TCE at 0.078 mM was oxidized by MnO_4^- concentration varying from 0.37 to 1.2 mM at pH 7.1. A slope $\beta = 1.05 \pm 0.03$ confirm a first order reaction with respect to MnO_4^-.

Figure 5. Degradation of chlorinated ethylenes by MnO_4^- (1 mM), at pH 7.1. Lines represent best fits using a pseudo-first-order kinetic model.

Figure 6. Liberation of Cl^- ions in the TCE oxidative transformation by 1 mM MnO_4^- at pH 7.1. The error bars for Cl^- ions are the standard deviation of triplicate samples. The solid lines were calculated from Eq. 10 with k_{obs} obtained from a best fit to TCE observations using Eq. 10(a).

Figure 7. Pseudo-first-order plot of TCE transformation in 1 mM MnO_4^- over the pH range of 4-8. Rate constant $k_{obs} = 0.67 \pm 0.03 \times 10^{-3}$ s^{-1} and half life $T_{1/2} = 17.3 \pm 0.5$ minutes.

Figure 8. Overlay of UV-vis spectra at time intervals of 10 minutes during TCE (3.81 mM) oxidation by MnO_4^- (0.23 mM) at pH 7.1. The solid bold line is the initial MnO_4^- spectrum and the dashed line is the final spectrum due to a product from the decomposition of MnO_4^-.

Figure 9. Log A versus log λ for the spectrum recorded at 80 minutes after the reaction between MnO_4^- (0.23 mM) and TCE (6.85 mM) at pH 8.2. The linear relationship with a slope =-4.22±0.05 obeys Rayleigh's law.

Figure 10. Comparison of TCE degradation by 0.13 mM (20 mg/L) MnO_4^- in Milli-Q water, ground water, and contaminated ground water (2% leachate). Lines represent best fits using a pseudo-first-order kinetic equation.

Figure 11. Plot of the maximum pseudo-first-order rate constant (k_{obs}) versus TOC concentration.

Figure 12. TCE degradation by MnO_4^- at various concentrations in a synthesized contaminated ground water containing 101 mg/L TOC. The solid lines were calculated using $k_{TCE\text{-}MnVII} = 0.67$ M^{-1} s^{-1} and $k_{TOC\text{-}MnVII} = 0.60$ M^{-1} s^{-1}at composite weight of 176 g for TOC. The dashed lines were calculated for TCE degradation in Milli-Q water without TOC.

Appendix 2. Manuscript of published article entitled:

KINETICS AND MECHANISMS FOR TCE OXIDATION BY PERMANGANATE

Y. Eugene Yan[1] and Franklin W. Schwartz[2]

Department of Geological Sciences
The Ohio State University
Columbus, OH 43210

ABSTRACT

The oxidation of trichloroethylene (TCE) by permanganate was studied via a series of kinetic experiments. The goal in product identification and parameterization of the oxidation kinetics was to assess the utility of this reaction as the basis for the in-situ remediation of ground water contaminated by chlorinated ethenes. TCE oxidation mainly involves the formation and decomposition of an organometallic compound (hypomanganate ester) to form carboxylic acids, and eventually, oxidation to the final product, CO_2. The initial and final reactions in the TCE oxidation are subject to rate-limiting steps, which control the destruction rate of TCE and formation rate of the final product. The fast reactions involved in the second step determine the nature of products. Four carboxylic acids, including formic, oxalic, glyoxylic and glycolic acids, and CO_2 were identified and quantified in kinetic measurements. The distribution of products is highly dependent upon experimental conditions, particularly pH. Based on our understanding of various processes involved with TCE oxidation, a kinetic model was developed and the model parameters (seven rate constants) were estimated. The kinetic model proposed in this study successfully simulates observed experimental data.

Key Words: Permanganate, Trichloroethylene, Oxidation, Kinetics, Remediation

INTRODUCTION

There is considerable interest in the in-situ oxidative degradation of chlorinated ethenes with a metal-oxo reagent (1-5). In terms of remediating contaminated ground water, this method is attractive due to the rapid degradation of chlorinated ethenes, the non-reactive nature of the reagent with carbonate and bicarbonate, the ease of field implementation, and the relatively low costs (1,5,6). Degradation kinetics for five chlorinated ethenes, including PCE, TCE, and three isomers of DCE were reported by (7). TCE degradation was postulated to involve the following three sequential reactions:

$$C_2HCl_3 + MnO_4^- \xrightarrow{k_1} I \xrightarrow{k_2} \gamma\, CA + MnO_2 + 3Cl^- \qquad \textbf{(1)}$$

$$\gamma\, CA \xrightarrow{k_3\,(MnO_4^-)} \eta\, CO_2 \qquad \textbf{(2)}$$

where I is a cyclic complex, CA are various carboxylic acids, γ and η are stoichiometric coefficients,

---

[1] Corresponding author. Current address: Environmental Research Division, Argonne National Laboratory, 9700 S. Cass Ave., Argonne, IL 60439. Fax: 630-252-5747, Tel: 630-252-6322. E-mail: eyan@anl.gov

[2] Fax: 614-292-7688. E-mail: frank@geology.ohio-state.edu

and k_1, k_2, and k_3 are rate constants. In the first reaction, TCE disappearance was found to be independent of pH. Complete chlorine liberation thought to occur in the second step of eq 1. However, the second and third reactions have not been studied in detail. Other work indicates that the oxidation of alkene and its products is highly pH dependent and that both permanganate and hydroxyl ions compete for a common cyclic intermediate (8). The purpose of our study here was to describe the kinetics and mechanisms involved with TCE oxidation by permanganate. Specific objectives of the study are (i) to identify reaction products, (ii) to elucidate reaction pathways and their pH dependence, (iii) to develop a kinetic model, and (iv) to determine the rate constants for all major reactions in $KMnO_4$-TCE-H_2O system.

EXPERIMENTAL METHODS

Materials.

Radiolabeled [1,2-^{14}C] TCE (3.1 mCi/mmol) was purchased from Sigma Chemical Co. (St. Louis, MO) and diluted with methanol in a 10-ml glass volumetric flask and stored at 4^{o}C in the dark. Carboxylic acids were obtained from Fluke (Buchs, Switzerland) with purity 99+% and used as received. All other chemicals were of the highest purity available and were described previously (7).

Product Studies and Kinetic Experiments

With TCE oxidation reaction by permanganate, carboxylic acids and carbon dioxide would be expected as the major intermediate and final products (7). Two types of kinetic experiments were designed to identify the carboxylic acids and to trace CO_2 formation. Each type consists of three experiments conducted at pHs 4, 6, and 8 and each experiment has one set of vials with two or three replicates and one control vial containing only TCE aqueous solution.

For investigating carboxylic acid distributions over time, a first kinetic experiment was conducted in 50-ml glass vials with PTFE/silicone septum-lined screw-top caps. Each vial was filled with a 50-ml TCE solution of 0.1 mM. The experiment began by injecting 5-ml of $KMnO_4$ of 6.3 mM through the septum. A second needle enabled an equal volume of TCE solution to be displaced. Vials were placed on a vibratory shaker until sampled. At each sampling time, one vial was taken. A 1-ml aliquot of reaction solution from the vial was transferred to a volumetric flask with appropriate dilution following immediate TCE analysis. To quench the reaction, 1-ml thiosulfate from the stock solution was added to the vial. The quenched solution was centrifuged at 3000 rpm for 20 minutes and filtered by 0.2-μm filter to separate the precipitated manganese dioxide. After filtration, the solutions were withdrawn for carboxylic acid analysis.

To trace the CO_2 production, we undertook a second kinetic experiment with radiolabeled ^{14}C TCE. To maintain the same initial conditions as the first kinetic test, experiments began with the addition of 0.1-ml permanganate stock solution to a set of 3-ml test tubes filled with a 2.9-ml of a 0.093 mM TCE solution. At predetermined intervals, a test tube was sacrificed with the reaction quenched by adding 0.1-ml of thiosulfate from the stock solution. The test solution was then analyzed for CO_2.

Chemical Analysis

The organic acids were analyzed on a Waters high performance liquid chromatography (HPLC) fitted with a Bio-Rad Aminex HPX-87H column (300 × 7.8 mm I.D.). CO_2 was determined by

retaining CO_2 under basic conditions and stripping CO_2 under acidic conditions. This method was adapted from (9). TCE concentrations were determined as described in (7).

RESULTS AND DISCUSSION

Products

In the experiments for identifying products, a 0.09 mM TCE solution was reacted with 0.63 mM permanganate. The solution was phosphate-buffered and had an ionic strength of 0.05 M at pH 4, 6, and 8, respectively. Four carboxylic acids, formic, oxalic, glyoxylic, and glycolic acids, were identified in the system as intermediate products. Either formic or oxalic acid predominated, depending on the pH. One hour after the reaction started, a maximum of 43% of the initial TCE was converted to either formic or oxalic acid and up to 25% of the TCE was transformed to glyoxylic acid. Glycolic acid was produced in small quantities (<2%).

The radiolabled product analysis indicates that the majority of TCE was eventually transformed to CO_2, the final product. Assuming TCE is stoichiometrically converted to CO_2, 57-88% of the initial TCE, varying depending on pH, was converted to CO_2 when the experiments were terminated at 8 hours.

The proposed chemical pathways for TCE oxidation (Figure 1) were developed from a basic understanding of alkene oxidation by permanganate in organic synthesis chemistry (8,10,11). The products and intermediates in the shadowed boxes were identified in our experiments. TCE oxidation is initiated by the attack of permanganate ion, as an electrophile, on the carbon-carbon double bond (7). An organometallic compound, cyclic hypomanganate ester **2** is formed via an activation complex in transition state (10,12-13). The rapid decomposition of cyclic ester **2** can follow several different pathways in an aqueous system such as oxidative hydrolysis and hydrolysis.

Oxidative hydrolysis transforms cyclic hypomanganate ester **2** rapidly to cyclic manganate (VI) ester **3** to form formic acid **5** via **4**. Two other possible pathways involve the hydrolysis of cyclic ester **2** to acyclic hypomanganate (V) ester **6**. The acyclic manganate (VI) ester **7**, oxidatively hydrolyzed from **6**, may undergo rapid electron transfer and then either hydrolysis to form glycolic acid **9** via **8** or release of one hydrogen chloride and hydrolysis to form glyoxylic acid **12** or oxalic acid **13** via **11**. In weak alkalinic to alkalinic solutions, acyclic ester **6** may simply hydrolyze to trichloroglycol **10**, which rapidly releases two hydrogen chlorides. This compound is subsequently hydrolyzed to either glyoxylic acid **12** or oxalic acid **13**. Carboxylic acids are further oxidized to carbon dioxide at a relatively slow rate.

The liberation of chlorine substitutes is hypothesized as a series of reactions, involving the transformation of hypomanganate ester to manganate ester, the electron transfer to release hydrogen chloride, and hydrolysis. A stoichiometrically consistent release of chloride was observed along with disappearance of TCE (7). Thus, the decomposition of the ester with chloride release is a very rapid process, which is much faster than its formation.

Kinetic Equations for TCE Oxidation

TCE oxidation by permanganate ion generally involves the formation and decomposition of cyclic hypomanganate ester (CHME), and the oxidation of carboxylic acids, based on the TCE transformation pathways in Figure 1. A second order reaction for the formation of CHME was suggested by (5):

$$C_2HCl_3 + MnO_4^- \xrightarrow{k_{1p}} CHME \quad \textbf{(3)}$$

where k_{1p} is a second-order rate constant. The decomposition of CHME via various pathways to form major carboxylic acids and the release of chlorides can be described by eqs 4-6:

$$\alpha\, CHME + \beta\, H_2O \xrightarrow{k_{2a}} 2\alpha\, HCOOH + \alpha\, MnO_2 + 3\alpha\, Cl^- + \gamma\, H^+ \quad \textbf{(4)}$$

$$\alpha\, CHME + \eta\, H_2O \xrightarrow{k_{2b}} \alpha\, OHC-COOH + \alpha\, MnO_2 + 3\alpha\, Cl^- + \nu\, H^+ \quad \textbf{(5)}$$

$$\alpha\, CHME + \xi\, H_2O \xrightarrow{k_{2c}} \alpha\, HOOC-COOH + \alpha\, MnO_2 + 3\alpha\, Cl^- + \zeta\, H^+ \quad \textbf{(6)}$$

where α, β, γ, η, ν, ξ and ζ are stoichiometric coefficients and k_{2a}, k_{2b}, and k_{2c} are rate constants for the formation of formic, glyoxylic, and oxalic acids, respectively.

The oxidation of formic, glyoxylic, and oxalic acids by permanganate involves a series of reactions. Most studies, however, have shown that the reaction at a rate limiting step can be described by second-order reaction for formic and oxalic acids (14-16). By analogy with the oxidation of formic and oxalic acids, it is reasonable to assume a second-order reaction for glyoxylic acid due to its similar structure to the other two acids. The rate laws for these three oxidation reactions are shown in eqs 7-9 (Table 1). With an excess of MnO_4^- in aqueous media at a fixed pH, the order of kinetic reaction can be reduced. The rates of disappearance/appearance for TCE, major intermediates and final product are summarized in Table 1, eqs 10-15.

Estimation of Rate Constants

To find the rate constants for transformation and/or formation of TCE, three carboxylic acids, and CO_2, equations of 10-15 were solved analytically using Laplace transformation. The solutions for TCE, formic, glyoxylic, and oxalic acids in terms of normalized concentration are:

$$\frac{[TCE]}{[TCE]_0} = e^{-k_1 t} \quad \textbf{(16)}$$

$$\frac{[C_t]_l}{[TCE]_0} = m k_1 k_{2l} \sum_i \frac{e^{-k_i t}}{\prod_{j(j\neq i)} (k_j - k_i)} \qquad i,j = 1,2,and\ 3l; \quad l = a,b,and\ c; \qquad m = \begin{cases} 2 & l = a \\ 1 & l = b,c \end{cases}; \quad \textbf{(17)}$$

where $[C_t]_l$ is the concentration of the carboxylic acids and the subscript l =a, b, and c denotes formic, glyoxylic, and oxalic acids, respectively. The formation of CO_2 can be described as

$$\frac{[CO_2]}{[TCE]_0} = 2\left\{1 - k_1 \sum_{l=a}^{c} \left(k_{2l}\, k_{3l} \sum_i \frac{e^{-k_i t}}{k_i \prod_{j(j\neq i)} (k_j - k_i)} \right) \right\} \qquad i,j = 1,2,and\ 3l \quad \textbf{(18)}$$

To establish a kinetic model, the seven rate constants, k_1, k_{2a}, k_{2b}, k_{2c}, k_{3a}, k_{3b}, and k_{3c} need to be estimated using kinetic data from the TCE oxidation experiments. Accordingly, the kinetic experiments, described previously, were conducted with a H_3PO_4-K_2HPO_4- KH_2PO_4-NaOH buffer at pHs 4, 6, and 8. The concentrations of TCE, the intermediates (including formic, glyoxylic and oxalic acids), and the final product, CO_2 were measured with time. Mass balances in these experiments ranged from 0.84 to 1.09. The results indicate that the experiments were well controlled, even though various analytical procedures were involved.

Rate constants were estimated with eqs 16-17 by fitting the measured concentration data. The fitted results (Figure 2) agree well with the experimental data across a pH range of 4 to 8. With the pseudo-first-order rate constant k_1 ranging from 4.11×10^{-4} to 4.30×10^{-4} s^{-1} (Table 2), the second-order rate constant k_{1p}, defined in eq 10, can be calculated. The calculated k_{1p} in the range of 0.65 - 0.68 M^{-1} s^{-1} agrees with (7) (i.e., k=0.67±0.03 M^{-1} s^{-1}).

To choose an appropriate k_2 for the second step in TCE oxidation, the concentration data for the carboxylic acids were fitted with eq 17 using various ratios of k_2 to k_1. The results indicate that determination coefficient (r^2) for curve fittings was improved with increasing k_2/k_1 ratio and reaches 0.9 at k_2/k_1>10. The large k_2/k_1 ratio supports the idea that the decomposition of cyclic ester is much faster than its formation, as suggested by (7,8). When $k_2 > 10^2$ k_1, r^2 does not show any obvious improvement. All other rate constants (k_{2a}, k_{2b}, k_{2c}, k_{3a}, $k_{3b,}$ and k_{3c}) remain constant with increasing k_2/k_1. Thus, $k_2 = 10^2$ k_1 was assumed in all curve fittings. The ratios, k_{2a}/k_2, k_{2b}/k_2, and k_{2c}/k_2, represent the fraction of the total decomposition rate along each pathway and quantify the contribution from the various pathways in Figure 1. Their values (Table 2) suggest that the pathway leading to formic or oxalic acid is dominant in the decomposition process.

The pseudo-first-order rate constants, k_{3a}, $k_{3b,}$ and k_{3c}, describe the oxidation of formic, glyoxylic, and oxalic acids in the final step. Compared to the other steps in TCE oxidation, the oxidation rates for the carboxylic acids are slower than any of the rates in the previous steps. The second-order rate constants, k_{3ap}, $k_{3bp,}$ and k_{3cp}, can be calculated with eqs 12-14. k_{3ap} for the oxidation of formic acid ranges from 0.075 to 0.16 $M^{-1}s^{-1}$. These results compare well with the range of 0.003-0.25 $M^{-1}s^{-1}$ obtained by (17). The observed range in k_{3c} values, 0.073-0.11 $M^{-1}s^{-1}$, for oxalic acid is also consistent with k = 0.005-0.02 $M^{-1}s^{-1}$ (16). Based on the estimated rate constants, the oxidation rates for formic and glyoxylic acids are greater than oxalic acid over a pH range of 4-8.

Using all the estimated rate constants, the calculated accumulation of CO_2 is plotted in Figures 2. The results for CO_2 are in general agreement with the experimental data, except at pH 8 where the predicted CO_2 is higher than the observed at later time. This overestimation may result from the adsorption of carboxylic acids on MnO_2, which is more readily precipitated at pH 8 than other pH conditions. Because the precipitates were left in the filtrates in our experiments for acid analysis, acid adsorption on MnO_2 could cause a mass deficiency, which occurs at late time (Figure 2c). Consequently, the rate constant k_3 at pH 8 may be slightly overestimated.

Effects of pH and Temperature

During the first step in TCE oxidation, the rate constant k_1 does not show strong correlation with pH. Our previous study (7) indicated that (i) the variation of k_1 at different pH is small and within the experimental error and (ii) the second-order rate constant k_{1p} is equal to 0.67±0.03 M^{-1} s^{-1}. Thus, the rate of TCE disappearance is independent of pH. However, the fate of hypomanganate ester and the product distribution are strongly dependent on pH. At pH = 4, the transformation of cyclic ester to formic acid is overwhelmingly dominant (k_{2a}/k_2 = 0.77). At pH of 6-8, decomposition favors the formation of oxalic and glyoxylic acids ((k_{2b}+ k_{2c})/k_2 = 0.95-96). Most of cyclic ester reacts to form oxalic and glyoxylic acids in this higher pH range.

The rate constants (k_{3a}, k_{3b}, and k_{3c}) for oxidation of carboxylic acids are strongly correlated with pH over a range of 4-8 (Figure 3). With decreasing pH, the oxidation rates (k_3) increase for all

three carboxylic acids. This pH effect on k_3 results in the relatively rapid formation of CO_2 at low pHs, as compared to higher pHs.

In order to investigate the effect of temperature on the rate TCE transformation, five sets of duplicated kinetic experiments were performed at temperatures varying from 5 to 25 ^oC. All experiments were initiated by reacting 0.06 mM TCE with excess of MnO_4^- (1mM) at pH 7 and an ionic strength of 0.05 M. The estimated logarithm of the second-order rate constant k_{1p} from the experiments is plotted against the reciprocal of temperature in Figure 4. The dependence of k_{1p} on temperature, as expected, follows the Arrhenius equation. The activation energy (E_a) and preexponential (A) were calculated and are listed in Figure 4. These values can provide a rate constant, k_{1p}, at any temperature relevant to ground water.

Based on the E_a=41.46 kJ/mol and A=1.678×10^7 M^{-1} s^{-1}, activation parameters, $\Delta H^{\ddagger}$ and $\Delta S^{\ddagger}$, can be calculated. The low activation enthalpy ($\Delta H^{\ddagger}$ = 39 kJ/mol) obtained here is comparable to the results from many other studies in alkene oxidation by permanganate. This result indicates that initial step of TCE oxidation may proceed via a similar transition state as other alkene oxidation. The negative entropy ($\Delta S^{\ddagger}$ = -14 J/mol) is consistent with a bimolecular reaction in which the transient intermediate may be highly structured and possibly solvated.

PROPOSED MECHANISM FOR TCE OXIDATION

The fact that the loss of TCE is independent of pH but that the nature and distribution of products are highly dependent on pH strongly supports the existence of a short-lived intermediate in the initial stage of oxidation. In the classical view, as summarized by (10), the formation of cyclic ester involves a 3+2 electrocyclic addition of permanganate ion to the carbon-carbon double bond

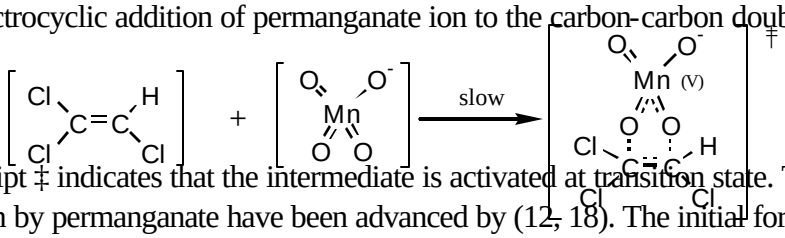

(19)

where the superscript ‡ indicates that the intermediate is activated at transition state. The modern ideas on alkene oxidation by permanganate have been advanced by (12, 18). The initial formation of transient organometallic intermediate proceeds with 2+2 insertion of an alkene π bond directly into a metal-oxo bond of manganese.

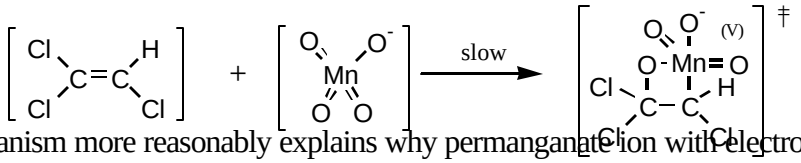

(20)

This reaction mechanism more reasonably explains why permanganate ion with electron-rich oxygen termini could attack carbon-carbon double bond electrophilically. The attack is controlled by orbital-overlap via delocalized charge-transfer interaction rather than net-charge (13, 19). In the initial TCE oxidation, TCE with electron-withdrawing group (Cl) is more likely attacked by permanganate ion via a transition state in eq 20. This reaction mechanism may also favor trans isomers with a charge-transfer interaction in the transition state (19). This view is supported by our early result that trans-DCE showed much greater reactivity than cis-DCE (7).

The small enthalpy $\Delta H^{\ddagger}$ (39 kJ/mol) and negative entropy $\Delta S^{\ddagger}$ (-14 J/mol) are consistent with the observations of the oxidation of other alkenic substrates by permanganate under various conditions, even though their products are different. The results suggest that TCE oxidation proceeds via similar

transition states but that these transformation products are subjected to various post-transition-state reactions, which are highly dependent on reaction conditions.

The existence of various reaction pathways is evidenced by the formation of different intermediate products as a function of pH. At pH 4, the decomposition of cyclic ester **2** involves both oxidative hydrolysis (following carbon bond cleavage) to form formic acid and hydrolysis (with subsequent reactions) to form oxalic acid (Figure 1). The calculated ratios of rate constants (k_{2a}/k_2 and k_{2c}/k_2) indicate that the former reaction pathway is predominant (77% of total production), while the latter one is much less importance (20%). With increasing pH, almost all the cyclic esters are hydrolyzed via **6**. Products are further decomposed via oxidative hydrolysis, hydrolysis and electron transfer to form either glyoxylic or oxalic acid. Decomposition of acyclic ester **7** via **8** to form glycolic acid is insignificant. The estimated k_2/k_1 ratio from our kinetic data also supports the postulate that the decomposition of cyclic ester is much faster than its formation. The series of reactions, during the fast ester decomposition, liberate almost all the chlorine substitutes on TCE (7).

In the final step, the oxidation of carboxylic acids is relatively slow compared to the previous steps. The oxidation may involve hydride abstraction by permanganate ion (20) and carbon-carbon bond cleavage. In the aqueous solution, carboxylic acids can be dissociated:

$$HCOOH \Leftrightarrow HCOO^- + H^+ \qquad pK_a = 3.74 \tag{21}$$

$$HOC-COOH \Leftrightarrow HOC-COO^- + H^+ \quad pK_b = 3.34 \tag{22}$$

$$HOOC-COOH \Leftrightarrow HOOC-COO^- + H^+ \quad pK_{c1} = 1.27 \tag{23}$$

$$HOOC-COO^- \Leftrightarrow {}^-OOC-COO^- + H^+ \; pK_{c2} = 4.28 \tag{24}$$

where K_a, K_b, K_{c1}, and K_{c2}, are ionization constant for formic, glyoxylic and oxalic acids, respectively. If all species are considered to react independently with permanganate, eqs 7-9 can be further developed to eqs 25-27 (Table 1). Because the pH range of 4-8 is higher than pK_a pK_b, pK_{c1}, $[H^+] << K_a$, $[H^+] << K_b$ and $[H^+]^2 << K_{c1}K_{c2}$ and $K_{c1}[H]^+$. As compared to eqs 25-27 with 7-9, the second-order rate constants for oxidation of formic, glyoxylic, and oxalic acids are

$$k_{3ap} = \frac{k_{3ap1}}{K_a}[H^+] + k_{3ap2} \tag{28}$$

$$k_{3bp} = \frac{k_{3bp1}}{K_b}[H^+] + k_{3bp2} \tag{29}$$

$$k_{3cp} = \frac{k_{3cp1}[H^+]^2 + k_{3cp2}K[H^+] + k_{3cp3}K_{c1}K_{c2}}{K_{c1}K_{c2} + K_{c1}[H^+]} \tag{30}$$

The relationship between logarithm of second-order rate constants with pH shown in Figure 3 is consistent with the mechanism described by eqs 28-30. Because of the relatively high oxidation rate of carboxylic acids at low pH, as illustrated in Figures 2, CO_2 is accumulated more rapidly with decreasing pH.

ACKNOWLEDGEMENTS

We thank Drs. O. H. Tuovinen, Y. P. Chin , S. Traina for their advice and assistance. This material is based upon work supported by the U. S. Department of Energy under Grant No. DE-FG07-96ER14735.

REFERENCES

(1) Vella, P. A.; Veronda, B., In *Chemical Oxidation Technologies for the Nineties*, Eckenfelder, W. W., ed., Technomic Publishing, Lancaster, Basel, **1992**.

(2) Truax, C.M. A. Sc. *Thesis*, Univ. Waterloo, Waterloo, Ontario, Canada, **1993**.

(3) Yan Y. E.; Schwartz F. W. *EOS*, **1995**, 76(46), F247.

(4) Gates D. D.; Siegrist, R. L.; Cline, S. R. In *Proceedings of 88th Annual Meeting and Exhibition*, Air & Waste Management Assoc., San Antonio, Texas, June 18-23, **1995**.

(5) Schnarr, M.; Truax, C.; Farquhar, G.; Hood E.; Gonullu, T.; Stickney, B. *J. Contam. Hydrol*. **1998**, 29, 205-224.

(6) Vella, P. A. In *Proceedings of 3rd Intl. Conf. on Advanced Oxidation Technologies for Water and Air Remediation*, Cincinnati, Ohio, Oct. 26-29, **1996**, 119-120.

(7) Yan, Y. E. and Schwartz, F. W. *J. Contam. Hydrol.* **1999**, 37, 343-365.

(8) Wiberg, K. B.; Saegebarth, K. A. *J. Am. Chem. Soc.* **1957**, 79, 2822-2824.

(9) Kriegman-King, M. R.; Reinhard, M. *Environ. Sci. Technol.* **1992**, 26, 2198-2206.

(10) Freeman, F. *Reviews on Reactive Species in Chemical Reactions* **1976**, 1, 179-226.

(11) Lee, D. G.; Chen, T. *J. Am. Chem. Soc.* **1989**, 111, 7534-7538.

(12) Sharpless, K. B.; Teranishi, A. Y.; Backvall, J. E. *J. Am. Chem. Soc.* **1977**, 99, 3120-3128.

(13) Lee, D. G.; Brown, K. C. *J. Am. Chem. Soc.* **1982**, 104, 5076-5081.

(14) Berka, A.; Koreckova, J. *Analytical Letters* **1973**, 6, 1113-1123.

(15) Rodriguez, J.; Sanchez Burgos, F. *Ion (Madrid)* **1975**, 35, 241-245.

(16) Mahmood, A. J.; Begum, M. *Dacca University Studies*, *Pt. B.*, **1975**, 23, 51-64.

(17) Perez-Benito, J. F.; Arias, C.; Brillas, E. *Int. J. Chem. Kinet.* **1990**, 22, 261-287.

(18) Rappe, A. K. and Goddard, W. A. III. *J. Am. Chem. Soc.* **1982**, 104, 448-456.

(19) Toyoshima, K.; Okuyama, T.; Fueno, T. *J. Organic Chem.* **1980**, 45, 1600-1604.

(20) Gardner, K. A.; Mayer, J. M. *Science* **1995**, 269, 1849-1851.

Figure 1. Proposed TCE oxidation pathways. Shadowed boxes are products identified in this study.

Figure 2. Product distribution with time in TCE oxidation at pH 4 (a), pH 6 (b) and pH 8 (c). Lines for TCE and carboxylic acids represent best fits using eqs 16-17, whereas the line for CO_2 is calculated by eq 18 using rate constants from the previous curve fitting.

Figure 3. Dependence of the pseudo-first-order rate constants (k_{3a}, k_{3b}, and k_{3c}) on pH for oxidation of carboxylic acids. The reaction involved reacting 0.09 mM TCE with 0.63 mM MnO_4^- in a phosphate buffered aqueous solution at ionic strength 0.05 M.

Figure 4. Arrhenius plot for the oxidation of TCE (0.06 mM) by potassium permanganate (1 mM) in a phosphate buffered solution at ionic strength 0.05M and pH 7.1. Error bars are standard deviation for each estimated second-order rate constant k_1.

Table 1: Listing of kinetic equations.

Equation	No
$\frac{d[HCOOH]_t}{dt} = -k_{3ap}[HCOOH]_t[MnO_4^-]$	7
$\frac{d[OHC-COOH]_t}{dt} = -k_{3bp}[OHC-COOH]_t[MnO_4^-]$	8
$\frac{d[HOOC-COOH]_t}{dt} = -k_{3cp}[HOOC-COOH]_t[MnO_4^-]$	9
$\frac{d[C_2HCl_3]}{dt} = -k_1[C_2HCl_3] \qquad k_1 = k_{1p}[MnO_4^-]$	10
$\frac{d[CHME]}{dt} = k_1[C_2HCl_3] - k_2[CHME] \qquad k_2 = k_{2a} + k_{2b} + k_{2c}$	11
$\frac{d[HCOOH]_t}{dt} = 2k_{2a}[CHME] - k_{3a}[HCOOH]_t \qquad k_{3a} = k_{3ap}[MnO_4^-]$	12
$\frac{d[HCO-COOH]_t}{dt} = k_{2b}[CHME] - k_{3b}[OHC-COOH]_t \quad k_{3b} = k_{3bp}[MnO_4^-]$	13
$\frac{d[HOOC-COOH]_t}{dt} = k_{2c}[CHME] - k_{3c}[HOOC-COOH]_t \; k_{3c} = k_{3cp}[MnO_4^-]$	14
$\frac{d[CO_2]}{dt} = k_{3a}[COOH]_t + 2k_{3b}[OHC-COOH]_t + 2k_{3c}[HOOC-COOH]_t$	15
$\frac{d[HCOOH]_t}{dt} = -(k_{3ap1}[HCOOH] + k_{3ap2}[HCOO^-])[MnO_4^-]$ $= -\left(\frac{k_{3ap1}[H^+] + k_{3ap2}K_a}{[H^+] + K_a}\right)[HCOOH]_t[MnO_4^-]$	25
$\frac{d[HOC-COOH]_t}{dt} = -(k_{3bp1}[HOC-COOH] + k_{3bp2}[HOC-COO^-])[MnO_4^-]$ $= -\left(\frac{k_{3bp1}[H^+] + k_{3bp2}K_a}{[H^+] + K_b}\right)[HOC-COOH]_t[MnO_4^-]$	26
$\frac{d[HOOC-COOH]_t}{dt} = -(k_{3cp1}[HOOC-COOH] + k_{3cp2}[HOOC-COO^-] + k_{3cp3}[^-OOC-COO^-])[MnO_4^-]$ $= -\left(\frac{k_{3cp1}[H^+]^2 + k_{3cp2}K_{c1}[H^+] + k_{3cp3}K_{c1}K_{c2}}{K_{c1}K_{c2} + K_{c1}[H^+] + [H^+]^2}\right)[HOOC-COOH]_t[MnO_4^-]$	27

subscript t for each acid denotes the total concentration; k_1, k_{3a}, k_{3b}, and k_{3c} are pseudo-first-order rate constants; k_{2a}, k_{2b}, and k_{2c} are first-order rate constants; $k_{3ap,}$ k_{3bp}, and k_{3cp} are second-order rate constants; k_{3ap1}, k_{3ap2}, k_{3bp1}, k_{3bp2}, k_{3cp1}, k_{3cp2}, and k_{3cp3} are rate constants.

Table 2 Rate constants obtained for TCE transformation pathways using equations, 16-17. Estimation was based on experiments conducted with an initial concentration of 0.63 mM MnO_4^-. $k_2 > 10^2\ k_1$.

pH	k_1 $10^{-4}\ s^{-1}$	k_{2a}/k_2	k_{3a} $10^{-4}\ s^{-1}$	r^2	k_{2b}/k_2	k_{3b} $10^{-4}\ s^{-1}$	r^2	k_{2c}/k_2	k_{3c} $10^{-4}\ s^{-1}$	r^2
4	4.30	0.77	2.19	0.98	0.03	2.34	0.98	0.20	0.70	0.95
6	4.11	0.02	1.53	0.91	0.32	1.05	0.99	0.63	0.64	0.95
8	4.11	0.04	0.47	0.97	0.42	0.80	0.99	0.55	0.46	0.95

Appendix 3. Manuscript of published article entitled;

PHASE-TRANSFER-CATALYSIS APPLIED TO THE OXIDATION OF NONAQUEOUS PHASE TRICHLOROETHYLENE BY POTASSIUM PERMANGANATE

Yongkoo Seol and Franklin W. Schwartz*

Department of Geological Sciences, The Ohio State University
Columbus, OH 43210, USA

Abstract

The use of potassium permanganate to oxidize chlorinated solvents has been demonstrated as an effective process for treating nonaqueous phase liquids in ground-water systems. This study evaluates the effectiveness of phase-transfer-catalysts (PTCs) in enhancing the degradation rate. PTCs work by transferring permanganate ion into the nonaqueous phase where it initiates oxidative decomposition. We studied the oxidation of trichloroethylene (TCE) by potassium permanganate, conducting kinetic batch experiments in conjunction with three PTCs that varied in terms of their extraction constants and molecular structures. Using the same batch technique, we examined whether PTCs could enhance the aqueous solubility of TCE. Solubilization could also increase oxidation rates in the aqueous phase. Rates of TCE oxidation in solutions containing the PTCs and a blank were estimated separately by measuring chloride concentration and UV/Vis absorbance in the aqueous phase. The enhanced rate of TCE destruction by the PTCs was reflected by an increase in the rate of consumption of permanganate ion and production of chloride ion. There was no tendency for the PTCs, however, to solubilize TCE in the aqueous phase. Therefore, the PTCs increased the rate of TCE decomposition by catalyzing permanganate oxidation in the organic phase. This study suggests that there is significant potential for testing this scheme under field conditions.

Keywords; Phase-transfer-catalyst; Potassium permanganate; Trichloroethylene; Nonaqueous phase, Remediation

1. Introduction

Chlorinated ethylenes such as trichloroethylene (TCE) and perchloroethylene (PCE) are common contaminants (Plumb, 1991; Westrick *et al.*, 1984). They occur in the subsurface as zones of residual saturation or occasionally as free products. Because of their inherently low solubility, dense nonaqueous phase liquids (DNAPLs) persist in aquifers and provide a long-term source of dissolved contaminants, capable of being transported (Johnson and Pankow, 1992).

Given the difficulties in remediating DNAPL contaminated sites, there has been a lot of effort to develop and to demonstrate new technologies. Our focus here is on oxidative schemes. In particular, oxidative decomposition with potassium permanganate (Schnarr *et al.*, 1998; Yan, 1998; Yan and Schwartz, 1999) or hydrogen peroxide (Glaze and Kang, 1988) has been

* Corresponding Author; frank@geology.ohio-state.edu, fax)614-292-7688

demonstrated as an effective process for mineralizing chlorinated solvents in the aqueous phase. Unlike reductive dechlorination, the oxidation of chlorinated solvents does not produce hazardous intermediates, such as dichloroethylene and vinyl chloride (Vella and Veronda, 1992; Vogel *et al.*, 1987).

Potassium permanganate ($KMnO_4$) has been widely examined for the oxidative dechlorination of TCE in bench scale or pilot scale experiments (Vella and Veronda, 1992; Yan, 1998; Yan and Schwartz, 1999). A recent study on the permanganate dechlorination of trichloroethylene (TCE) has documented reaction mechanisms and pathways, and has identified main intermediate products at different pHs (Yan, 1998). Our group has completed a model capable of simulating permanganate oxidation under field situations (Zhang and Schwartz, 2000).

Both laboratory and modeling results pointed out how constraints on the solubility of chlorinated solvents in the aqueous phase ultimately control the rate of oxidative destruction. Permanganate oxidation occurs only in the aqueous phase and involves dissolved species such as permanganate ion (MnO_4^-) and the chlorinated ethylenes. Thus, the solubility of the contaminants indirectly controls the utilization of MnO_4^- in the reaction and keeps the reaction rate relatively small.

Our efforts to increase the permanganate oxidation rate were initially concentrated on methods to enhance the solubility of chlorinated ethylenes in the aqueous phase. We first tried to exploit cosolvency effects, utilizing various alcohol-water mixtures to increase TCE solubilization and ultimately the rate of oxidation. However, nonideal behavior of MnO_4^- in the cosolvent phase, as yet poorly understood, and competition between the cosolvent and the target contaminant for MnO_4^- frustrated this approach.

This paper outlines a new concept, which is based on phase transfer catalysis, to accelerate the oxidation of chlorinated solvents. Phase transfer catalysis attempts to speed up the overall rate of DNAPL oxidation by enabling the oxidation to occur in both the aqueous and DNAPL phases. In a conventional oxidation scheme with two immiscible phases in contact (water and DNAPL), the oxidation of chlorinated compounds only occurs in the aqueous phase because that is where the MnO_4^- is present. Adding a phase-transfer catalyst (PTC) transfers some of MnO_4^- to the nonaqueous phase. Thus, MnO_4^- can oxidize chlorinated compounds both in the aqueous phase and in the pure-phase solvent.

The specific objectives of this study are to introduce the concept of phase transfer catalysis for the oxidation of chlorinated solvents and to evaluate whether the catalyzed oxidation scheme can enhance the oxidation of TCE with MnO_4^-. We conducted kinetic batch experiments to verify the hypothesis that PTCs would promote the oxidation of TCE in the nonaqueous phase and speed up the overall rate of TCE decomposition. We also examined whether the accelerated TCE decomposition in the presence of PTCs might be related to the enhanced solubilization of TCE in the aqueous phase by PTCs.

2. Theoretical background

Since Starks (1971) proposed a mechanistic concept for catalytic reactions occurring in the presence of two phases and catalysts, phase transfer catalysis has become a powerful tool for developing new types of reactions and chemicals in the field of synthetic organic chemistry.

Phase transfer catalysis is a technique for converting similar chemical species situated in two or more phases. Because of its polarity, an ionic species cannot normally enter nonpolar organic substances. However, once it combines with a PTC, the organic phase can extract the association of ionic species with the PTC from the aqueous phase.

Common PTCs include organic-soluble cations such as quaternary ammonium or phosphonium ions, which contain both liphophilic and hydrophilic moieties. Due to their amphiphilic nature, the catalysts distribute themselves between aqueous and organic phases, form an association with the reactive anion (e.g. MnO_4^-), and bring them into the organic phase in a form suitable for reactions. It is presumed that PTCs would not be consumed but perform the transfer function repeatedly.

When PTCs dissolve in water, they dissociate into catalytic cations (Q^+) and counter anions (X^-), which occur as free ions like MnO_4^-. In nonpolar solvents, the associations of catalysts and ionic species exist as ion pairs (Bränström, 1977). Ion pairs are neutral entities formed by the coulombic binding of oppositely charged ions (Dehmlow and Dehmlow, 1983). An important distinction between free ions and ion pairs is that solutions containing only ion pairs are not electrically conductive. Ion pairs are thermodynamically in equilibrium with the free ions;

$$Q^+ + X^- \longleftrightarrow [Q^+X^-] \qquad (1)$$

where $[Q^+X^-]$ is an ion pair.

The reaction of an organic compound with MnO_4^- in the presence of PTCs (Figure 1) can be represented by an overall equation (Eq. 2), conceptually involving two separate steps (Starks *et al.*, 1994), a transfer step (Eq. 3) and an intrinsic displacement reaction step (Eq. 4);

$$K^+_{aq}MnO^-_{4\,aq} + RX_{org} \xrightarrow{[Q^+X^-]} K^+_{aq}X^-_{aq} + RMnO_{4\,org} \qquad (2)$$

$$[Q^+X^-]_{org} + K^+_{aq} + MnO^-_{4\,aq} \longleftrightarrow [Q^+MnO^-_4]_{org} + K^+_{aq} + X^-_{aq} \qquad (3)$$

$$RX_{org} + [Q^+MnO^-_4]_{org} \longrightarrow RMnO_{4\,org} + [Q^+X^-]_{org} \qquad (4)$$

where R is the organic reactant (e.g. TCE) with a leaving group X (e.g. Cl^-). As depicted in Figure 1, the transfer step involves the extraction of MnO_4^- from the aqueous to the organic phase and the release of Cl^- back into the aqueous phase. Intrinsic displacement reaction describes the displacement of chloride ion on the target organic compound with MnO_4^-. It occurs when the transferred MnO_4^- is dissociated from the ion pair, oxidizes the chlorinated solvent, and disengages Cl^- from the organic compound.

Eq. (3) includes two simpler conversion processes (Eq. 5 and 6) consisting of equilibria between free ions and ion pairs and transfer of ion pair into the organic phase;

$$Q^+_{aq} + MnO^-_{4\,aq} \longleftrightarrow [Q^+MnO^-_4]_{org} \qquad (5)$$

$$Q^+_{aq} + X^-_{aq} \longleftrightarrow [Q^+X^-]_{org} \qquad (6)$$

The ability of MnO_4^- to transfer into the organic phase is reflected by the relative distribution of MnO_4^- between the two separate phases. From Eq. (5), one can define the extraction constant (K_E). It represents the capability of the nonpolar solvent to extract an ionic species from the

aqueous phase, and is expressed in Eq. (7). This constant is related in turn to experimentally determined solubilities (Karaman *et al.*, 1984) by way of Eq. (8);

$$K_E = \frac{[Q^+MnO_4^-]_{org}}{[Q^+]_{aq} \cdot [MnO_4^-]_{aq}} = \frac{[Q^+MnO_4^-]_{org}}{[MnO_4^-]_{aq}^2} \quad (7)$$

$$K_E = \frac{\text{solubility of } QMnO_4 \text{ in organic solvent (M)}}{(\text{solubility of } QMnO_4 \text{ in water})^2\ (M^2)} \quad (8)$$

Thus, the degree of extraction (K_E) increases in direct proportion to the solubilities of the ion pair in the organic phase.

Conceptualization of the extraction process in terms of an extraction constant can be somewhat misleading because other side processes could be important (Bränström, 1976). They impact the concentration of either the ion pairs in the organic phase or the ionic species in the aqueous phase, which subsequently can change the degree of extraction. Despite this limitation, there were reasonable agreements between the calculated extraction constants and the experimentally obtained values (Karaman *et al.*, 1984). Therefore, a rough estimate of the extraction constants provides a useful guide in predicting the magnitude of MnO_4^- transfer.

Successful use of phase transfer catalysis for enhancing the oxidation of TCE by MnO_4^- requires the optimal matching of organic phases and PTCs to obtain the maximum ionic transfer. For illustrative purposes, consider a case where an oxidation scheme is used to remediate a ground-water system contaminated by a single chlorinated solvent. The contaminant in this case is considered as an organic phase as well as a target organic reactant (RX_{org}). The extraction capability of the chlorinated solvent depends on the chemical structure (Bränström, 1976). Generally, somewhat more polar solvents have greater capabilities in extracting ion pairs but strongly nonpolar solvents reduce the solubility of PTCs in the organic phase to such an extent that reactions are slowed or inhibited (Table 1).

Although some organic solvents (e.g., TCE) have small extraction constants, significant extraction can be achieved by selecting an appropriate ionic reactant and PTC. Because MnO_4^- has a high affinity for association with most of the catalytic cations and the ion pair has a high lipophilicity (Makosza and Bialecka, 1976), the selection of catalysts is a key element in the design of an effective catalytic oxidation scheme. Extensive solubility measurements made by Karaman *et al.* (1984) reveal that the structure of the catalyst is one of the most important factors determining the efficiency of catalysis. There is a linear relationship between the solubility of the ion pair and the number of carbon atoms for quaternary ammonium with different solvents (Table 2). Quaternary cations with larger radii also have the advantage of a smaller activation energy, which facilitates the release of the ionic reactant from the ion pair and participation in the displacement reaction (Starks, 1997; Ugelstad *et al.*, 1966). However, the use of quaternary ammonium with long alkyl groups would promote the generation of a stable emulsion that inhibits the transfer of aggregated ion pairs (Rao and Rao, 1991; Starks, 1971). The increasing activation efficiency with symmetrical quaternary cations having longer alkyl groups also levels off in the range of pentyl to octyl (Starks, 1997). Therefore, quaternary cations with extremely long alkyl chains would not be recommended in choosing a PTC.

In addition to the structure, the concentration of the catalyst is also an important factor in speeding up the catalysis reaction. Because the reaction rate is dependent on the catalyst concentration, using a small quantity of catalyst would only make sense if the conversion is

highly exothermic or the catalyst is very expensive. However, care is required in increasing the concentration of a catalyst beyond the solubility of catalyst-anion salts in the aqueous phase in order to avoid potential aggregation or precipitation of solids causing pore plugging.

Physical disturbance of the phases in the reaction system is also an important factor controlling the transfer step. Without the agitation, which is the case in ground-water systems, interfacial diffusion would be the main driving force for anion transfer. Phase transfers could be increased when tiny droplets of one phase end up scattered in the other. This distribution of phases maximizes the interfacial area for diffusional anion transfers. This effect could be important in ground-water settings. The relatively intimate dispersal of one phase in another is often found with the residual saturation of the nonwetting fluid in ground-water/DNAPL systems (Wilson and Conrad, 1984). In laboratory experiments, some agitation is essential not only to enhance the transfer but also to break down the thin stagnant layer occurring at the interface (Tomoi and Ford, 1981). With an increasing agitation rate, the overall rate of the catalytic reaction increases. Eventually, the point is reached where the intrinsic displacement process becomes rate controlling rather than the transfer step (Landini *et al.*, 1986).

There have been many studies of the reactions between MnO_4^- and various alkenes in the organic phase (Harris and Case, 1983; Lampman and Sharpe, 1983; Ogito and Mochizuki, 1979; Sala and Sargent, 1978; Sam and Simmons, 1972; Starks, 1971; Weber and Shepherd, 1972). Due to the high reactivity of MnO_4^-, fast reactions between MnO_4^- and alkenes were reported in common solvents such as benzene and methylene chloride. Nonetheless, few experimental results are available for TCE degradation in an organic phase. Also, the lack of solubility data for common PTCs except tetra-n-butylammonium in TCE makes it difficult to predict MnO_4^- transfer into the pure TCE phase. As a proof-of-concept work, our study was concentrated on the enhancement of overall TCE decomposition with permanganate oxidation in the presence of pure TCE phase and selected PTCs, instead of individual processes like MnO_4^- transfer and organic-phase displacement reactions.

3. Materials and methods

3.1. Phase transfer catalyst

Three PTCs, tetra-n-ethylammonium bromide (TEA, $(C_2H_5)_4NBr$, 99.9 %), tetra-n-butylammonium bromide (TBA, $(CH_3(CH_2)_3)_4NBr$, 99.9 %), and pentyltriphenylphosphonium bromide (PTPP, $CH_3(CH_2)_4P(C_6H_5)_3Br$, 99.8 %) were obtained from Aldrich Chem. Co. The catalysts were selected on the basis of their extraction constants (K_E) and molecular structures (Table 3). Due to the lack of available solubility data for TCE, estimated extraction constants for methylene chloride were used to guide the selection of PTCs. The concentration of selected PTCs in all experiments was kept below the aqueous phase solubility in order to avoid aggregation and precipitation of catalyst-permanganate salts.

3.2. Permanganate Oxidation

We conducted kinetic batch experiments to study the rate of permanganate oxidation of TCE in the presence of the selected catalysts. The $KMnO_4$ solution (2.5 mM) was prepared by dissolving $KMnO_4$ crystals in a phosphate-buffered solution (0.1 M, $KH_2PO_4 : K_2HPO_4$, pH=8). Concentrated catalyst stock solutions were also prepared with the buffer solution. Based on previous research (Makosza and Bialecka, 1976; Dehmlow and Dehmlow, 1983), it was assumed that the catalysts would hardly mobilize phosphate ion and as a result, the interference on the interaction between permanganate ion and the catalyst would be negligible. Four sets of 9-mL test tubes with Teflon-lined caps were utilized. Each set was made up of 12 tubes and the four sets were allocated to the three catalysts and one control, respectively. 3.0-mL of $KMnO_4$ solution was placed in the test tubes. 0.1-mL of concentrated catalyst solution was added to the tubes to provide a final catalyst concentration of 10-mole % $KMnO_4$. After the solution was homogenized with gentle shaking, we added 1.0-mL of TCE (99.5 %, Aldrich Chem. Co.) to the permanganate solution. All of the test tubes were stirred frequently to keep the solution homogeneous but not mixed so intensely that a TCE macroemulsion formed or the surface area of the TCE changed. A 1.5-mL sample from the aqueous phase was taken from one tube of each set every five minutes. We evaluated samples for TCE degradation by measuring the chloride concentration and UV absorbance for MnO_4^-.

A 1.0-mL sample was transferred into a quartz cuvette with 1-cm pathline and scanned using a Varian Cary 1 UV-visible spectrophotometer at wavelengths ranging from 400 to 600 nm. The phosphate buffer solution was scanned as a reference. In this range of wavelengths, MnO_4^- has a maximum absorbance at 525 nm and is almost transparent at 418 nm (Stewart, 1965). The absorbance at 418 nm is a measure of the concentration of either cyclic hypomanganate ester (Lee and Brownridge, 1973; Wiberg *et al.*, 1973) or a soluble form of colloidal manganese dioxide (Mata-Perez and Perez-Benito, 1985; Simandi and Jaky, 1976).

The addition of PTCs to the permanganate solution did not impact the UV absorbance across the range of wavelengths of interest. UV absorbance was also used to monitor the consumption of PTCs in the permanganate reaction. UV absorbance, measured for a control without TCE, did not show any difference from the initial scan after more than 30 days.

Chloride concentration was measured using a Labconco Digital Chloridometer, which works by a coulometric titration of chloride ions (Cotlove, 1958). A 0.1-mL aliquot was mixed with 0.1-mL of sodium thiosulfate (6 mg/mL) in 5.0-mL reaction vessel. The sodium thiosulfate acts as reducing agent to quench the oxidation reaction in the sample solution. 3.0-mL of concentrated acid reagent (0.4 N HNO_3 and 40 % glacial acetic acid) was added to the reaction vessel before finally adding 4 drops of gelatin reagent. The samples in the reaction vessel were titrated at the HIGH switch position. The measured concentrations (mEq/L) for Cl^- in the sample were compared with those for standards. Chloride standards were prepared using KCl dissolved in the same phosphate buffer solution with the same concentration of $KMnO_4$ and catalysts. Thus, a separate set of standard was prepared for each catalyst and the control. All experiments were conducted at room temperature of $22 \pm 1°C$.

3.3. Solubility Enhancement

The kinetics of TCE dissolution in the aqueous phase was measured in order to examine the influences of the catalysts on TCE solubility. The same kind of kinetic batch experiments was also employed, except that $KMnO_4$ was absent from the aqueous phase. 6.0-mL of

phosphate buffer (0.1 M) was mixed with a 0.2-mL solution of concentrated catalyst in 9.0-mL test tubes, before adding a 1.0-mL of TCE. Three samples (4.0-mL) were collected from the aqueous phase at 0.5, 1, and 24 hours. The sample solution was transferred into a 9.0-mL centrifuge tube and centrifuged for 10-minutes at 2500 rpm. The solution was diluted with deionized water (1/1000). 1.8-mL of diluted sample was mixed with 5.0-mL of pentane in 25-mL amber bottles in order to extract the organic compounds. The bottles were agitated on a platform shaker for 30 minutes and equilibrated for 1 hour before taking samples for GC analysis. The pentane extractant was analyzed using a Fisons Instruments 8060 gas chromatograph equipped with a Ni^{63} electron capture detector and a DB-5 capillary column (J&W Scientific, Rancho Cordova, CA), 30 m $\times$ 0.32 mm I.D. with a film thickness of 1.0 μm. Helium was the carrier gas and nitrogen the make-up gas. For calibration standards, TCE in methanol was mixed with phosphate buffer solution containing catalysts. We kept the volume of methanol added small (0.1 % of total volume) in order to minimize cosolvent effects. For consistency, the same procedures were followed in preparing the standards for consistency. Separate standards were prepared for each catalyst and the control.

4. Results and discussion

4.1. Chloride Concentration Measurements

Because of the pure TCE phase in the system, it was not feasible to monitor TCE loss with time as a measure of oxidation rate. However, the time variation in the concentration of chloride ion can serve as an indicator for the TCE breakdown. The rates of TCE degradation with time were estimated for three catalysts and a blank as a control. As Figure 2 illustrates, the extent of reaction speedup provided by the catalysts was variable. PTPP led to a marked increase in the Cl^- concentration in the aqueous phase during the first 20 to 25 minutes of the experiment. These results suggest a remarkable enhancement to the rate of TCE degradation. After this early response, the rate of Cl^- release with time slowed. Although the greatest enhancement was evident with PTPP, the slopes obtained with two ammonium salts in Figure 2 also reflect a noticeable increase in TCE destruction as compared to the control experiment. The pattern of reaction speedup, PTPP > TBA > TEA >Blank, is consistent with the extraction constants (K_E) calculated based on the solubilities in the organic phase of methylene chloride (Table 3). In other words, PTPP with the largest extraction constant of the three was the most efficient in transferring MnO_4^- to the TCE phase. These results indicate that PTPP would be the most effective catalyst in speeding up the oxidation of TCE by MnO_4^-.

The noticeable change in reaction rates occurring at 20 to 25 minutes coincides with a concentration of Cl^- of 3.5 mEq/L (Figure 2). This Cl^- production represents about 93 % of the total Cl^- that would be expected (i.e., 3.75 mEq/L) from the stoichiometry, given an initial permanganate concentration (2.5 mM). Our calculation is based on Eq. (9);

$$C_2Cl_3H + 2MnO_4^- \longrightarrow 2CO_2 + 2MnO_2 + 3Cl^- + H^+ \qquad (9)$$

During the early phase of the reaction, MnO_4^- would mainly participate in the oxidation. After the complete consumption of MnO_4^-, less efficient oxidation can be accomplished with MnO_2,

causing TCE to breakdown more slowly. The breakpoint in reaction rates probably indicates the transition in oxidants from MnO_4^- to MnO_2.

Although MnO_4^- would form ion pairs with the catalytic cations and be transferred into the nonpolar media, we were not sure whether the catalysts would impact the oxidation of TCE by MnO_2 in the aqueous phase. The catalysts could influence the extent of hydration shell formation around MnO_2 molecules and consequently the interaction between MnO_2 and dissolved TCE could be affected. Additional work is required to study the behavior of catalysts in solution with the suspended colloidal materials.

4.2. UV/Vis Absorbance Monitoring

Once catalysts were added to the system, we observed that the color of TCE phase, initially colorless and transparent, changed to a purple color due to the permanganate transfer. The TCE phase became clear once the reaction was completed and the MnO_4^- was used up. The purple color of the TCE phase was most distinct with PTPP. We measured of the concentration of MnO_4^- in the aqueous phase with time using UV/Vis absorbance measurements. Figure 3 displays UV/Vis spectra successively changing with time for the four different treatments. Decreases in the maximum absorbance at 526 nm indicated the loss of MnO_4^- as it reacted with TCE. The rapid decrease of maximum absorbance with PTPP confirms that PTPP is the most efficient catalyst in transferring MnO_4^- into the TCE phase, and in enhancing the permanganate consumption. This result is consistent with the other observations, such as the rapidly increasing Cl^- concentration observed in the PTPP-catalyzed reaction and the distinct coloration of TCE phase with permanganate transfer.

The UV/Vis spectra showed an isobestic point at 469 nm until the point shifted to a lower wavelength after about 40 minutes (Figure 3). This shift in the isobestic point in the spectra was observed earlier with PTPP than with other catalysts. The shift might be caused by the precipitation of MnO_2. Variation in absorbance at 418 nm (Figure 4) indicates the precipitation of MnO_2 (Mata-Perez and Perez-Benito, 1985). The highest absorbance at 418 nm corresponded to the starting point for MnO_2 precipitation. The subsequent decrease in the magnitude is due to the removal of MnO_2 from the solution by precipitation. The time taken to reach the maximum absorbance at 418 nm was about 30 minutes with PTPP, less than any of the other treatments. The time for conversion of soluble manganese species to MnO_2 was likely reduced due to the rapid permanganate oxidation. The more rapid loss of MnO_4^- and formation of MnO_2 were evidence for accelerated TCE oxidation with PTPP.

The disappearance of MnO_4^- with TCE oxidation can be quantified with UV/Vis absorbance at 526 and 418 nm. Because MnO_4^- is almost transparent at 418 nm and both species absorb light at 526 nm (Stewart, 1965), the absorbance (A) at 418 and 526 nm can be given as;

$$A_{418} = \varepsilon_{MnO_2}^{418}(c_o - c_t) \tag{10}$$

$$A_{526} = \varepsilon_{MnO_4^-}^{526} c_t + \varepsilon_{MnO_2}^{526}(c_o - c_t) \tag{11}$$

where ε is the molar absorptivity of the manganese species (MnO_2 or MnO_4^-) at the wavelength (418 or 526 nm), c_o is the initial MnO_4^- concentration, c_t is the concentration of MnO_4^- at time t (Freeman and Kappos, 1985; Mata-Perez and Perez-Benito, 1985). From Eq. (10) and (11), we can deduce an equation for MnO_4^- concentration;

$$\frac{c_t}{c_o} = \frac{A_{526} - (\varepsilon_{MnO_2}^{526} / \varepsilon_{MnO_2}^{418}) A_{418}}{\varepsilon_{MnO_4^-}^{526} c_o} \qquad (12)$$

The denominator on the right side of Eq. (12) is equal to the absorbance of initial permanganate solution at 526 nm. The ratio of molar absorptivity for MnO_2 in the numerator was measured after MnO_4^- had been used up completely. This equation is based on assumptions that there are no other manganese species except MnO_4^- and MnO_2 and that flocculation or precipitation of MnO_2 in the solution is minimal over the time of concern.

The variation in MnO_4^- concentration, expressed as log (c_t/c_o) with time, is depicted in Figure 5. As expected, the MnO_4^- concentration was reduced faster with PTPP than with other treatments. The functions were convex, which probably result from the shortage of MnO_4^- available to react with TCE later in the experiment. As MnO_4^- concentration decreases with consumption in the reaction, TCE concentration increases slightly because of the continuous dissolution of pure phase. Because these two parameters vary in the course of the reaction, it cannot be considered strictly as a pseudo-first-order reaction. However, to help compare results, pseudo-first-order rate constants (k) were determined from the slopes of the log (c_t/c_o) versus time data in Table 4, using only the early straight portion of curves. We calculated stoichiometrically destroyed TCE amounts with chloride concentrations, assuming that MnO_4^- was present in excess in the system and that chloride release is a zero-order reaction within 15 minutes of reaction time (Table 4). The rate constants and destructed TCE amount verified that the consumption of MnO_4^- and the degradation of TCE were more rapid with PTPP than the other catalysts and potassium permanganate by itself.

4.3. Dissolution of TCE

Quaternary ammonium or phosphonium salts used as PTCs have structural features in common with surfactants employed in remedial systems. The capability of surfactants to solubilize nonpolar organic solutes in the aqueous phase is well known (Rosen, 1978; Schwartz and Perry, 1978). The problem for our experiments is that the solubilization in the aqueous phase, if it occurred, might enhance rates of TCE destruction. Effectively, enhanced solubility could increase the rate of transfer of TCE into the aqueous phase. Accordingly, we undertook experiments to examine the potential for the solubility enhancement of TCE by PTCs (TBA and PTPP). The experiments involved kinetic batch experiments, looking at TCE increase in the solution with time, as a function of the additives. The results showed no significant difference in TCE concentration for the first 30 minutes, as compared to trials without PTCs (Figure 6). Overall, there was a tendency for somewhat reduced solubilities with the PTCs after 24 hours of equilibrium.

Commonly surfactants consist of a long hydrophobic alkyl chain and a large hydrophilic head. PTCs are different in that they are relatively short chains. Because of this structural difference with other surfactants, the formation of pseudophase micelles through self-association is minimal even at the high concentration of PTCs. As a result, the solubilization power of PTCs is not comparable to common surfactants, as our experiments show. In addition, below the critical micelle concentration of surfactants, no significant enhancement in the solubility of nonpolar organic solutes is usually observed (Kile and Chiou, 1989; Moroi *et al.*, 1983). Considering the relatively large solubility of TCE in the aqueous phase (≅ 1100 mg/L), a small increase in TCE concentration with the addition of small amount of PTC would not measurably increase rates of permanganate oxidation of TCE in the aqueous phase.

Our experiments suggest that there is no enhancement in the rate of TCE decomposition due to solubilization by the PTCs. To the contrary, the concentration of TCE is reduced with the addition of PTCs. This behavior is explainable as a salting-out effect, whereby the solubility of organic compounds would be reduced in high salinity solutions.

5. Conclusions

These preliminary experiments point to significant opportunities for enhancing the oxidation of chlorinated solvents, like TCE, by MnO_4^-. Speedup in oxidation rates was evidenced in our experiments by (1) an increase in the rate of Cl^- production, (2) a more rapid disappearance of MnO_4^- from the aqueous phase, and (3) qualitative changes in the coloration of the TCE phase (clear, to purple, and to clear). Experimental evidence discounted the possibility that the solubilization of TCE in the aqueous phase contributed to the rate enhancement. All of the results confirm that the enhancement in TCE decomposition is due to reactions between MnO_4^- and TCE in the nonaqueous phase, in addition to oxidation of TCE in the aqueous phase.

Of all the catalysts, PTPP was most effective in transferring the reactant into the nonaqueous phase and promoted the greatest increase in the oxidation rate. Theory also provides a useful way to screen potential PTCs for use in remedial applications, for example, the largest extraction constant (K_E), was determined for PTPP, which turned out to be the most efficient catalyst for MnO_4^- transfer.

We think that phase transfer catalysis has some potential for application in DNAPL remediation. Catalyzed nonaqueous phase reactions could not only increase contaminant degradation rates but also help reduce costs for permanganate recirculation by increasing permanganate participation in the remedial scheme. The catalytic reaction would be most effective for contaminants with an extremely low solubility in the aqueous phase. Such contaminants are often hard to treat in aqueous reaction systems. Extensive studies on the nonaquatic decomposition of the contaminants would be required to explore more efficient PTCs and target contaminants.

In field situations, contaminants can occur as a mixture of various organic compounds in a field situation. A catalytic reaction system could be designed to optimize the effectiveness of the destruction, when individual compounds are considered separately as organic solvents for catalysts or target solutes for the reactions. Some chlorinated ethylenes such as TCE, *trans*-DCE and 1,1-DCE are very reactive with MnO_4^- but they are poor solvents for quaternary ammonium salts. Some chlorinated ethanes including perchloroethane and trichloethane are not very

reactive with MnO_4^- but they are excellent solvents for quaternary ammonium salts. The effectiveness of the catalysis would be maximized in the field when these two groups of compounds are found together. Clearly, additional experimental work is required to study DNAPL mixtures in order to elucidate processes of phase transfer catalysis in a more realistic situation.

There is a concern that MnO_4^- might be consumed by organic matter in soils and sediments prior to reaching the target contaminant. The same kind of problem could develop with PTCs because they are cationic and may be strongly attracted by cation exchange sites on soil and sediment surfaces. Work is needed to examine the affinity of PTCs for adsorption and whether this process might reduce their effectiveness as catalysts. There are potential work-arounds to this problem. For example, one could pretreat the geological medium to add other cations to exchange sites, or develop an injection technology that delivers the solution directly to the target contaminants.

We are continuing work to develop the catalytic scheme for permanganate oxidation. We are interested in further studying mechanisms of catalytic reaction in nonaqueous phase with various PTCs and the impact of PTC addition on DNAPL mobility and solubility. Evaluation of phase transfer assisted solvent oxidation at larger scales including column or tank experiment is required before any field demonstrations.

Acknowledgements

We thank Mr. Sang-suk Lee for his help with the experimental work over the course of the study. This material is based upon work supported by the Department of Energy under Grant No. DE-FG07-96ER14735.

References

Bränström, A., 1976. Preparative ion pair extraction. Apotekarsocieteeten/Hassle, Lakemedel, Sweden, 168 pp.

Bränström, A., 1977. Principles of phase-transfer catalysis by quaternary ammonium salts. Adv. Phys. Org. Chem., 15: 267.

Cotlove, E., 1958. An instrument and method for automatic, rapid, accurate and sensitive titration of chloride in biologic samples. J. Lab. Clin. Med., 51: 461-468.

Dehmlow, E.V. and Dehmlow, S.S., 1983. Phase transfer catalysis. Verlag Chemie, Weinheim, Germany, 386 pp.

Freeman, F. and Kappos, J.C., 1985. Permanganate ion oxidations. 15. Additional evidence for formation of soluble (colloidal) manganese dioxide during the permanganate ion oxidation of carbon-carbon double bonds in phosphate-buffered solutions. J. Am. Chem. Soc., 107(23): 6628-6633.

Glaze, W.H. and Kang, J.K., 1988. Advanced oxidation processes for treating groundwater contaminated with TCE and PCE; laboratory studies. J. AWWA, 80: 57-63.

Harris, J.M. and Case, M.G., 1983. Poly(ethylene glycol) ethers as recoverable phase-transfer agents in permanganate oxidations. J. Am. Chem. Soc., 48: 5390-5392.

Johnson, R.L. and Pankow, J.F., 1992. Dissolution of dense chlorinated solvents into groundwater. 2. Source functions for pools of solvent. Environ. Sci. Technol., 26(2): 896-901.

Karaman, H., Barton, R.J., Robertson, B.E. and Lee, D.G., 1984. Preparation and properties of quaternary ammonium and phosphonium permanganates. J. Org. Chem, 49: 4509-4516.

Kile, D.E. and Chiou, C.T., 1989. Water solubility enhancements of DDT and Trichlorobenzene by some surfactants below and above the critical micelle concentration. Environmental Science and Technology, 23(7): 832-838.

Lampman, G.M. and Sharpe, S.D., 1983. A phase transfer catalyzed permanganate oxidation preparation of vanillin from lsoeugenol acetate. J. Chem. Edu., 60(6): 503-504.

Landini, D., Maia, A. and Rampoldi, A., 1986. Stability of quaternary onium salts under phase-transfer conditions in the presence of aqueous alkaline solutions. J. Org. Chem., 51: 3187-3192.

Lee, D.G. and Brownridge, J.B., 1973. The oxidation of cinnamic acid by permanganate ion. spectrophotometric detection of an intermediate. J. Am. Chem. Soc., 95: 3033-3034.

Makosza, M. and Bialecka, E., 1976. A simple preparation of anhydrous tetraalkyammonium salts. Synth. Commun., 6(4): 313-318.

Mata-Perez, F. and Perez-Benito, J.F., 1985. Identification of the product from the reduction of permanganate ion by trimethylamine in aqueous phosphate buffers. Can. J. Chem, 63: 988-992.

Moroi, Y., Noma, H. and Matura, R., 1983. Solubilization of N-Alkylphenothiazine in aqueous anionic surfactant micelles. J. Physic. Chem., 87(5): 872-876.

Ogito, T. and Mochizuki, K., 1979. Homogeneous permanganate oxidation in non-aqueous organic solution. Selective oxidations of olefins into 1,2-diols or aldehydes. Chemistry Letters: 443-446.

Plumb, R.H., 1991. The occurrence of appendix 1X organic constituents in disposal site groundwater. Ground Water Monitoring Review(Spring): 157-165.

Rao, K.H. and Rao, M.B., 1991. Studies in phase transfer catalysis. part-1. Permanganate oxidation. J. Indian Chem. Soc., 68: 132-134.

Rosen, M.J., 1978. Surfactants and interfacial phenomena. John Wiley and Sons, New York, NY.

Sala, T. and Sargent, M.V., 1978. Tetrabutylammonium permanganate: an efficient oxidation for organic substrates. J.C.S. Chem. Comm.: 253-254.

Sam, D.J. and Simmons, H.E., 1972. Crown polyether chemistry. potassium permanganate oxidation in benzene. J. Am. Chem. Soc., 94(11): 4024-4025.

Schnarr, M. *et al.*, 1998. Laboratory and controlled field experiments using potassium permanganate to remediate trichloroethylene and perchloroethylene DNAPLSs in porous media. J. Contam. Hydro., 29: 205-224.

Schwartz, A.M. and Perry, J.W., 1978. Surface active agents- their chemistry and technology. Robert E. Krieger Publishing Co., Huntington, NY.

Simandi, I. and Jaky, M., 1976. Nature of the detectable intermediate in the permanganate oxidation of trans-cinnamic acid. J. Am. Chem. Soc., 98: 1995-1997.

Starks, C.M., 1971. Phase-Transfer Catalysis. I. Heterogeneous Reactions Involving Anion Transfer by Quaternary Ammonium and Phosphonium Salts. J. Am. Chem. Soc., 93(1): 195-199.

Starks, C.M., 1997. Modern perspectives on the mechanisms of phase-transfer catalysis. In: M.E. Halpern (Editor), ACS Symposium Series, 659. Phase-transfer catalysis; mechanism and synthesis. ACS, Washington, DC, pp. 10-28.

Starks, C.M., Liotta, C.L. and Halpern, M., 1994. Phase-transfer catalysis; fundamentals, applications, and industrial perspectives. Champman & Hall, New York, NY, 668 pp.

Stewart, R., 1965. Oxidation by permanganate. In: K.B. Wiberg (Editor), Oxidation in organic chemistry, part A. Academic Press, New York, NY, pp. 1068.

Tomoi, M. and Ford, W.T., 1981. Mechanisms of plymer-supported catalysis. 1. Reaction of 1-bromeoxtane with aqueous sodium cyanide catalyzed by polystyrene-bound benzyltri-n-butylphosphonium ion. J. Am. Chem. Soc., 103: 3821-3827.

Ugelstad, J., Ellingsen, T. and Berge, A., 1966. The effect of the solvent on the reactivity of potassium and quaternary ammonium phenoxides in nucleophilic substitution reactions. Acta Chem. Scand., 20: 1593-1598.

Vella, P.A. and Veronda, B., 1992. Oxidation of trichloroethylene; comparison of potassium permanganate and Fenton's reagent, The third international symposium on chemical oxidation technology for the nineties, Nashville, TN.

Vogel, T.M., Criddle, C.S. and McCarty, P.L., 1987. Transformation of halogenated aliphatic compounds. Environ. Sci. Technol., 21: 722-736.

Weber, W.P. and Shepherd, J.P., 1972. An improved procedure for the $KMnO_4$ oxidation of olefins to cis-1,2-glycols by use of phase transfer catalysis. Terahedron Letters, 48: 4907-4908.

Westrick, J.J., Mello, J.W. and Thomas, R.F., 1984. The groundwater supply survey. J. AWWA(May): 52-59.

Wiberg, K.B., Deutch, C.J. and Rocek, J., 1973. Permanganate oxidation of crotonic acid. spectrometric detection of an intermediate. J. Am. Chem. Soc., 95: 3034-3035.

Wilson, J.L. and Conrad, S.H., 1984. Is physical displacement of residual hydrocarbon a realistic possibility in aquifer restoration?, Proc. of the NWWA.API conference on petroleum hydrocarbon and organic chemicals in groundwater-prevention, detection, and restoration. National Water Well Association, Dublin, OH, pp. 274-298.

Yan, Y.E., 1998. Abiotic remediation of ground water contaminated by chlorinated solvents. Ph.D. Thesis, The Ohio State University, 105 pp.

Yan, Y.E. and Schwartz, F.W., 1999. Oxidative degradation and kinetics of chlorinated ethylenes by potassium permanganate. J. Contam. Hydro., 37: 343-365.

Zhang, H. and Schwartz, F.W., 2000. Simulations of oxidative treatment of chlorinated compounds by permanganate. Submitted.

Table 1. Effect of selected organic solvents on extraction constants of tetrabutylammonium bromide (Bränström, 1976)

Solvent	$K_{E\text{-NBu4Br}}$
CH_3CHCl_2	0.5
$ClCH_2$-CH_2Cl	6.1
$ClCH_2$-$CHCl_2$	8.6
Cl_2CH-$CHCl_2$	145
C_6H_5Cl	<0.1
o-$Cl_2C_6H_4$	<0.1
$CH_2=CCl_2$	<0.1
trans-ClCH=CHCl	<0.1
cis-ClCH=CHCl	33
$ClCH=CCl_2$	0.2

Table 2. Effect of catalyst structure on solubilities (M) of quaternary ammonium and phosphonium permanganates (Karaman, et al. 1984)

cation	CH_2Cl_2	$CHCl_3$	$C_6H_5CH_3$	CCl_4	H_2O
tetraethylammonium	0.235	a	b	b	7.30×10^{-2}
tetra-n-butylammonium	0.076	a	b	b	3.83×10^{-2}
tetra-n-propylammonium	0.417	0.221	3.44×10^{-4}	2.96×10^{-5}	2.10×10^{-2}
tetra-n-pentylammonium	0.482	0.261	5.59×10^{-5}	2.42×10^{-5}	9.29×10^{-5}
tetra-n-hexylammonium	0.545	0.339	5.81×10^{-5}	3.51×10^{-5}	b
tetra-n-heptylammonium	0.645	0.604	6.28×10^{-5}	7.48×10^{-5}	b
tetra-n-octylammonium	0.713	0.229	4.02×10^{-4}	5.93×10^{-4}	b
n-propyltriphenylphosphonium	0.083	1.03	3.57×10^{-5}	b	1.09×10^{-4}
n-butyltriphenylphosphonium	1.16	1.15	3.18×10^{-5}	b	3.80×10^{-4}
n-pentyltriphenylphosphonium	1.46	1.56	2.38×10^{-4}	b	2.40×10^{-4}
n-hexyltriphenylphosphonium	1.36	1.28	2.02×10^{-4}	b	7.63×10^{-4}
n-heptyltriphenylphosphonium	1.36	1.28	2.02×10^{-4}	b	7.53×10^{-4}

a; unstable, b;insoluble

Table 3. Chemical properties of selected PTC- MnO_4^- ion pairs.

Name/PTCs	Abbr.	FW[a]	S_w[b]	S_o[b]	$\log K_E$[c]
tetraethylammonium	TEA	165.71	7.30×10^{-4}	0.235	1.64
tetrabutylammonium	TBA	277.92	2.10×10^{-4}	0.417	4.98
pentyltriphenylphosphonium	PTPP	413.35	2.40×10^{-4}	1.460	7.40

FW; formula weight (g/mole), S_w; solubility (M) in water, S_o; solubility (M) in methylene chloride, a; formula weight of bromide salts only, b; Karaman, et al., (1984), c; calculated with Eq. (8)

Table 4. Pseudo-first order rate constants for permanganate consumption and TCE degradation by oxidation with permanganate

catalyst	Control	TEA	TBA	PTPP
[a] k (min^{-1})	0.0475	0.0424	0.0408	0.0791
r^2	0.9857	0.9926	0.9962	0.9927
[b] TCE destroyed (mg/min.)	0.0169	0.0188	0.0185	0.0248

[a] calculated from straight portion of relationships between log (c_t/c_o) and time (15 min).

[b] calculated with chloride concentration assuming zero-order destruction rate within 15 min in the presence of excessive amount

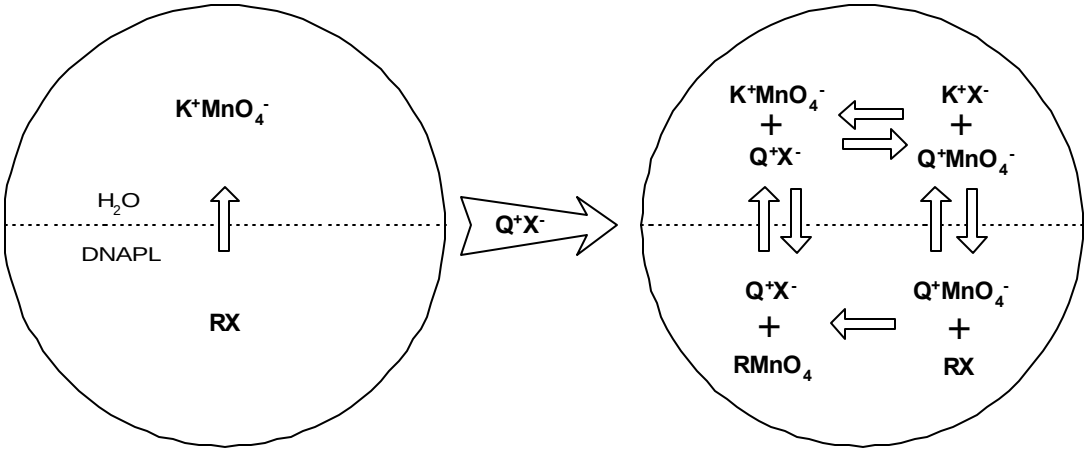

Figure 1. Schematic Diagram of Phase-Transfer Catalyst Facilitated Permanganate Oxidation of nonaqueous phase TCE. RX is the organic reactant (e.g., TCE) with leaving group X^- (e.g., Cl^-). Q^+ is the catalytic cation.

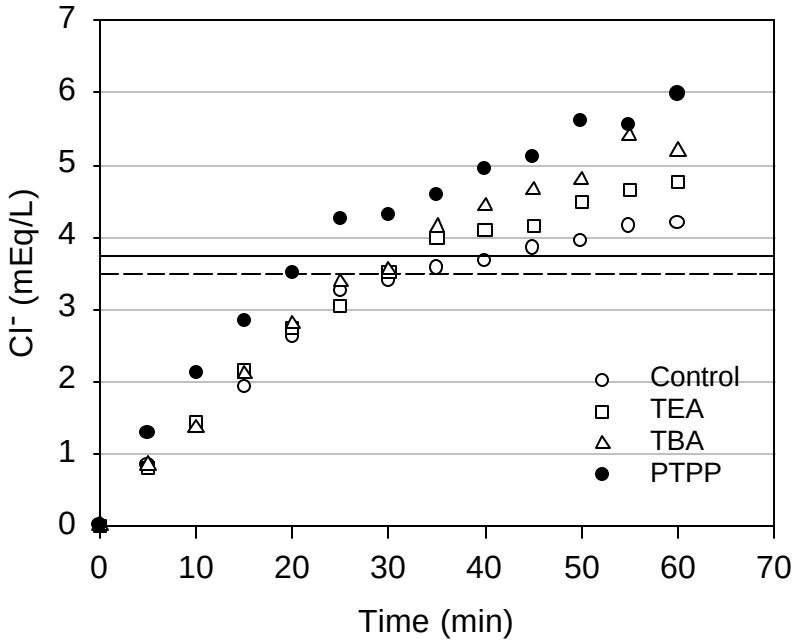

Figure 2. Concentration of chloride ion released from permanganate oxidation of TCE with different PTCs. Horizontal lines indicate the stoichiometrically expected chloride concentration from complete consumption of MnO_4^- (solid) and the experimentally measured chloride concentration (dotted).

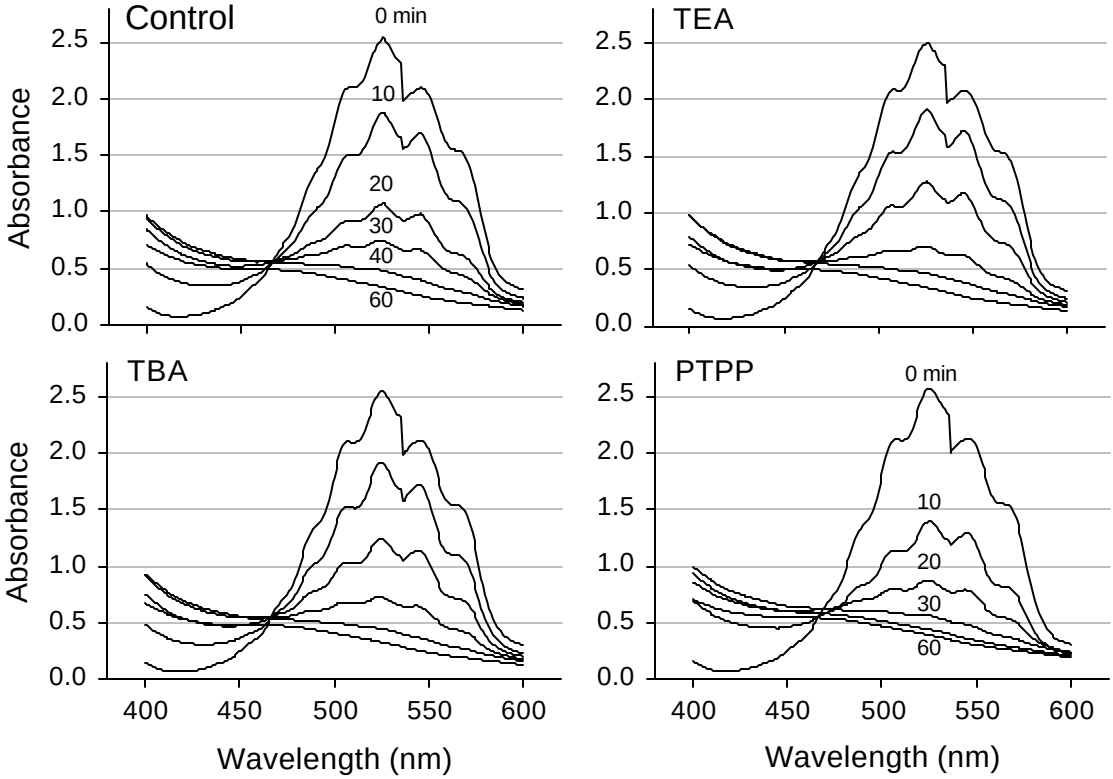

Figure 3. UV-Vis spectra of aquous phase in permanganate oxidation of TCE facilitated with diffetent PTCs. Numbers on graphs indicate the reaction time (min).

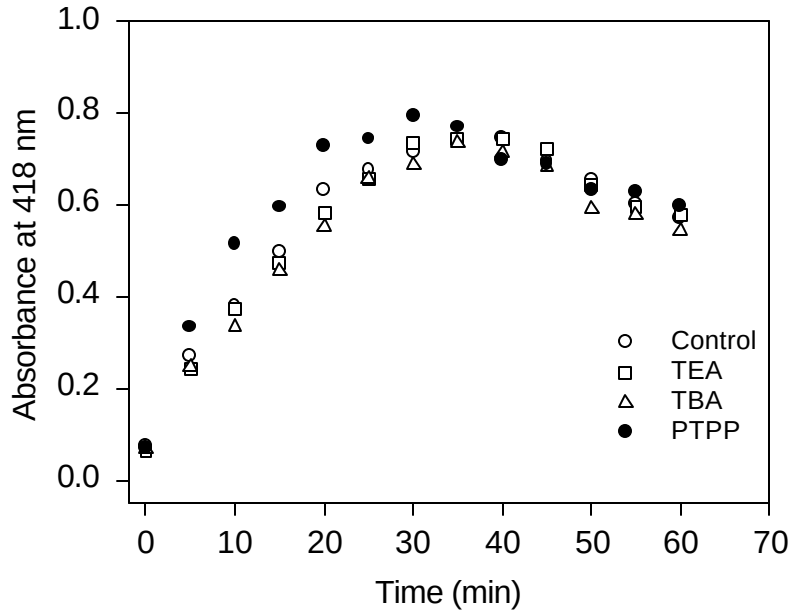

Figure 4. Variation of the absorbance at 418 nm with time in the aqueous phase as a consequence of TCE oxidation by MnO_4^- catalyzed with different PTCs

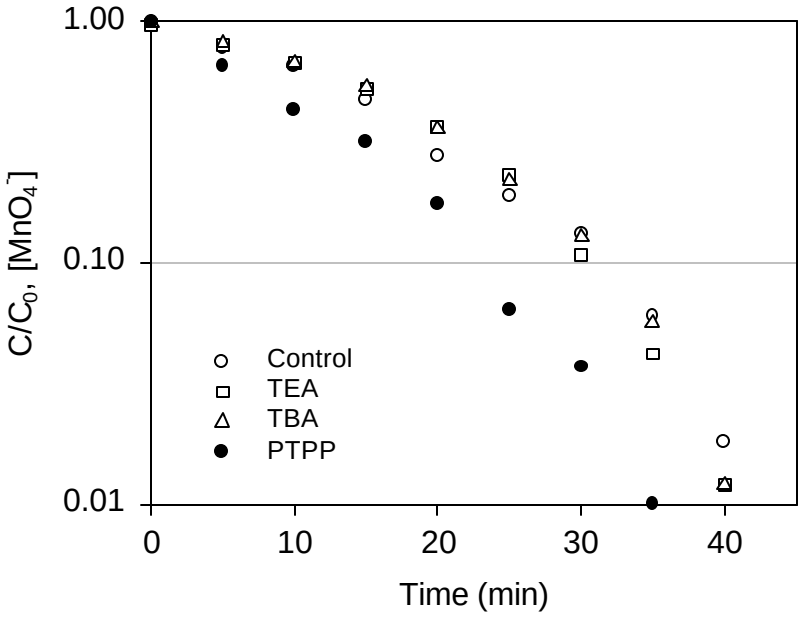

Figure 5. Relative concentration of MnO_4^- in aquous phase as a consequence of TCE oxidation catalyzed with different PTCs

OXIDATION OF BINARY DNAPL MIXTURES USING POTASSIUM PERMANGANATE WITH A PHASE-TRANSFER-CATALYST

by

Yongkoo Seol[a]*, Franklin W. Schwartz[a,b] , and Sangsuk Lee[b]
[a]Department of Geological Sciences and
[b]Environmental Sciences Graduate Program
The Ohio State University,
Columbus, OH 43210 USA

Submitted to;

Ground Water Monitoring and Remediation

August 16, 2000

*Corresponding Author
Phone: (614) 292-0585
Fax: (614) 292-7688
e-mail: seol.2@osu.edu

Oxidation of Binary DNAPL Mixtures Using Potassium Permanganate with a Phase-Transfer-Catalyst

Yongkoo Seol[a]*, Franklin W. Schwartz[a,b] , and Sangsuk Lee[b]
[a]Department of Geological Sciences and
[b]Environmental Sciences Graduate Program
The Ohio State University,
Columbus, OH 43210 USA

ABSTRACT

Phase-transfer-catalysts (PTCs) can enhance the oxidation of pure DNAPLs using potassium permanganate by facilitating reactions in the organic phase. This study examined the influence of pentyltriphenylphosphonium bromide (PTPP) as a PTC on the rate of permanganate (MnO_4^-) oxidation of DNAPLs in pure phases and mixtures. Kinetic batch experiments with trichloroethylene (TCE), 1,1,2-trichloroethane (TCA), tetrachloroethylene (PCE), 1,1,2,2-tetrachloroethane (TECA), and their mixtures (1:1, v/v) were performed in test tubes to assess reaction rates. The disappearance of MnO_4^- was quantified by capturing digital images of the tubes. This rapid photographic monitoring approach was validated by comparison with an UV-Vis spectrometer method. The PCE/TCA mixture was selected to examine the impact of relative contents of a component in the binary mixture on the MnO_4^- disappearance. The comparative rates of MnO_4^- consumption for pure phases were TCE > TECA > PCE > TCA. PTPP increased MnO_4^- consumption rates, especially for TCE and TECA as pure phases. The consumption rates of mixtures without PTPP were lower than those including the pure phases. However, due to their high extraction capability for PTPP-MnO_4^- ion pairs, TCA and TECA appeared to increase the MnO_4^- consumption significantly when they were mixed with TCE or PCE. The increase in consumption rates with PTPP was most remarkable with the mixture of PCE and TCA. Chloride concentration showed faster increases for the mixtures with relative PCE contents ranging about

5 to 90%, maximum at about 50% PCE, than for pure phases of PCE and TCA when the PTC-assisted the reactions. The PTC appears to be promising in its ability to increase oxidation rates of DNAPL mixtures.

INTRODUCTION

There has been considerable interest in the use of potassium permanganate for the in-situ destruction of chlorinated solvents. Proof-of-concept studies in the field have demonstrated the potential for mineralizing chlorinated ethenes (e.g., TCE, PCE) occurring as a dissolved phase in aqueous solution or as a pure phase (Schnarr *et al*., 1998, Siegrist *et al*., 1999). Laboratory studies have documented the reaction mechanisms, pathways, and kinetics (Yan, 1998; Yan and Schwartz, 1999; Yan and Schwartz, 2000).

At the present stage of development, significant opportunities remain in increasing the overall efficiency of flooding schemes and in speeding up the oxidation reaction. In some cases, the oxidation reactions are relatively slow in part because the reactions occur only in the aqueous phase and typical chlorinated compounds, like TCE or DCE, are not particularly soluble in water. In other cases, the oxidation reactions themselves are slow for some chlorinated ethenes (e.g., PCE) and chlorinated ethanes (e.g. TCA and TECA).

Our recent work has shown that phase-transfer-catalysts (PTCs) can speed up the overall rates of DNAPL oxidations. PTCs work by having the oxidation reaction take place in both the aqueous and DNAPL phases. A preliminary study on the effect of PTCs on TCE oxidations (Seol and Schwartz, 2000) showed that the rates of the oxidative decomposition increased considerably with the addition of PTCs.

The goal of this present study is to extend understanding on the behavior of PTCs in

mixtures of chlorinated solvents. Theory suggests that the rate of oxidation of DNAPLs can be enhanced in mixtures of solvents (e.g., PCE+TCA). This study was designed to test whether or not adding a PTC could enhance the oxidation rates of most common chlorinated solvents, occurring either as pure phases or binary mixtures. Main hypotheses of this study are (1) that the overall oxidation rates of pure DNAPLs or DNAPL mixtures in solutions carrying a PTC would be noticeably higher than would otherwise be the case with MnO_4^- only in aqueous phases; and (2) that some organic solvents may be reactive with MnO_4^- in binary organic solvents, even though they are recalcitrant in the aqueous phase. In other words, (2) examines whether the combination of a PTC with mixtures of DNAPLs could lead to a meaningful increase in the oxidation rate of a compound like PCE that is slow to be oxidized in the aqueous phase.

The relative complexity of the experimental design pushed us to develop a rapid method for collecting data from a large number of kinetic experiments. A further objective of this research then was to develop and describe a digital image-based monitoring method for measuring MnO_4^- consumption. The approach is sufficiently general that it could be applied to a variety of kinetic experiments routinely conducted for the design of remedial systems.

BACKGROUND

Generally, permanganate-oxidation reactions occur in the aqueous phase because the potassium permanganate is soluble and ends up dissolved only in the aqueous phase. Because of its polarity, MnO_4^- is not soluble in DNAPL phases. Transfer of MnO_4^- into the DNAPL phase can be accomplished using a phase-transfer agent, like quaternary ammonium or phosphonium salt or crown ether (Starks, 1971). Phase transfer catalysis is a technique for facilitating reactions between two or more agents in two or more phases, when the reaction otherwise might

be inhibited. The reaction works by complexing MnO_4^- with a PTC. The DNAPL phase can extract the association of ion and PTC, called an ion pair (Bränström, 1976) out of the aqueous phase. PTCs distribute themselves between aqueous and organic phases by forming ion pairs with the reactive anions (e.g. MnO_4^-), and bringing them into a common (organic) phase in a form suitable for reactions.

The reaction of an organic compound with MnO_4^- in the presence of a PTC (Figure 1) involves two reaction steps. The extraction step partitions the ionic pairs into the nonaqueous phase (Eq. 1). The intrinsic displacement reaction (Eq. 2) attaches the MnO_4^- to the organic reactant;

$$[Q^+X^-]_{aq} + K^+_{aq} + MnO^-_{4\,aq} \longleftrightarrow [Q^+MnO^-_4]_{org} + K^+_{aq} + X^-_{aq} \qquad (1)$$

$$RX_{org} + [Q^+MnO^-_4]_{org} \longrightarrow RMnO_{4\,org} + [Q^+X^-]_{org} \qquad (2)$$

where R is the organic reactant (e.g. TCE) with a leaving group, X (e.g. Cl^-) and Q^+ is the quaternary cation as a PTC.

The ability of a nonpolar solvent to extract ion pairs from an aqueous phase is traditionally represented by an extraction constant, K_E, (Karaman *et al*., 1984), which can be experimentally determined using solubility data with Eq. 3;

$$K_E = \frac{\text{solubility of } QMnO_4 \text{ in organic solvent (M)}}{(\text{solubility of } QMnO_4 \text{ in water})^2\ (M^2)} \qquad (3)$$

A rough estimate of extraction constants provides a useful guide for predicting the relative magnitude of the MnO_4^- transfer into different organic phases. The extraction constant appears to depend on the chemical structure (Bränström, 1976) and the dielectric constant of the organic solvent (Table 1).

Yan and Schwartz (1999) documented the rates of MnO_4^- oxidation for common

chlorinated ethenes in an aqueous phase. In general, TCE is degraded much more rapidly than PCE; alkenes are oxidized much more rapidly than alkanes, which hardly react at all. Experiments involving MnO_4^- and PTCs so far (Seol and Schwartz, 2000) have only involved a single component DNAPL system, where the organic phase is the target compound (reactant) as well as the solvent (extractant). In this earlier work, we did not examine whether PTCs would be effective in speeding up the oxidation of pure-phase PCE (Seol and Schwartz, 2000). Indications given by extraction constant (Table 1) were that PTCs would be of little help because the extraction capability for MnO_4^- ion pairs in PCE was small. In other words, the oxidation reaction in the PCE phase would be negligible because only an infinitesimal amount of MnO_4^- could be transferred as the ion pair. Extractions, however, would be higher for a mixture of PCE and a chlorinated ethane, such as TCA or TECA, which both are excellent extractants for permanganate ion pairs according to reported extraction constants (Table 1). It is likely that a catalytic reaction system will work better in a mixture than in a single component DNAPL, when one of the compounds is efficient in extracting MnO_4^- ion pairs into the mixture and providing reaction conditions. Our experiments here will examine this issue in detail with tests of binary DNAPL mixtures and a selected combination of DNAPL with varying relative contents.

MATERIALS AND METHODS

Chemicals

Four chlorinated organic solvents, trichloroethylene (TCE, 99.5%, Aldrich), 1,1,2-trichloroethane (TCA, 98%, Acros), tetrachloroethylene (PCE, 99%, Aldrich), 1,1,2,2-tetrachloroethane (TECA, 99.5%, Acros) were selected. The solvents vary in their molecular structures, extraction constants (K_E) and dielectric constants (e) (Table 1), which indicate the

variability in their reactivity with MnO_4^- and the solubility of the catalyst-MnO_4^- ion pair in the organic phase.

The study used pentyltriphenylphosphonium bromide (PTPP, 99.8%, Aldrich) as the PTC for the oxidation of pure or two-component DNAPLs (Table 2). The selection of PTPP was based on results from Seol and Schwartz (2000), which showed it to be the most efficient catalyst for the oxidation of pure-phase TCE, relative to other quaternary ammonium salts such as triethylammonium or tetrabutylammonium bromide. The extraction constants given in Table 1 are for ion pairs with tetrabutylammonium bromide, because values for PTPP are not available. However, the general trend implied by the values in Table 1 is valuable in predicting the relative magnitude of extraction for PTPP. The concentration of the PTC in all experiments was kept below its aqueous phase solubility in order to avoid any potential problems of aggregation or precipitation of catalyst-permanganate salts.

UV absorbance was used to monitor the consumption of MnO_4^- by reactions between MnO_4^- and PTPP. Spectrophotometric measurements for MnO_4^- concentration were performed as described in Seol and Schwartz (2000). A 1.0-mL sample was transferred into a quartz cuvette with 1-cm pathline and scanned using a Varian Cary 1 UV-visible spectrophotometer at wavelengths ranging from 400 to 600 nm. The phosphate buffer solution was scanned as a reference. In this range of wavelengths, MnO_4^- has a maximum absorbance at 525 nm and is almost transparent at 418 nm (Stewart, 1965). UV absorbance, measured without DNAPLs, did not show any difference from the initial scan after more than 30 days, indicating the reaction between MnO_4^- and PTPP was significantly slower than DNAPL oxidation reactions.

Photographically Monitored DNAPL Oxidation

The first set of kinetic batch experiments was performed in duplicate in test tubes with selected chlorinated solvents and their mixtures (1:1, v/v). The $KMnO_4$ solution (1.25 mM) was prepared by dissolving $KMnO_4$ crystals in a phosphate-buffered solution (0.1 M, KH_2PO_4 : K_2HPO_4, pH=8). A catalyst stock solution (3.78 mM) was also prepared with the same buffer solution. 3.0 mL of $KMnO_4$ solution was added over the DNAPL phase (1.0 mL) in each tube. 0.1 mL of concentrated catalyst solution was then added to bring the final catalyst concentration to about 10 mole % of the $KMnO_4$. All test tubes in this experiment were separated into two groups, one for the TCE group and the other for the PCE group. Each group was further divided into two sets of tubes, one of which contained PTPP as a PTC and one that did not. Each set consisted of five tubes containing three single phases; (TCE or PCE), TCA and TECA, and two mixtures; (TCE or PCE) + TCA and (TCE or PCE) + TECA, respectively. All the tubes were mechanically agitated on a reciprocating platform shaker at 200 rpm. As the MnO_4^- disappeared, the solutions changed in color from purple to clear. This pattern of change was recorded by taking digital photographs of each set of test tubes at several pre-selected times.

The conventional approach for measuring MnO_4^- concentrations in aqueous solutions relies on UV-Vis spectrophotometry. The analytical procedure requires several experimental steps, including solution transfer from a reaction vessel to a cuvette and scanning a certain range of wavelengths. During the transfer step and one or two minutes of scanning, reactions are still underway. There are obvious difficulties then in simultaneously handling a number of samples with rapid reaction rates.

To overcome this problem, we have developed a quick quantification scheme for measuring the concentration of MnO_4^- in aqueous phases. This digital image-processing method provides the relative concentration of residual MnO_4^- indirectly as a function of the transmittance

(T) of visible light. The transmittance is the ratio of the emerging light intensity (I) to the incident light intensity (I_o). It is logarithmically related to the absorbance (A) of light passing through the solution (Eq. 4).

$$A = \log\left(\frac{I_0}{I}\right) = -\log T \tag{4}$$

The absorbance of light in a permanganate solution is directly proportional to the concentration of an absorbing species (e.g. MnO_4^-). This effect is known as the Beer-Lambert Law;

$$A = a \cdot [C] \cdot l \tag{5}$$

where [C] is the concentration of the absorbing species in the solution, a is the molar absorptivity, and l is the length of a light path. Therefore, the concentration can be obtained from the negative logarithmic relationship with the transmittance as;

$$[C] = -s \cdot \log T + b \tag{6}$$

where s is the slope of the relationship between the transmittance and the concentration and b is the intercept. Both parameters, s and b, are estimated from the calibration of standards.

MnO_4^- exhibits a maximum absorbance at a wavelength of 525 nm (Stewart, 1965), which falls in the range (500-578 nm) for green in the visible spectrum. Thus, the transmittance of green light through the potassium permanganate solution will be influenced mostly by the absorbance by MnO_4^-. The brightness level, or in other words, the luminance in the green channel for a selected area in an image can then be interpreted as the transmittance of light in the green spectral range. The luminance level in the green channel provided by image processing software can be compared with those of standards and converted to some concentration of MnO_4^- using equation (Eq. 6). However, the concentration of standards would be represented on a relative scale, as would the unknowns.

Digital images were taken using a Nikon Coolpix® 950 Digital Camera under ambient light. In order to minimize any interference, test tubes were placed in the center of a rounded screen set, which was made of non-reflective white panels (Figure 2). The positions of tubes, exposure and shutter speed for the camera were optimized from a series of test shots. The same conditions were applied to the entire set of digital photographs. The digital photographs were taken at 0, 5, 10, 30, and 150 min for TCE group and at 0, 20, 45, 90, 140, and 180 min for PCE group.

Adobe Photoshop® was used to obtain the brightness level in the green channel, or in other words, the transmittance in green, for an 1100-pixel square in the center of each tube image (Figure 2). Due to a slight variation in the brightness over the course of experiments, a small correction was applied to the data to maintain consistency in the brightness. Standards for the residual permanganate concentration (%) were prepared by mixing the initial permanganate solution (100 %) with a solution (0 %) in which MnO_4^- was used up through the oxidation reaction. Calibration of the standards showed a linear relationship between log [transmittance in green] and the residual permanganate concentration (%). For some cases where there were significant reactions in the DNAPL phase, diffusive transfer of reaction products from the organic phase caused the aqueous phase to become dark brown and cloudy with suspended particles. Because this effect resulted in an abnormally low transmittance in green, the image-based monitoring scheme couldn't be used once these products started to accumulate and affected the brightness. Fortunately, this problem tended to develop midway through an experiment so that the rate of MnO_4^- loss could be estimated using early-time data that were unaffected by the formation of particles.

Validation of Digital Photographic Monitoring

The image-based monitoring approach was validated using a kinetic batch experiment with TCE and MnO_4^-, where the MnO_4^- concentration was monitored using both the conventional analytical approach (UV-Vis spectrophotometer) and photographic monitoring. Two sets of four test tubes were prepared in the manner described above. All tubes were shaken for only 2.5 minutes in every five minutes. One tube from each set was removed from the shaker every five minutes for measurements via digital image capture and UV-Vis spectrometer. Spectrophotometric measurements for MnO_4^- concentration were performed as described earlier.

Chloride Production from Oxidation of PCE/TCA Mixtures

We conducted a second set of kinetic batch experiments to study the rate of chloride production from the permanganate oxidation of PCE/TCE mixtures in the presence of the catalyst. The solutions were prepared as described earlier. Nine sets of 9-mL test tubes with Teflon-lined caps were utilized. Each set was made up of 12 tubes and was allocated to nine mixtures of PCE and TCA with volumetric fraction that varied from 0 to 100%, respectively. All the experimental conditions were identical to those for first batch experiments. A 1.5-mL sample from the aqueous phase was taken from one tube of each set at each pre-selected time. We evaluated samples for DNAPL degradation by measuring the chloride concentration.

Chloride concentration was measured using a Labconco Digital Chloridometer, which works by a coulometric titration of chloride ions (Cotlove, 1958). A 0.1-mL aliquot was mixed with 0.1-mL of hydrazine hydrate (6 mg/mL) in 5.0-mL reaction vessel. The hydrazine hydrate acts as reducing agent to quench the oxidation reaction in the sample solution. 3.0-mL of concentrated acid reagent (0.4 N HNO_3 and 40 % glacial acetic acid) was added to the reaction

vessel before finally adding 4 drops of gelatin reagent. The samples in the reaction vessel were titrated at the LOW switch position. The measured concentrations (mEq/L) for Cl^- in the sample were compared with those for standards. Chloride standards were prepared using KCl dissolved in the same phosphate buffer solution with the same concentration of catalyst. All experiments were conducted at room temperature of 22 ± 1°C.

RESULTS AND DISCUSSION

Validation of Digital Image-based Monitoring Method

One way to quantify reaction rates in a $KMnO_4$-DNAPL system is to monitor the change in concentration of MnO_4^- in the aqueous phase. As mentioned, the concentration of MnO_4^- can be determined simply by observing how fast the purple color disappears. We tested this photographic approach by comparing results from the digital image method with conventional spectrophotometric measurement. It is worth recognizing that the spectrometric method may underestimate the concentration because the scanning starts from the upper wavelength for a certain range of wavelengths. Absorbance at the lower wavelength (418 nm) for the reaction product (MnO_2) could be higher than what it should be at the time when absorbance at the higher wavelength (526 nm) for the reactant (MnO_4^-) is measured because the reaction has been progressing during the scanning time.

Generally, the photographic estimates of MnO_4^- consumption agreed reasonably well with the results obtained from the UV-Vis spectrometer (Figure 3), even though the former were slightly higher than the latter. Pseudo-first order rate constants (k) were calculated with the relative concentrations (C/C_o) during the first 5 or 10 minutes of the reaction time (Table 3). The

digital-photographic monitoring approach appears to provide a fast and inexpensive alternative to the conventional spectrophotometric analysis.

Rates of Pure DNAPL Oxidation

The first series of experiments looked at the rates of oxidation of TCE, PCE, TECA, and TCA as pure phases. The experiments were monitored photographically, as described above, to obtain rates of the MnO_4^- consumption. MnO_4^- consumption is a good indication for the susceptibility of DNAPLs to oxidative attack by MnO_4^-. However, higher rates of MnO_4^- consumption do not necessarily indicate the quickness of complete DNAPL mineralization but it only implies rapid utilization of MnO_4^-. Because it is possible that intermediate products would be more hazardous or recalcitrant than the parent contaminants, each substance should be subject to detail examination on degradation and reaction mechanism, and until then, interpretation of the results applies to the initial response of the solvents to permanganate oxidation.

The most rapid utilization of MnO_4^- was evident with TCE and TECA (Figure 4). The slow to negligible decline of MnO_4^- in test tubes containing PCE and TCA provided indications of near-zero oxidation rates (Figure 4). We fitted pseudo-first order rate constants to obtain the estimates of MnO_4^- consumption. The rates of MnO_4^- consumption were TCE > TECA > PCE > TCA (Table 4).

When the reactions with the set of unmixed DNAPLs were catalyzed with PTPP, there was visual evidence that MnO_4^- was being transferred and reacting in the DNAPL phases. The normally clear and colorless organic phase became purple colored. Quantitatively, this change was more evident with TCA and TECA, and to a lesser extent with TCE. The color of the PCE did not appear to change. As the oxidation reaction progressed, the purple solvents gradually

changed in color to light brown, pointing to the oxidation of pure-phase DNAPLs. This second color change was most evident in TCE and TECA, while TCA remained purple.

As before, the digital monitoring looked specifically at color changes in the aqueous phase for direct comparison with noncatalyzed systems. The same relative order in MnO_4^- consumption was observed with small increases (Table 4). The increases were most obvious in test tubes containing TCE and TECA, which already exhibited large reaction rates without the PTC. Also, the increases were proportionally large for the alkanes as compared with the alkenes. These results show that MnO_4^- promoted oxidative reactions with the alkanes because these compounds were able to extract significant quantities of the MnO_4^--catalyst ion pairs. The rates of MnO_4^- consumption were barely increased for PCE and TCA with the addition of the PTC due to the extremely low extraction capability or the lack of reactivity with MnO_4^- in the nonaqueous phase.

Some of these kinetic results are in agreement with data from Yan and Schwartz (1998). The initial stage of oxidation reaction may involve a slow electrocyclic addition of permanganate ion to alkenic bond to afford cyclic manganese ester (Freeman, *et al*., 1981). PCE degradation is slower than TCE because the deficiency of electrons in the carbon double bond of PCE is too high for electrophile addition (Burdon and Tatlow, 1958). However, this idea cannot explain why TECA utilizes MnO_4^- more rapidly than TCA. Reportedly, the permanganate oxidation of alkanes may proceed via abstraction of a hydrogen atom from a tertiary position to yield alkyl hypomanganate ester (Stewart and Spitzer, 1978; Wiberg and Fox, 1963). The presence of a tertiary hydrogen atom in alkanes would determine the rates of MnO_4^- consumption through the initial bond-breaking step. However, because the elaboration of pathways was beyond the scope of this study, we cannot yet explain the faster consumption of permanganate with TECA than

TCA.

Rates of Oxidation in Binary DNAPL Mixtures

The rates of MnO_4^- consumption in DNAPL mixtures without the PTC were about the same as the weighted average of consumption for the single components. For example, the MnO_4^- consumption rates for TCE and TECA were 0.102 and 0.0435 min^{-1} (Table 4). The consumption rate for the 1:1 mixture of TCE and TECA was 0.0749 min^{-1} (Table 4). The reduction in the consumption rates might be caused by reduced dissolution of reactive components (e.g. TCE) into the aqueous phase only where the permanganate reaction would take place. For compounds that have nearly the same molecular weight in the mixture, the weight percent abundance in aqueous phase will not differ greatly from the mole fraction (Schwarzenbach, *et al*., 1993, Broholm and Feenstra, 1995). Therefore, the dissolution of reactive components such as TCE decreases in proportion to the mole fraction and the consumption rate diminishes consequently.

When the PTC was added to the system to oxidize the DNAPL, the consumption rates of MnO_4^- increased (Figure 4). The rates with the various TCE mixtures were two or three times higher as compared to those without PTPP (Table 4). The observed rate for TCE+TCA (0.145 min^{-1}) was greater than that of pure TCE (0.124 min^{-1}). The presence of TCA enhances the ability of the mixture to extract MnO_4^--PTPP ion pairs for the reaction of TCE in the DNAPL phase, even though TCA itself does not have a fast oxidation rate.

TECA not only was effective in extracting the ion pair but also tended to utilize MnO_4^- at a rapid rate. Thus, the MnO_4^- consumption rate was highest (0.155 min^{-1}) when one component (e.g., TECA) of the mixture especially promoted the extraction of the PTC and both components

had relatively large consumption rates. However, as stated earlier, permanganate consumption does not directly mean the complete mineralization of the DNAPLs. Because TECA consumes permanganate rapidly, it is not as preferred as an extractant of MnO_4^- ion pair for oxidations of other DNAPLs such as TCE or PCE.

The increase in the consumption rates of MnO_4^- with PTPP was most remarkable with the mixture of PCE and TCA (Figure 4), considering that neither compound by itself reacts with MnO_4^-, even with the catalyst added. Based on the results from pure phase experiments, it was believed that TCA barely reacts with MnO_4^- in both the aqueous and the TCA phase. Therefore, the large increase in the consumption rates for the PCE mixtures with the catalyst suggested that PCE became more reactive to MnO_4^- in the DNAPL phase. In this case, TCA acts as an extractant for MnO_4^- which oxidizes the reactant, PCE.

Chloride Production from Oxidation of PCE/TCA Mixtures

Digital image-based monitoring in the experiments discussed above revealed that PCE/TCA mixtures increase the effectiveness of oxidation by permanganate as a remediation technique. However, the experiments used only a 50:50 mixture of the two DNAPLs and typically, one DNAPL is dominant at most contaminated sites. Therefore, there was a need to examine mixtures with varying relative contents of DNAPLs in order to establish what conditions would be most amenable for PTC-assisted oxidation. By monitoring the aqueous concentration of chloride, which is an oxidation product of chlorinated solvents, we are able to quantify the rates of DNAPL oxidation in both phases.

Results of batch experiments with varying mixtures of chlorinated compounds are compared with results for pure phases (Figure 5). Chloride concentration increases as the

reaction progresses and increases faster with a higher PCE content in the various mixtures. Even with 10% PCE, chloride concentration increases more rapidly than with pure PCE. With PCE comprising 50 % of the mixture, chloride concentration increases most rapidly. As the relative proportion of PCE in mixtures is increased above 50%, chloride production shows down and approaches values for pure PCE.

Figure 6 is a summary diagram that recasts these experimental results in terms of production rates. The rates of chloride production increase rapidly as the relative abundance of PCE increases to 10 % in mixtures (Figure 6). At 10% PCE, the rate is twice that for pure PCE. Rates of chloride production reached a peak at about 50% PCE. Once the proportion of PCE was increased further, the rate of chloride production gradually decreased to approach the rate for pure PCE. The production rate did not behave in a symmetrical manner about the maximum. The rate rose much more quickly than it fell. A 90% PCE mixture has nearly same release rate as pure PCE.

In TCA-dominated DNAPL mixtures (<10% PCE), TCA efficiently extracts MnO_4^- ion pairs into the DNAPL mixture and with the assistance of PTC, provides optimal conditions for oxidation of PCE in the DNAPL phase. As the abundance of one reactant (PCE) increases, rates of chloride production from MnO_4^--PCE oxidation increase linearly because MnO_4^- is efficiently extracted into TCA by the catalyst and is present at sufficiently high concentrations. With a PCE-dominated mixture (>90% PCE), however, the chloride release rate is not much higher than for pure PCE because the oxidation reaction is predominately occurring in the aqueous phase and there is limited MnO_4^- transfer into nonaqueous phase.

The results show that the presence of TCA (>10%) as an extractant in DNAPL mixtures will be beneficial for PCE remediation with permanganate when a PTC is employed.

Unfortunately, other treatment measures will be required for the TCA because it is not reactive with MnO_4^-. However, when the relative abundance of TCA is lower than 10%, the enhancement in the rate of PCE oxidation is negligible even with the PTC. For problems where TCA is dominant in the PCE/TCA mixture (< 10% PCE), clearly the main emphasis in remediation effort would be TCA. Thus, PTC-assisted oxidation would be marginally useful, perhaps as a scheme to remediate PCE.

CONCLUSION

Oxidation of four chlorinated solvents by permanganate along with a PTC was quantified by monitoring MnO_4^- consumption. The rates of MnO_4^- consumption depend on the reactivity and the extracting power of solvents. Extraction of the MnO_4^- ion pair with the assistance of PTC is most significant for the ethanes (TCA and TECA), while reactivity with MnO_4^- is greatest for the ethenes. TCA is found to be the best extractant because it does not consume MnO_4^- in either aqueous or nonaqueous condition as much as TECA does.

Results of this study suggest that PTCs will be useful in field situations where contaminants occur as a mixture of DNAPLs. In a mixture of DNAPLs, reaction rates are enhanced when one component is effectively oxidized by MnO_4^- and the other is capable of extracting the PTC from the aqueous phase. Thus, there is hope of oxidizing a compound like PCE in a mixture rather than the aqueous phase. Apparently PCE is quite reactive in the DNAPL phase, if MnO_4^- can be provided. However, potential applications of PTC-assisted permanganate oxidation for DNAPL mixtures depend on which component is dominant in the mixtures.

Although PTCs increase the effectiveness of MnO_4^- as an oxidant for organic contaminants, there is still a need for research on mechanisms and pathways for reactions

occurring in nonaqueous phase. This research would contribute to a better understanding of the potential applicability of this oxidative approach for remedial schemes and any potentially adverse impacts of possibly hazardous intermediate or final products.

ACKNOWLEDGEMENTS

This research was supported in part under Grant No. DE-FG07-96ER14735, Environmental Management Science Program, Office of Science and Technology, Office of Environmental Management, United States Department of Energy (DOE). However, any opinions, findings, conclusions, or recommendations expressed herein are those of the authors and do not necessarily reflect the views of DOE. The paper benefited considerably from comments by the journal's reviewers.

REFERENCES

Bränström, A. 1976. Preparative ion pair extraction. Apotekarsocieteeten/Hassle, Lakemedel, Sweden, 168 pp.

Broholm, K. and Feenstra, S. 1995. Laboratory measurements of the aqueous solubility of mixtures of chlorinated solvents, *Environmental Toxicology and Chemistry* 14, no. 1: 9-15.

Burdon, J. and Tatlow, J.C. 1958. The reactions of highly fluorinated organic compounds. X. The oxidation of fluoro-olefins by potassium permanganate in acetone. *Journal of Applied Chemistry* 8, May: 293-296.

Cotlove, E. 1958. An instrument and method for automatic, rapid, accurate and sensitive titration of chloride in biologic samples. *Journal of Laboratory and Clinical Medicine* 51: 461-468.

CRC 1999. Handbook of Chemistry and Physics, 80th edition. David R. Lide, Editor-in-Chief, CRC Press, New York, NY.

Freeman, F., Fuselier, C.O., Armstead, C.R., Dalton, C.E., Davidson, P.A., Karchesfski, E.M. Krochman, D.E., Johnson, M.N., Jones, N.K. 1981. Permanganate ion oxidations .13. soluble manganese(iv) species in the oxidation of 2,4(1h,3h)-pyrimidinediones (uracils), *Journal of the American Chemical Society* 103, no. 5: 1154-1159.

Karaman, H., Barton, R.J., Robertson, B.E. and Lee, D.G. 1984. Preparation and properties of

quaternary ammonium and phosphonium permanganates. *Journal of Organic Chemistry* 49, no. 23: 4509-4516.

Schnarr, M. *et al*., 1998. Laboratory and controlled field experiments using potassium permanganate to remediate trichloroethylene and perchloroethylene DNAPLs in porous media. *Journal of Contaminant Hydrology* 29, no. 3: 205-224.

Schwarzenbach, R.P., Gschwend, P.M., and Imboden, D.M., 1993. Environmental Organic Chemistry, John Wiley and Sons, New York, NY, pp. 681

Seol, Y. and Schwartz, F.W., 2000. Phase-transfer-catalysts applied to the oxidation of nonaqueous phase trichloroethylene by potassium permanganate. *Journal of Contaminant Hydrology* 44, no. 2: 185-201.

Siegrist R.L., Lowe, K.S., Murdoch, L.C. and Case T.L., and Pickering D.A., 1999. In situ oxidation by fracture emplaced reactive solids, *Journal of Environmental Engineering, ASCE* 125, no. 5: 429-440

Starks, C.M., 1971. Phase-Transfer Catalysis. I. Heterogeneous Reactions Involving Anion Transfer by Quaternary Ammonium and Phosphonium Salts. *Journal of the American Chemical Society* 93, no. 1: 195-199.

Stewart, R., 1965. Oxidation by permanganate. In: K.B. Wiberg (Editor), Oxidation in organic chemistry, part A. Academic Press, New York, NY, p. 1-68.

Stewart, R. and Spitzer, U.A., 1978. Aqueous trifluoroacetic acid as a medium for organic reactions. II. The oxidation of hydrocarbons by manganese (VII). *Canadian Journal of Chemistry* 56, no. 9: 1273-1279.

Wiberg, K.B. and Fox, A.S., 1963. The mechanisms of permanganate oxidation. Oxidation of tertiary hydrogens. *Journal of the American Chemical Society* 85: 3487-3491.

Yan, Y.E., 1998. Abiotic remediation of ground water contaminated by chlorinated solvents. Ph.D. Thesis, The Ohio State University, 105 pp.

Yan, Y.E. and Schwartz, F.W., 1999. Oxidative degradation and kinetics of chlorinated ethylenes by potassium permanganate. *Journal of Contaminant Hydrology* 37, no. 3-4: 343-365.

Yan, Y.E. and Schwartz, F.W., 2000. Kinetics and Mechanisms for TCE oxidation by permanganate. *Environmental Science and Technology* 34, no. 12: 2535-2541.

Table 1. Characteristics of selected chlorinated DNAPLs.

DNAPL	Formula	M.W.	S_W[a]	S.D.[a]	ε[a]	$K_{E\text{-NBu4Br}}$[b]
TCE	$ClCH=CCl_2$	131.39	1101	1.48	3.39	0.2
PCE	$Cl_2C=CCl_2$	165.83	260	1.50	2.27	n.a.
TCA	$ClCH_2\text{-}CHCl_2$	149.32	4439	1.44	7.19	8.6
TECA	$Cl_2CH\text{-}CHCl_2$	167.85	3009	1.49	8.50	145

M.W. (molecular weight, g/mole), a; S_W (solubility in water, mg/L), S.D. (specific density, g/cm^3) and ε (dielectric constant) from CRC (1999), b; $K_{E\text{-NBu4Br}}$ (extraction constant of ion pair with tetrabutylammoniumbromide) from Bränström (1976).

Table 2. Chemical properties of selected catalyst-MnO_4^- ion pairs.

Name/PTC	Abbr.	M.W.	S_w [a]	S_o [a]	$\log K_E$ [b]
pentyltriphenylphosphonium $CH_3(CH_2)_4P(C_6H_5)_3$	PTPP	333.45	2.4×10^{-4}	1.46	7.40

M.W.; molecular weight (g/mole), S_w; solubility (M) in water, S_o; solubility (M) in methylene chloride, a; Karaman, et al., (1984), b; calculated with Eq. (8) in Seol and Schwartz (2000).

Table 3. Comparison of pseudo-first order rate constants (min^{-1}) for MnO_4^- consumption obtained with digital image capture (DIC) and UV-Vis spectrophotometer (UV).

	DIC	UV
Control	0.0365 - 0.0539	0.0484 - 0.0716
PTPP	0.0671 - 0.0932	0.0777 - 0.102

Values obtained with the data from the reaction time of 5 and 10 minutes

Table 4. Pseudo-first order rate constants for MnO_4^- consumption (min^{-1}) of pure and mixed DNAPLs calculated from the linear portion of the MnO_4^- concentration (%)–time curves obtained with digital image capture.

DNAPL		2nd DNAPL	
		TCA	PCA
TCE	0.102	0.0459	0.0749
PCE	0.0012	0.0007	0.0066
TCA	0.0004		
PCA	0.0435		

Phase Transfer Catalyst; PTPP

DNAPL		2nd DNAPL	
		TCA	PCA
TCE	0.124	0.145	0.155
PCE	0.0012	0.0112	0.0407
TCA	0.0009		
PCA	0.0561		

LIST OF FIGURES

Figure 1. Schematic representation of phase-transfer-catalyzed MnO_4^- displacement on chlorinated organic solvents.

Figure 2. Schematic procedure of digital photographic approach for rapid measurements of MnO_4^- concentration.

Figure 3. Comparison of results from the digital image capture technique (DIC) for the rapid detection of MnO_4^- consumption with absorbance measurements from a UV-Vis spectrophotometer (UV).

Figure 4. Selected diagrams for permanganate consumptions of (a) selected chlorinated DNAPLs and (b) PCE/TCA mixtures with phase transfer catalyst (PTPP).

Figure 5. Chloride releases from oxidation of PCE/TCA catalyzed by PTPP. The volumetric percentage of PCE in the mixture varied from 0 to 100 %.

Figure 6. Changes of chloride release rate as PCE volumetric percentage increases in the mixture of PCE and TCA.

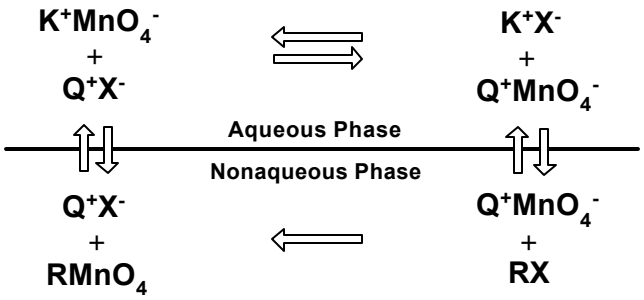

Figure 1. SEOL

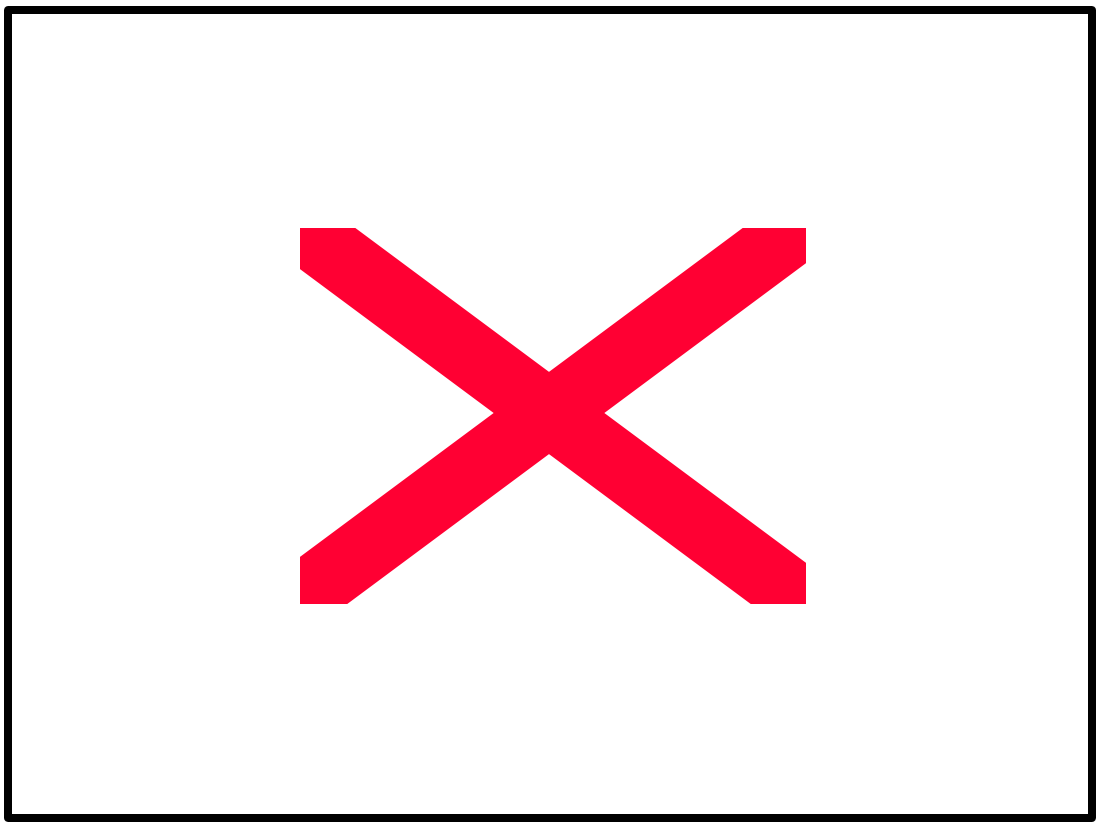

Figure 2. SEOL

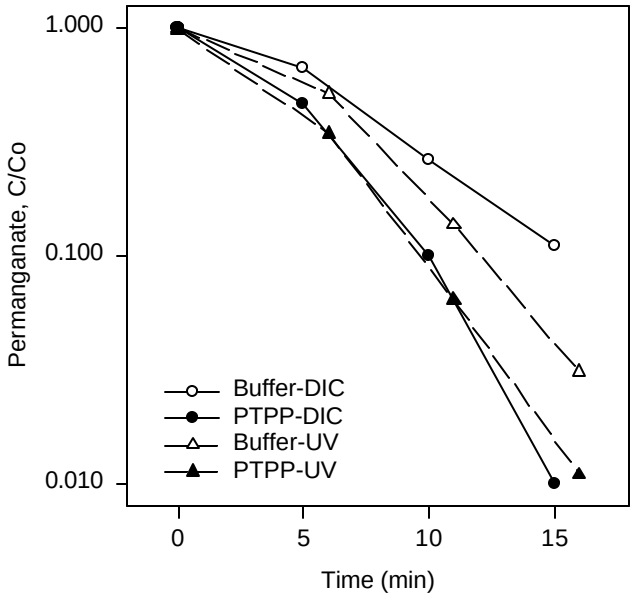

Figure 3. SEOL

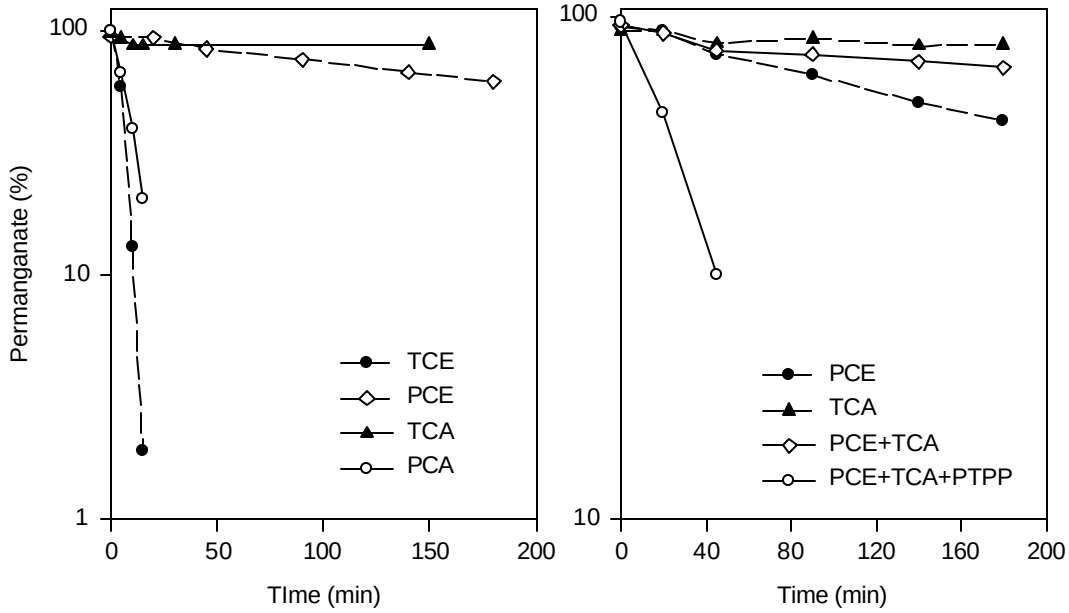

Figure 4. SEOL

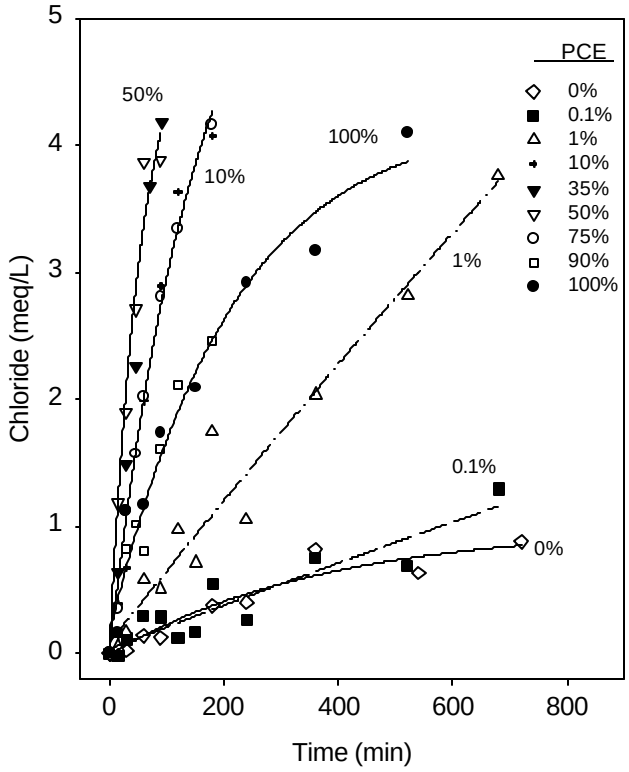

Figure 5. SEOL

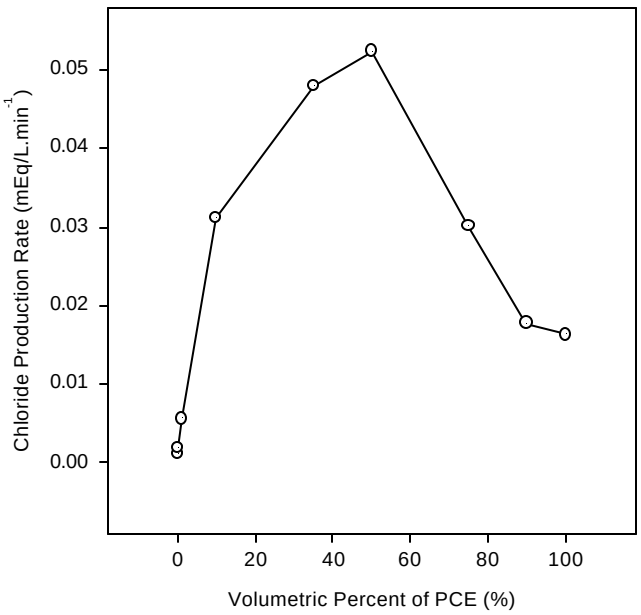

Figure 6. SEOL

Appendix 5. Manuscript of published article entitled;

EFFICIENCY PROBLEMS RELATED TO PERMANGANATE OXIDATION SCHEMES

X. David Li and Franklin W. Schwartz
The Ohio State University, Columbus, Ohio, USA

ABSTRACT: This study investigates problems that potentially could impact a permanganate oxidation scheme, such as competitive permanganate utilization in reactions with aquifer materials, MnO_2 precipitation around zones of high DNAPL saturation, and permeability-related flow bypassing. A series of batch experiments were conducted to examine whether typical aquifer materials (glacial deposits, alluvium and carbonate-rich sand) reacted with permanganate. The results show a dramatic consumption of the oxidant and a significant change in the concentrations of some chemical species, which may be of environmental concern. 1-D column and 2-D flow tank experiments have been conducted to examine mass removal rates and related flushing efficiencies. The results indicate that mass removal rates are also greatly influenced by the MnO_2 precipitation and flow bypassing. It is anticipated that in actual field settings, the issue of flushing efficiency needs to be considered in the design.

INTRODUCTION

Oxidation schemes for the *in situ* destruction of chlorinated solvents, using potassium permanganate, are receiving considerable attention. Potassium permanganate is a powerful oxidant that has been used for long time in wastewater treatment. Batch scale experiments have demonstrated the rapid mineralization of contaminants with final products that are environmentally safe (Yan and Schwartz, 1999). Researchers at the University of Waterloo (Schnarr et al., 1998) and Oak Ridge National Laboratory have conducted experiments to investigate permanganate-oxidation schemes in field and laboratory tests. The results suggested that permanganate oxidation is a promising technology for the remediation of chlorinated solvents. This approach also has been implemented by consultants at several sites in Florida and California.

Indications from these field studies and our work are that permanganate oxidation schemes have inherent problems that could severely limit their applicability. As a powerful oxidant, permanganate is not only capable of oxidizing chlorinated ethylenes, but also inorganic compounds in ground water and solid aquifer materials. For example, Drescher and others (1998) reported the significant consumption of permanganate by humic acid in a system consisting of sand, TCE, permanganate and humic acid. With aquifer materials consuming some of the permanganate, the overall efficiency of the cleanup is reduced and costs are increased. Reaction also can release metals (e.g. Cr^{3+}) to the aqueous phase at concentration of regulatory concern. Given the present, relatively limited understanding of the oxidation reactions, there is a

need for studies to understand these problems and to improve the efficiency of permanganate delivery.

Another potential problem is that key reaction products, manganese dioxide and carbon dioxide, can cause plugging and flow diversion. There is little research on the impact of these problems on mass removal rate and on possible approaches to inhibit precipitation. This study specifically addresses gaps in knowledge that bear on the realistic use of permanganate-oxidation schemes in DNAPL clean ups. Here, we present preliminary data on the likely metals that can be released due to permanganate-aquifer interaction. We also discuss the results of various column and flow tank experiments that elucidate problems of flooding inefficiencies, and pore plugging related to reaction products.

MATERIALS AND METHODS

The study involves two types of experiments. We utilize batch studies to investigate the consumption of MnO_4^- by aquifer materials and the release of potentially hazardous metals. Column (1-D) and flow tank studies (2-D) are used to examine the impact of oxidation products on DNAPL removal efficiencies.

Permanganate Consumption/Metal Release. Batch experiments with natural aquifer materials are used to examine the interaction of potassium permanganate with aquifer material and the extent to which metals are released. Samples were collected from various aquifer materials, such as, alluvium, glacial till, glacial outwash, and carbonate sand. Special efforts were made to collect samples at depth, away from soil horizons.

Samples were placed in aluminum pans to air dry for two to three days. Experiments were conducted at room temperature in 25 mL vials. 15 gram of each sample was mixed with 15 mL of 0.5 g/L potassium permanganate solution. A control was prepared with the same potassium permanganate solution, but without any aquifer material. After the permanganate solution was added to the aquifer solids, the vials were covered with aluminum foil and black cloth, and kept in the dark to avoid photo-induced degradation of potassium permanganate. Sample vials were shaken by hand once a day to ensure mixing during the experiment. At predetermined time steps, 5 mL of solution was removed from the vial and filtered through a 0.22 μm glass fiber membrane to remove any suspended solids immediately prior to the concentration measurement. Permanganate concentrations were measured with a Varian Cary 1 UV–visible spectrophotometer at a wavelength 525 nm.

The study of metals released by the oxidation of aquifer materials followed a similar procedure. The controls in this case were mixtures of 15 mL Milli-Q deionized water and aquifer materials. By comparing the differences between metals released from the control experiments and oxidized materials, the effect of MnO_4^- treatment could be established. After ten days, when the permanganate had mostly been consumed, solutions of both the controls and samples were separated from large solid particles and filtered to remove suspended solids. The samples were analyzed by a Perkin-Elmer Sciex ELAN 6000 Inductively Coupled Plasma Mass Spectrometer (ICP-MS). As a first step, a semi-quantitative screening analysis was performed to identify the elements with most dramatic change in concentration. A quantitative

analysis was then carried out with specific external standards. 12 elements were quantitatively analyzed. The results were then converted to the pore water concentration, based on the porosity of the media.

1-D Column Experiment. The 1-D column experiment was conducted using a glass column with Teflon end fittings and packed with medium silica sand (US Silica, Ottawa, IL). Details of the experimental set up are summarized in Table 5.1. Once the column was packed, it was positioned upside down. 1 mL of TCE was added to the column evenly across the opening to create a zone of residual DNAPL saturation. The column was returned to an upright position and fluid was pumped upward through the column using an Ismatec tubing bed pump (Cole Parmer Instrument Co. Vernon Hills, IL). Effluent samples were collected periodically for chemical analysis. MnO_4^- concentration was measured with a UV-visible spectrophotometer as mentioned earlier. TCE was measured with a Fisons Instruments 8060 gas chromatograph equipped with a Ni^{63} electron capture detector and a DB-5 capillary column (J&W Scientific, Rancho Cordova, CA). Cl^- ion concentration was measured with a Buchler Digital Chlorodometer. Samples were taken at 12 hour intervals over a two week period. The experiment was concluded when the effluent TCE concentration fell below 5 μg/L. After the experiment finished, several porous medium samples were taken along the column. The samples were treated with thiosulfate to dissolve the MnO_2. The resulting solution was analyzed by ICP-MS to quantify the distribution of MnO_2 along the column.

Table 5.1. Experimental design for the 1-D column and 2-D flow tank experiments

Column/ tank	Dimension (mm)	Medium	Q (mL/min)	$KMnO_4$ concentration	Porosity
1 – D	605(L)x50 (ID)	Silica sand	1.2	1 g/L	0.385
2 – D	305(L)x50(H)x3 (T)	Glass beads	0.5	0.2 g/L	0.42

2-D Flow Tank Experiments. A thin, small 2-D glass flow tank with Teflon end fittings was constructed for the experiment (Table 5.1). The flow tank was filled with transparent borosilicate glass beads with a mean grain size of 1 mm. Two PTFE tubes with inside diameter of 1.32 mm were installed in the two ends of the column to function as recharge and discharge wells. Both tubes had ends open at a depth of 0.5 cm from the bottom of column. Once the column was packed, it was saturated with Milli-Q water. A Spectroflow 400 solvent delivery system (Kratos analytic, NJ) was used to maintain inflow to the tank, the Ismatec pump removed fluid at the outlet.

With both pumps running at the same steady rate, flow was horizontal along the length of the tank. 1 mL of the TCE was added to the tank from the top to form a zone of residual DNAPL saturation across the vertical depth of the tank and a small DNAPL pool at the bottom. The tank was flushed for about two weeks with $KMnO_4$. Effluent samples were taken three times a day and were analyzed as before. Images of the column were taken with a digital camera to monitor the development of the growing zone of MnO_2 precipitation.

RESULTS

Results of batch experiments to examine the consumption of MnO_4^- by natural materials are plotted in Figure 5.1. After 10 days, the MnO_4^- concentration dropped to near zero for every sample of natural aquifer material, irrespective of the type of sample. There are two exceptions, with virtually no change in the MnO_4^- concentration with time. These two samples are the silica sand and the glass beads, which were used later for the column experiments. The decrease in the MnO_4^- concentration appears follow a first order kinetic rate law. Because permanganate is likely conservative in the aqueous phase, it is unlikely concentration reductions were caused by sorption onto the solids.

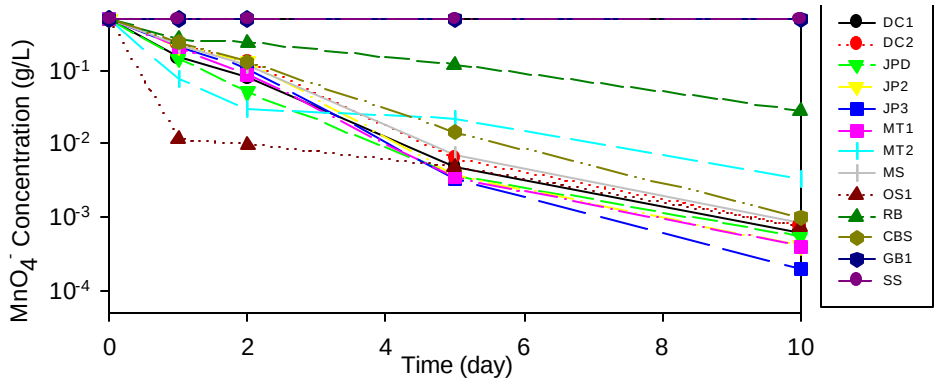

FIGURE 5.1. Utilization of MnO_4^- through oxidation of various aquifer materials.

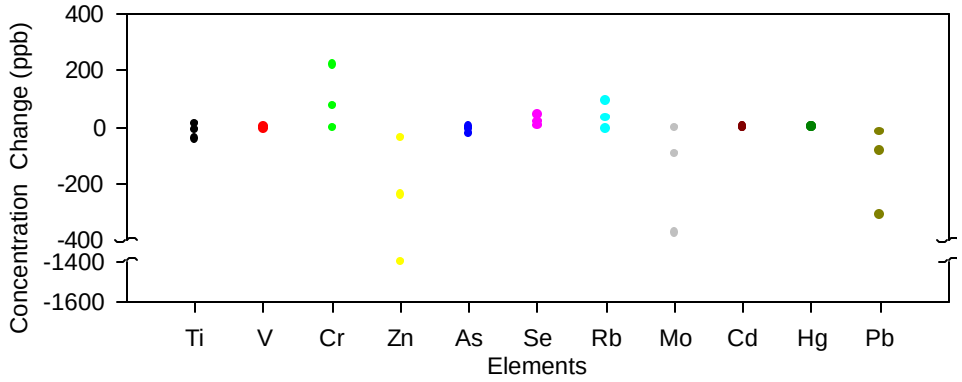

FIGURE 5.2. Average, maximum and minimum concentrations for the elements in pore water after treatment with 0.5 g/L $KMnO_4$ for ten days.

The decreasing MnO_4^- concentrations with time implies that the aquifer materials have being oxidized. Results of the ICP-MS analysis of the pore water MnO_4^- treatment (Figures 5.2, 5.3) confirmed this conclusion. In spite of the variability in the types of sample, there are common features among the results. Of the 12 elements that were quantitatively analyzed, chromium, selenium and rubidium generally increased in concentration; and vanadium, zinc, cadmium and lead, decreased. The remaining elements (titanium, arsenic, molybdenum, cesium and mercury) generally showed no significant change. While the pattern of change is relatively consistent, the magnitude of the change is variable. In some cases, the concentration could change several hundred fold.

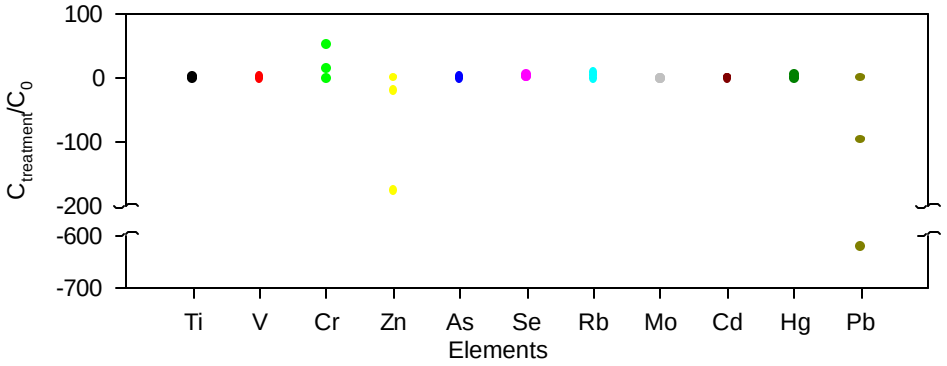

FIGURE 5.3.Average, maximum and minimum ratio of concentrations of elements in pore water before and after treatment with 0.5 g/L $KMnO_4$ for ten days.

The 1-D column experiment confirms the capability of MnO_4^- to oxidize TCE present in the column. Mass balance calculations, based on the measured TCE and chloride concentration in the effluent from the column, indicated the nearly complete removal of the pure TCE in a relatively short time (Figure 5.4). Intergrating the TCE removal curve shows that after 365 hours of permanganate flushing, 96.9% of the initial TCE was removed from the column. The rate of TCE removal was highest when MnO_4^- first fully saturated the column, and decreased with time dramatically. 90% of the TCE was removed in the first 115 hours of the experiment, while another 250 hours was required to remove the last 7%. Flushing by MnO_4^- was halted when Cl^- measurements suggested that the oxidation reaction had stopped. Flushing continued with Milli-Q water being pumped through the column. Interestingly, TCE concentrations rebounded to about 130 µg/L. Apparently, the Cl^- measurements were not sensitive at the lower level of detection to indicate that small quantities of TCE remained in the column. It is estimated that another couple hundred hours would be needed for the TCE concentration drop to below 5 µg/L.

The distribution of manganese dioxide precipitation in the column after the experiment is presented in Figure 5.5. The majority of the Mn was presented at or very close to the DNAPL zone. These precipitates tended to plug the column and toward the end of the experiment flushing was increasingly difficult.

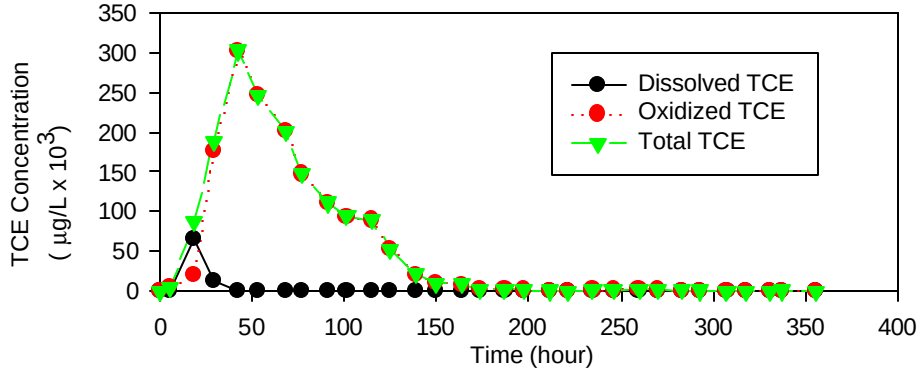

FIGURE 5.4. TCE concentration with time in the effluent of the 1 – D column and calculated removal based on Cl^- stoichiometry.

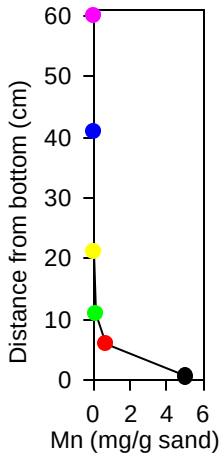

FIGURE 5.5. Distribution of Mn along the column.

experiment, except that removal rates were noticeably smaller. After 313 hours of flushing with MnO_4^-, only 34.9% of the initial TCE was removed from the column. Half of the TCE was removed in the first 25% of the elapsed time. Note that in Figure 5.6 at the end of the experiment TCE concentration rebounded, once the injection of MnO_4^- had stopped.

The visual observation system provided a useful way to monitor the growth of the zone of MnO_2 precipitation. Precipitation started once MnO_4^- came in contact with residual DNAPL. There was a tendency for the MnO_4^- flood to bypass the zone with the highest DNAPL saturation, moving instead through a much less saturated zone in the upper portion of the tank. The results from the 2-D flow tank experiment (Figure 5.6) were similar to the 1-D With time, the precipitation of MnO_2 reduced the permeability. MnO_2 rapidly formed a precipitation rind above the DNAPL pool. Greater injection pressure was required to maintain the flow close to the end of the experiment. The experiment came to a halt when MnO_2 plugged the tank nearly completely and MnO_4^- could no longer be injected. Carefully examination of the tank after the experiment indicated the presence of tiny CO_2 bubbles, produced from the oxidation reaction. The gas bubbles likely played a role in reducing the permeability and the flow in the system. Flushing with MnO_4^- appears effective in removing residual DNAPL. However, much of the original volume of the pool of DNAPL at the bottom of the tank was evident at the end of the experiment.

SUMMARY AND DISCUSSION

In the batch experiments, the gradual disappearance of MnO_4^- and the change in chemistry of the aqueous phase pointed to significant interactions between the porous medium and the MnO_4^-. Given the variability in mineralogy

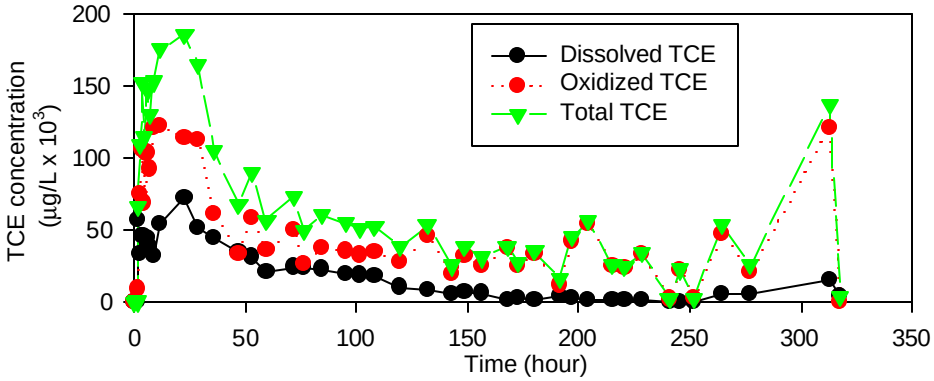

FIGURE 5.6. Effluent TCE concentration change with time in the 2 – D column experiment.

and grain coatings, it is not possible to propose reaction mechanisms. We are now in the processes of elucidating the MnO_4^-- solid reactions in more detail. The permanganate likely oxidizes the solid metal oxide. For example, chromium, Cr (III), which often exists as Cr_2O_3 solid, was probably oxidized to Cr (VI), a dissolved species of chromium. Any metals sorbed to organic matters would be added to solution as MnO_4^- oxidizes the organic matter. Clearly, MnO_4^- is a powerful oxidant that is capable of oxidizing solids and organic contaminants indiscriminately. The heavy metal loading is of regulatory concern, although it is not clear how mobile these constituents might be. The ability for most natural aquifer materials to consume MnO_4^- reduces concern that the presence of MnO_4^- in solution would emerge as a major problem of contaminant at most sites.

Understanding how the chemical composition of the aqueous phase will change is more complicated because the oxidation of TCE is capable of shifting the equilibra of dissolved-precipitated phase, sorbed-solution phase and complexations by changing pH, E_h and the concentration of Cl^-. For example, selenium tends to much more mobile in the oxic rather than reducing condition (Alloway, 1995) as the E_h goes up with the treatment. Mobilization of several metals (Hg, Cd, Pb) was found to be very sensitive to the concentration of Cl^-. A given element will likely respond to the permanganate treatment differently. Our results suggest caution in the application of oxidation schemes to environmentally sensitive areas and aquifers containing high concentrations of metal oxides at lower oxidation states.

Results from both the 1-D and 2-D experiments indicate that early in the flushing process, the mass removal rate is greatest. As the treatment proceeds, the rate decreases dramatically. Running the experiments to achieve complete DNAPL removal will produces a long tail in the later part of the treatment, which points to inefficiencies in the flushing. This tailing effect has also been noted by researchers studying DNAPL dissolution. Towards the end of their experiments when a large portion of the contaminant was dissolved, small droplets remained in hydraulically stagnant zones in the medium. Preferential flow paths appear to develop even with the homogeneous media. With MnO_4^- oxidation schemes, the tendency for preferential flow paths to develop will be further promoted as MnO_2 precipitates in the zones of higher DNAPL saturation or CO_2 bubbles are trapped in the porous medium. The rapid oxidation and relatively slow mass transfer rate from the DNAPL to the aqueous phase means that MnO_2 would tend to precipitate at or immediately adjacent to the DNAPL, which results in a zone of more concentrated precipitates around the zones of greatest saturation. Flow would tend to bypass these zones and follow a more permeable flow path, causing the DNAPL oxidation process to become diffusion controlled.

These effects are most obvious in the 2-D tank experiment where DNAPL is present in zones of high residual saturation or pools. The pooled DNAPL persisted because the interfacial area is relatively small and MnO_4^- moved around but not through these zones. In zones of residual saturation, DNAPL oxidization was more efficient because MnO_4^- could move through the zones. With the opportunities for MnO_4^- to move around zones of DNAPL saturation in the two dimensional system, there was a much smaller overall destruction of TCE in the 2-D tank as compared to the 1-D column. These results suggest that with 3-D flow conditions, evident at actual contaminated sites, the efficiency of removal would probably be smaller. It appears that MnO_4^- oxidation is more effective in cleaning up residually saturated DNAPLs rather than pool of DNAPL. Clearly, in actual field settings, the issue of

flushing efficiency will be of concern in the design. Experiments are underway to find an effective additive that minimizes the precipitation effects.

ACKNOWLEGEMENTS: This paper is based on research supplied by the Department of Energy under Grant No. DE-FG07-96ER14735.

REFERENCES

Alloway, B.J. (Eds.). 1995. *Heavy metals in soils* (2nd edition). Blackie academic & Professional, London, pp. 106-351.

Drescher, E., A. R. Gavaskar, B. M. Sass, L. J. Cumming, M. J. Drescher and T. K. J. Williamson. 1998."Batch and column testing to evaluate chemical oxidation of DNAPL source zones." In G. B. Wickramanayake and R. E. Hinchee (Eds.), *Physical, Chemical, and Thermal Technologies, Remediation of Chlorinated and Recalcitrant Compounds*, pp. 425-432. Battelle Press, OH.

Schnarr, M., C. Truax, G. Farguhar, E. Hood, T. Gonullu, and B. Stickney. 1998. "Labortory and controlled field experiments using potassium permanganate to remediate trichloroethylene and perchloroethylene DNAPLs in porous media." *Journal of Contaminant Hydrology*. 29(3): 205-224.

Yan, Y.E. and F.W. Schwartz. 1999. "Oxidative degradation and kinetics of chlorinated ethylenes by potassium permanganate." *Journal Of Contaminant Hydrology*. 37(3-4): 343-365.

Table 5.1. Experimental design for the 1-D column and 2-D flow tank experiments

Column/tank	Dimension (mm)	Medium	Q (mL/min)	$KMnO_4$ concentration	Porosity
1 – D	605(L)x50 (ID)	Silica sand	1.2	1 g/L	0.385
2 – D	305(L)x50(H)x3 (T)	Glass beads	0.5	0.2 g/L	0.42

FIGURE 5.1. Utilization of MnO_4^- through oxidation of various aquifer materials.

FIGURE 5.2. Average, maximum and minimum concentrations for the elements in pore water after treatment with 0.5 g/L $KMnO_4$ for ten days.

FIGURE 5.3.Average, maximum and minimum ratio of concentrations of elements in pore water before and after treatment with 0.5 g/L $KMnO_4$ for ten days.

FIGURE 5.4. TCE concentration with time in the effluent of the 1 – D column and calculated removal based on Cl^- stoichiometry.

FIGURE 5.5. Distribution of Mn along the column.

FIGURE 5.6. Effluent TCE concentration change with time in the 2 – D column experiment.

Appendix 6. Manuscript of published article entitled;

Simulating the *In Situ* Oxidative Treatment of Chlorinated Ethylenes by Potassium Permanganate

Hubao Zhang[1] and Franklin W. Schwartz[2]

[1] Duke Engineering & Services
1650 University Blvd., Suite 300
Albuquerque, NM 87102

[2] The Ohio State University, Department of Geological Sciences
275 Mendenhall Laboratory, 125 South Oval Mall
Columbus, OH 43210

Abstract

Several laboratory and field studies have demonstrated the potential viability of oxidation schemes using MnO_4^- for the in-situ treatment of DNAPL source areas, which are contaminated by chlorinated ethylenes (PCE, TCE and DCE). Chemically, the chlorinated ethylenes are oxidized to CO_2, Cl^-, and MnO_2. The goal of this study was to develop a theoretical framework for the chemical and physical processes involved. To this end, a computer model was developed to simulate the coupled processes of NAPL dissolution, chemical reactions, and solute mass transport in the in-situ chemical oxidization scheme. The model incorporates a kinetic description of reactions between the MnO_4^- and the chlorinated ethylenes and the rate of dissolution of the NAPL. A Strang operator-splitting method, which coupled the different physical and chemical processes and an exponentially-expressed solution of the kinetic equations, led to a significant speed up in the solution process. The products in reactions were calculated based on the stoichiometry of the reaction. We demonstrated the capabilities of this code using already published results of column, test cell, and field experiments. Generally, the simulated results matched well with experimental measurements. The computer model provides a useful tool for assisting the design and the prediction of the oxidization processes under field conditions.

Introduction

In recent years, MnO_4^- oxidation of chlorinated ethylenes (PCE, TCE and DCE) has emerged as a potentially useful approach for destroying these compounds in water (Vella and Veronda, 1992; Gates et al., 1995; Schnarr et al., 1998; Yan and Schwartz, 1998 and 1999). The ability of MnO_4^- to oxidize some organic compounds has been known for a long time. Steward (1965) extensively reviewed the role of $KMnO_4$ in organic reactions. Colthust and Singer (1982) noticed that adding $KMnO_4$ to drinking water reduced the concentration of trihalomethane (THM) precursors. Moreover, the concentration of these humic substances was further reduced in the presence of Ca^{2+} through sorption on manganese dioxide, a product of the oxidation reaction.

Recently, more applied studies have looked at whether $KMnO_4$ could be used in remediating sites contaminated by chlorinated solvents. Schnarr et al. (1998) reported the results of laboratory and controlled field experiments using $KMnO_4$ to remediate trichloroethylene and perchloroethylene. West et al. (1997) undertook a field demonstration of the *in situ* scheme for source-zone remediation at a DOE facility. Yan and Schwartz (1998, 1999) examined the kinetic behavior of chlorinated ethylenes in reactions with MnO_4^-. Drescher et al. (1998) demonstrated that organic matter in the soils exerts a greater competitive demand for MnO_4^- than the NAPL. Pilot tests for treatment of TCE were also performed in unsaturated zones (LaChance et al., 1998; McKay et al., 1998).

Almost all of the work to date has been concerned with understanding the nature and kinetics of key reactions, and assessing the remedial concept in controlled laboratory and field experiments. There is no published work on numerical models that could be used in the design and evaluation of this scheme under field conditions. However, development of a three-dimensional model is a natural step in the development of this technology. Such a model could help to optimize the engineering designs to reduce the cost and potential adverse side effects.

This paper describes a new computer code (ISCO3D), which was developed to simulate the coupled processes of NAPL dissolution, chemical reactions, and solute mass transport in the *in-situ* oxidization scheme. The code is also capable of simulating key reactions between the aquifer material and MnO_4^- and the kinetic sorption of chemicals, and has been optimized for computational efficiency. The code fills the gap between the laboratory studies and field operations by providing a numerical model capable of assisting with the design of systems and the interpretation of field observations.

The first few sections of this paper will provide numerical framework of the model. The code is demonstrated in applications involving column experiments (Schnarr et al., 1998), a test cell experiment (Schnarr et al., 1998), and a field demonstration (West et al., 1997).

Mathematical Formulation

In the following development of mathematical equations, it is assumed that there exists a zone of residual NAPL or a dissolved plume of chlorinated compounds in the saturated zone. MnO_4^- is injected into an aquifer as an oxidant and assumed to follow some flow path. The MnO_4^- is assumed to react with natural organic carbon and other oxidizable aquifer materials, as well as the dissolved chlorinated compounds in the aqueous phase. With the injection of MnO_4^- into a NAPL zone, the utilization of contaminants in the aqueous phase accelerates the dissolution of the NAPL.

Assuming that the NAPL is immobile and the saturation of the NAPL in the medium is small, the

ground-water flow equation can be written as (Bear, 1972; Frind, 1983)

$$\nabla(\mathbf{K}\nabla h) + Q = S_s \frac{\partial h}{\partial t} \tag{1}$$

where **K** is the hydraulic conductivity tensor (L/T), h is the water head (L), Q is the source (L^3/T), t is the time (T), and S_s is the specific storage (L^{-1}).

The mass-transport equation (modified from Bear, 1972; Huyakorn and Pinder, 1983) for mobile species is expressed as

$$\nabla(n\mathbf{D}\nabla c_i) - \nabla(nV c_i) + r_i = \frac{\partial(n c_i)}{\partial t} \tag{2}$$

where n is porosity, **D** is the dispersion coefficient tensor (L^2T^{-1}), V is the linear groundwater velocity vector (LT^{-1}), c_i is the concentration for species i (ML^{-3}), and r_i is the reaction rate for species i ($ML^{-3}T^{-1}$).

Yan and Schwartz (1999) found that the oxidation of PCE, TCE, and three isomers of DCE involved two sequential reactions, illustrated here for TCE

$$C_2HCl_3 + MnO_4^- \xrightarrow{k_1} I \xrightarrow{k_2} g\,CA + MnO_2 + 3Cl^- \tag{3}$$

where I is a cyclic complex, CA are various carboxylic acids, and k_1, and k_2 are rate constants. Our modeling approach is sufficiently general to accommodate reactions of this kind. We conducted preliminary trials to examine the overall behavior of the various carboxylic acids that formed. Unfortunately, for large multi-dimensional problems, large execution times made solving this reaction network infeasible. A simplified approach was adopted which abstracted the chemical reactions between MnO_4^- and tetrachloroethene (PCE), trichloroethene (TCE), and dichloethene (DCE), and aquifer material (for example, natural organic carbon) as follows:

(a) PCE

$$C_2Cl_4 + 2MnO_4^- \Rightarrow 4Cl^- + 2CO_2 + 2MnO_2(s) \tag{3}$$

(b) TCE

$$C_2HCl_3 + 2MnO_4^- \Rightarrow 3Cl^- + 2CO_2 + H^+ + 2MnO_2(s) \tag{4}$$

(c) DCE

$$C_2H_2Cl_2 + 2MnO_4^- \Rightarrow 2Cl^- + 2CO_2 + 2H^+ + 2MnO_2(s) \tag{5}$$

(d) Natural organic carbon

$$C + MnO_4^- \Rightarrow CO_2 + MnO_2(s) \tag{6}$$

(5) Sorption reaction

$$C_2Cl_4 \Leftrightarrow C_2Cl_4(s) \tag{7}$$

The equations for the oxidation of chlorinated compounds (3) through (5) have a form that is similar to that as illustrated here for TCE

$$\frac{d(TCE)}{dt} = -k_{TCE}(TCE)(MnO_4^-) \tag{8}$$

where ( ) indicate concentrations and k_{TCE} is the rate constant (s^{-1}) for the oxidation of TCE. The values for these constants come from kinetic batch experiments (Table 1). In these experiments, initial TCE

concentration varied from 0.031 to 0.083 mM while initial MnO_4^- concentration changed from 0.37 to 1.2 mM.

The reaction rate data indicate that it is much easier to oxidize DCE with MnO_4^- than TCE. Similarly, the reaction rate between TCE and MnO_4^- is faster than that between PCE and MnO_4^-.

Equation (6) represents the oxidization of aquifer materials by MnO_4^- as a single reaction. In reality, MnO_4^- reacts with a variety of oxidizable species in solid and dissolved phases. It is assumed that the oxidation of aquifer materials by MnO_4^- has this rate law

$$\frac{d(OAM)}{dt} = -k_{OAM}(OAM)(MnO_4^-) \tag{9}$$

where (OAM) is the concentration of oxidizable aquifer material and k_{OAM} is the pseudo rate constant. Our simplified treatment is in keeping with the limited information related to MnO_4^- consumption by aquifer materials. There is little published information as to values of k_{OAM}. The column experiments by Schnarr et al (1998) show the breakthrough of MnO_4^- to be considerably delayed as a consequence of competitive utilization by the oxidation of the porous medium. These results indicate that the reaction between the MnO_4^- and the oxidizable aquifer material is much faster as compared to contaminant transport time. In the simulations that follow, we assume k_{OAM} >> rate constants for the chlorinated compounds. In effect, this assumption produces an MnO_4^- transport velocity that depends on (OAM).

Equation (7) is a kinetic sorption/mass transfer equation for PCE. Kinetic sorption of other compounds can be expressed in a similar way. There is some evidence from field experiments that a kinetic approach is appropriate. Roberts et al. (1986) showed that the retardation factor increases from 2.7 at 15 days to 5.9 at 650 day for PCE transport in the Borden aquifer. The increase of retardation factor with time is one of the indicators of kinetic sorption (Zhang et al., 1998).

The chemical reactions are included in (2) through the source term. All of the transport equations are written in terms of the concentration, although provision is made in the code to provide mass-law expressions in terms of activity.

Kinetic Dissolution Model for NAPLs

The rate of organic dissolution can be described by

$$n\frac{dc_i}{dt} = k_{Ni}(c_{Si} - c_i) \tag{10}$$

where c_i is the aqueous concentration corresponding to NAPL species i (ML^{-3}), k_{Ni} is the mass transfer coefficient (T^{-1}), and c_{Si} is the equilibrium concentration with pure organic liquid or solubility of species i (Pfannkuch, 1984; Sleep and Sykes, 1989; and Miller et al., 1990). Some investigators (Sleep and Sykes, 1989) used a lumped mass transfer coefficient in their sensitivity analysis for mass transfer between phases. Others (Pfannkuch, 1984; Miller et al., 1990; and Powers et al., 1992) used correlation expressions to relate the mass transfer coefficient to Reynolds and Schmidt numbers, and other physical parameters. The correlation expressions were chosen in this study because they are more closely related to ground-water flow and properties of NAPLs. To summarize these correlation expressions, several dimensionless numbers need to be defined. The Reynolds number is:

$$Re = \frac{v_w \rho_w d_{50}}{\mu_w} \tag{11}$$

and the Sherwood number is:

$$Sh = \frac{k_{Ni} d_{50}^2}{D_m} \tag{12}$$

where v_W is the linear groundwater velocity (LT^{-1}), ρ_W is the density of aqueous phase fluid, μ_W is the viscosity of the aqueous phase fluid ($ML^{-1}T^{-1}$), d_i means i% of the particles smaller than d_i (L), and D_m is the aqueous molecular diffusion coefficient of the NAPL (L^2T^{-1}). The Sherwood number relates mass transfer coefficient to particle diameter and molecular diffusion coefficient. Several empirical expressions were determined from column experiments (Miller et al., 1990; Imhoff et al., 1994; and Powers et al, 1994). Although these expressions are all useful to determine mass transfer coefficient, a simplified relationship adopted in this study matched better with simulations.

$$Sh = \alpha' Re^{\beta_1'} S_N^{\beta_2'} \tag{13}$$

where α', β_1', and β_2' are fitting parameters, respectively, S_N is the NAPL saturation, and Re is the Reynolds number. Comparison between the equation (13) and models formulated by other researchers are shown in Table 2. The variables δ, U_i, and S_{N0} in the Power's model are the normalized grain size, the uniformity of the grains, the original saturation of NAPL, respectively. The variable X in the Imhoff's model is the distance from the flux entry point of a column to the measurement point in the column. The equation (13) is a generic expression of the models proposed by Miller et al. (1990), Imhoff et al. (1994), and Powers et al (1994). The original models by Imhoff et al. (1994), Power et al. (1994), and Miller et al. (1990) were tied to constant coefficients α', β_1', and β_2' for their experiments. These constant coefficients are different in the three models, and are functions of the grain size, grain shape, grain packing, porosity of media, and other factors. Fitting α', β_1', and β_2' to some values in our simulations provides equation (13) the flexibility to reflect the heterogeneity of geological materials in a variety of conditions.

Numerical Formulation

Solution Procedures for Coupled Nonlinear Equations

This section describes the approach to solve the problem of reactive mass transport. To facilitate the description, consider the transport equation expressed in operator notation as:

$$\frac{\partial c_i}{\partial t} + L(c_i) = r_i \tag{14}$$

where

$$L = \nabla \bullet (n v - n D \nabla) \tag{15}$$

In general, there are three approaches to couple transport equations with chemical reactions: global implicit, sequential iterative and sequential non-iterative (Steefel and MacQuarrie, 1996). The global implicit approach solves the concentrations of all species at all nodes using Newton or other non-linear procedures. The global implicit approach may be feasible for multiple species mass transport in one dimension, but is considered costly in terms of computational time and computer memory for 3-D

problems (Yeh and Tripathi, 1989). The sequential iteration approach accomplishes coupling by iterating between the reaction and transport terms and may not converge in some cases. The sequential non-iterative approach solves the transport and reaction equations in separate steps but may result in errors for a large time step (Valocchin and Malmstead, 1992). To improve the accuracy of reactive transport in the sequential non-iterative approach, a time-centered method, Strang splitting, was used to couple the physical transport and chemical reactions. Strang splitting is similar to the alternating operator-splitting scheme proposed by Valocchin and Malmstead (1992) to reduce mass balance errors. In the Strang-splitting approach, changes in solute mass are calculated in two transport time steps and one reaction time step. The solution steps may be summarized as follows (modified from Zysset et al., 1994):

(1) Specify initial and boundary conditions.

(2) Solve the ground-water flow equation.

(3) Solve the mass transport equation (2) for each species without reaction for half a time step, or

$$\frac{c_i^T - c_i^k}{\Delta t/2} + L(c_i) = 0 \tag{16}$$

where c_i^T is the concentration at time step k+1/2, Δt is the time step size in the numerical solution of the advection-dispersion equation, and c_i^k is the concentration of species i at time step k.

(4) Calculate the dissolution of NAPLs according to equation (10) with an equation of this form:

$$\frac{c_i^D - c_i^T}{\Delta t} = k_{Ni}(c_{Si} - c_i^T) \tag{17}$$

where c_i^D is the concentration of species i after a dissolution step for the current time step. The concentration of species without a corresponding NAPL phase does not change during the dissolution step. The size of the time step cannot exceed the inverse of mass transfer coefficient k_{Ni}, maintaining the maximum concentration at or below the aqueous solubility of the species. Mathematically, this constraint is expressed as:

$$\Delta t \le \frac{1}{k_{Ni}} \tag{18}$$

The time step size is also constrained by the NAPL available for dissolution in each time step. This constraint has the following form:

$$\Delta t \le \frac{S\rho_N}{k_{Ni}(c_{Si} - c_i^T)} \tag{19}$$

where ρ_N is the density of the NAPL, and S is the saturation of the NAPL at a node.

(5) The next step is to solve the reaction equation for each species without transport term, solving a set of equations that have this general form:

$$\frac{c_i^R - c_i^D}{\Delta t} = r_i(c_1, c_2, ..., c_n) \tag{20}$$

where c_i^R is the concentration of species i after a reaction step.

(6) Solve the following form of the transport equation (2) for each species without reaction for half a time-step size:

$$\frac{c_i^{k+1} - c_i^R}{\Delta t/2} + L(c_i) = 0 \tag{21}$$

where c_i^{k+1} is the concentration at time step k+1.

(7) Depending upon the accuracy requirement for the problem, a non-iterative or iterative procedure may be selected for the operator-splitting algorithm. In the iterative procedure, once convergence of the solutions in this step is achieved, you proceed to the next time. For a non-iterative option, go to the next time step.

In this study, the size of the time steps is kept reasonable to make the Strang-splitting approach accurate and efficient for the reactive transport simulation. The numerical procedures for solving mass transport equations (16) and (21) and reaction equation (20) will be discussed in the following sections.

Finite-volume discretization of flow and transport equations

The flow and transport equations were discretized by the finite-volume method. In this discretization scheme, the simulation domain consists of a finite number of control volumes. Each control volume maintains its mass balance (Letniowski and Forsyth, 1991). Flow-balance equations can be obtained by integrating equation (1) over a control volume:

$$\iiint_{\Delta V} \nabla(K\nabla h)dxdydz + \iiint_{\Delta V} Qdxdydz = \iiint_{\Delta V} S_s \frac{\partial h}{\partial t} dxdydz \tag{22}$$

Similarly, solute mass balance equations can be written as:

$$\iiint_{\Delta V} [\nabla(nD\nabla c_i) - \nabla(nV c_i)]dxdydz + \iiint_{\Delta V} r_i dxdydz = \iiint_{\Delta V} \frac{\partial(n c_i)}{\partial t} dxdydz \tag{23}$$

The first term in these two equations represent the flux-in or flux-out from boundaries of the control volume, the second term is the source of flux within the control volume, and the third term is the change in storage. In words, the flux-in from boundaries plus the flux generated within the control volume are equal to the storage change. These equations can be discretized by both finite-element and finite-difference methods. Unlike the traditional finite-element method, the control-volume finite-element method maintains the mass balance for each node instead of mass balance for the entire simulation domain. The mass balance at each node is calculated by summing mass fluxes from adjacent elements. Details on the method for solving equations (22) and (23) can be found in Zhang (1995).

Kinetic reactions

A predictor-corrector procedure was applied by Zysset et al. (1994) for solving kinetic reaction equations. The method was implemented by separating reaction rates into production rates and first-order loss rates.

$$r_i = \boldsymbol{x}_i - \boldsymbol{J}_i c_i \qquad \text{i=1, …, } N_{sp} \tag{24}$$

where ξ_i and ϑ_i are production and loss rates, respectively, and are non-linear functions of all species, and N_{sp} is the total number of reactive species. The reaction equation of a species is said to be stiff if

$$\Delta t^0 \boldsymbol{J} > 1 \tag{25}$$

where Δt^0 is the time step size in the integration of equation (22) (Zysett et al, 1994). The predictor-

corrector procedure is a very robust algorithm in terms of convergence. However, the computation is very intensive because the time step size Δt^0 is constrained by

$$\Delta t^0 = \alpha \min \left| c_i / r_i \right| \tag{26}$$

where α is a scale factor (estimated as 1×10^{-3} by Zysset et al, 1994). For a small value of $|c_i/r_i|$, an extremely tiny time step is required. Our test problems indicate that such a small time step is feasible for one-dimensional problems, but it took weeks on a Sun workstation to finish a run using the time step size. To overcome the stiff condition in equation (25) and improve the efficiency of reaction calculations, we implemented a variable time step procedure for solving equation (20), which is summarized as follows:

(1) Assign k=1 and $t_k = 0.0$. Here k is the time step index in the reaction calculations.

(2) Calculate first-order loss rate ϑ_i for each species and determine the maximum loss rate ϑ_{max} among the species.

(3) The time step size without causing the stiffness for the solution is

$$\Delta t_k = \frac{1}{J_{\max}} \tag{27}$$

(4) The first-order loss reaction is calculated by

$$c_{i,m}^{R,t_k+\Delta t_k} = c_i^{R,t_k} e^{-J_{i,m}\Delta t_k} \tag{28}$$

where m is the index number for the m*th* iteration, and R is an index number for the reaction. Equation (28) ensures that no negative concentration is generated by the reaction step. The reaction rates $\vartheta_{i,m}$ are calculated by the average concentrations at the previous iteration of the current time step and at the previous time step.

(5) Calculation of the production rate is related to first-order loss rates by stoichiometric coefficients. The calculation is expressed as

$$c_{i,m}^{R,t_k+\Delta t_k} = c_i^{R,t_k} + \Delta c_{i,m}^{t_k+\Delta t_k} \tag{29}$$

The first term at left side of equation (29) is the concentration of species i at the current time step and the current iteration, and the first term on the right side of the equation (24) is the concentration of species i at the previous time step. The second term on the right side of equation (29) is a function of reactant changes in equation (28) so that one mole of reactant produces the corresponding number of moles of products, as determined by the stoichiometric coefficients in equations (3) through (7).

(5) Test the convergence of reaction solutions by

$$\left| c_{i,m+1}^{R,t_k+\Delta t_k} - c_{i,m}^{R,t_k+\Delta t_k} \right| < \varepsilon \left| c_{i,m+1}^{R,t_k+\Delta t_k} \right| \tag{30}$$

where ε is a small number defined as relative error. If the condition (30) is met, go to step (6); otherwise, go to step (4).

(6) Assign k=k+1 and $t_k = t_k + \Delta t_k$, and go to step (2) if $t_k < \Delta t$; otherwise stop calculations.

With such a modification, there was a significant speedup in the solution. Simulations were finished overnight with a Sun workstation or a powerful PC, as compared to weeks with a constant time step.

Simulation Results

Verification of Numerical Models

This section describes two verification tests with the ISCO3D code. We compare model results against a column experiment of NAPL dissolution to test the dissolution model. The column experiment data come from a study by Imhoff et al. (1994) who looked at the dissolution of NAPLs in saturated media. They packed washed silica sand in an aluminum cylinder with a diameter of 8.25 cm and a height of 7 cm. At the start of the experiment, the average TCE saturation was 0.16 throughout the column. During the experiment, a Darcy flux of 0.91 m/day was maintained to flush the DNAPL out of the sand column. We tested three empirical equations (Miller et al., 1990; Imhoff et al., 1994; and Powers et al, 1994) to match the TCE saturation at x = 31.5 mm (as Figure 5 in Imhoff et al., 1994), a measurement point that reflects a complete loss of TCE from the pores (Figure 1). All empirical equations generally matched the experimental saturation data. Miller's model matched the early-time part of the saturation curve better, but not the late-time part. Both Imhoff's and Powers' models matched the late-time part of the saturation curve better. In the verification exercise, the dissolution parameters for the three models are determined from respective references (Miller et al., 1990; Imhoff et al., 1994; and Powers et al, 1994) and the transport parameters are from Imhoff et al. (1994).

The second test compares our model results with an analytical solution that includes first-order decay reaction to test the coupling of mass transport and kinetic reactions. The purpose of this test is to verify that the operator-splitting approach works for a simple example. We used the USGS code , FINITE (Wexler, 1992), to provide the analytical solution. A column, 40 m long, was set up with a third-type (variable flux) boundary condition at x = 0 with unit concentration. The other specified parameters were the linear ground water velocity (v) = 0.6 m/h, the effective diffusion coefficient (D_{eff}) = 0.6 m^2/h, and the decay constant (λ) = 0.001 h^{-1}. Breakthrough curves at x =5, 10, 20, and 40 m created using the operator-splitting approach matched exactly with the analytical solution (Figure 2).

General Description of Simulation Exercises

We demonstrate the application of the code using three examples. The first simulation attempted to reproduce column flushing experiments by Schnarr et al. (1998), using aquifer materials from the Canadian Forces Base Borden. The second set of simulations sought to match the Cl^- mass production rate in a field test designed as a proof-of-concept of source-zone flooding by MnO_4^- (Schnarr et al., 1998). The third set of simulations was based on a similar field-demonstration of $KMnO_4$ flooding at a DOE facility (West et al, 1997). In all of simulations, kinetic rates in Table 1 were used. In the following simulations, fitting parameters include dissolution rate constants α', β_1', and β_2', mass transfer coefficients k_f and k_r for the flowing-stagnant region model in the simulations of column experiments, and the quantity of the oxidizable aquifer materials (OAM). Other input parameters are kept constant during the try-and-error calibration process.

Various properties of chemical compounds and species relevant to these trials are listed in Table 3. The solubility of PCE varies from 150 to 200 mg/L (Callahan et al, 1979). A solubility value of 160 mg/L is selected in our study because the column experiments by Schnarr et al. (1998) exhibited a somewhat smaller effluent concentration (~100 mg/L) at the beginning of their experiments. The diffusion coefficient for all of the compounds and ion species was set to zero because diffusion is likely

negligible in all of the experiments as compared to the mechanical dispersion.

Simulation of Permanganate Treatment of PCE in Column Experiments

Schnarr et al. (1998) undertook column experiments to study PCE oxidation by $KMnO_4$. The glass columns (30 cm long, 5.2 cm ID) were packed with fine-grained sand from Canadian Forces Base Borden. This sand had a f_{oc} of 0.02%, and a porosity of 0.41. They flushed the 10 cm DNAPL zone placed near the top of the columns with a 10g/L $KMnO_4$ solution for 214 h, and then with deionized water to 680 hours . Because of the upward flow, the MnO_4^- oxidized organic matter and other reactive materials in the column, before it reached the NAPL zone. With time destruction of PCE in the aqueous phase enhanced the solubilization of the DNAPL.

Figure 3 shows the simulation domain and basic data for the five column experiments. The domain is discretized by 40 rectangular blocks with $\Delta x = 0.01$ m, and $\Delta y = \Delta z = 0.045$m (Figure 3). To maintain a Peclet number of 2, a longitudinal dispersivity of 0.02 m was specified in the model. The measured porosity of 0.41 was assigned uniformly. A constant-head boundary condition was assumed at the end of column. The simulations utilized the experimental Darcy fluxes, which ranged from 42 to 68 cm/day (Figure 3). The initial concentrations of $KMnO_4$ ranged from 7.5 to 10 g/L w except for column 5. The initial PCE saturation was 1%.

Modeling the kinetic dissolution of pure-phase PCE requires various medium and NAPL parameters. The soil grain diameter d_{50} at the Borden site, 0.13 mm, was inferred from O'Hannesin (1981) and Ball et al. (1990). We defined a variable proportionality factor α' in the dissolution model (Eqn.13) to reflect the difference in dissolution rates in different column experiments, while keeping $\beta_1' = 0.598$ and $\beta_2' = 0.938$ constant (within the range of values in the Powers' model, 1994 and see Table 2). The difference in the dissolution rates in the five column experiments may be caused by the heterogeneity of aquifer materials, NAPL distribution, and variations in flow rates.

In each column experiment, there were three kinetic reactions of interest. A reaction rate constant from batch experiments (Table 1) (Yan and Schwartz, 1999) was used to describe oxidation of PCE by MnO_4^-. A large reaction rate constant of 450 $M^{-1}s^{-1}$ is assumed for reactions between oxidizable aquifer materials (OAM) and MnO_4^-. The approximate magnitude was estimated by the relative rate of migration of MnO_4^- as compared to the linear ground-water velocity.

The quantity of oxidizable material in the medium was a fitting parameter. Our simulations indicated that around 2.62 g/kg of soil materials, including natural organic carbon in the column provided the best match with the experimental results. This consumption of MnO_4^- by oxidizable compounds in the porous medium is evident in the delayed breakthrough curve of MnO_4^- in column experiment 3.

Figure 4 shows the breakthrough curves of MnO_4^- for column experiments 1 through 4. The simulated breakthrough curves for MnO_4^- are similar to the measured ones in terms of arrival times. However, as Figure 4 illustrates, the measured breakthrough curve for column 3 exhibits a lower concentration at early times. This may be due to preferential flow paths in the column along which the reactions could occur first. Diffusion carried reactive species from immobile regions in the column to flow paths as time progressed.

The simulated breakthrough curves for PCE are comparable to the measurements (Figures 5a through 5e). We were able to reproduce the dramatic concentration decrease in the aqueous phase

once MnO_4^- was applied to the NAPL zone. When the MnO_4^- was replaced by water in the injection fluid the PCE concentrations were rebounded to a higher level. A difficulty in simulating PCE effluent concentrations in columns 1 through 4 is that a non-zero PCE concentration was observed when MnO_4^- effluent concentration approached its injection concentration. This result was not expected because MnO_4^- with large concentration (mg/L) should be able to oxidize PCE completely. There are several possible explanations for why this behavior occurred. With the data we have available from the column experiments it is not possible to interpret these results unambiguously. The presence of PCE might be caused by the kinetic sorption of PCE on the surface of the aquifer materials or more likely, preferential flow paths within the column. In effect, local scale heterogeneities in PCE distribution would provide zones that are not effectively being swept by the MnO_4^-. Mathematically, this process can be represented by the kinetic sorption/mass transfer model expressed by equation (7). Forward reaction rate constant k_f is the rate of mass transfer from a flowing region to a stagnant region. Reverse reaction rate constant k_r is the rate of mass transfer from a stagnant region to a flowing region. Table 4 lists the best-matched dissolution and mass transfer coefficients for the five column experiments. Clearly, there remains some uncertainty in the actual interpretation of the results of the column experiments that could not be resolved in our analysis.

The basic characteristics of the breakthrough curves of Cl^- were also simulated reasonably well (Figure 6) although there were differences between the measured and the calculated breakthrough curves.

Simulations of MnO_4^- Flooding in a Three-dimensional Test Cell Experiment

The next demonstration is based on a field-scale experiment at CFB Borden that demonstrated the potential of MnO_4^- flooding for removing pure-phase PCE (Schnarr et al., 1998). The model conceptualization of the field experiment cell is shown in Figure 7. The experimental cell was 3 m in length, 1 m in width, and 2.5 m in height. We only simulated their first experiment where a PCE source at 8% saturation was emplaced in a zone of 0.3m x 0.3m x0.35m. Flow across the cell was maintained through a system of injection and withdrawal wells. In the simulation, we simulated this condition by maintaining constant heads in the six injection wells and by pumping the other six wells. The total extraction rate was 100 L/day from the beginning of the experiment to 50 days, and 50 L/day afterward to 180 days. Flooding with a MnO_4^- solution at 10 g/L continued over the first 120 days. Water was injected from 120 to 180 days. In the simulation, we used three stress periods (0 to 50 days for stress period 1, 50 to 120 days for stress period 2, and 120 to 180 days for stress period 3) to account for the variable mass loading and extraction rates during the experiment.

The complexity of this system requires a three-dimensional model (Figure 8). The simulation grid consists of 15 columns in the x direction, 9 slices in the y direction, and 10 rows in the z direction. Grid intervals range from 0.16 to 0.28 m in the x direction, 0.125 m in the y direction, and 0.175 to 0.5 m in the z direction. A horizontal hydraulic conductivity of 8.2×10^{-3} m/s and a vertical hydraulic conductivity of 6.3×10^{-3} m/s (Sudicky, 1986) were specified uniformly in the entire simulation domain. Longitudinal and transverse dispersivities of the aquifer material are 0.36 and 0.039 m (Freyberg, 1986), respectively. No flow boundary conditions were assumed on six sides of the domain except at wells. Other transport and reaction parameters are the same as that in the previous one-dimensional column

simulations, except for 1.05 g/kg of soil materials reacting with MnO_4^-, and a dissolution rate constant α = 434. There were no measurements for these two parameters in the original field experiment. Their values were established through calibration using patterns of Cl^- production. We suspect that the difference in flow heterogeneity between the column and the field materials and preferential flow paths may result in different reactivity and dissolution behaviors between one-dimensional and three-dimensional experiments.

Simulated mass removal rate in terms of Cl^- was compared with measurements (Figure 9). The two results exhibit a relatively close match after trial and error adjustment of reaction parameters. Interestingly, the mass removal rate could not be simulated without accounting for MnO_4^- oxidation of the aquifer materials. Thus, for both column and field cell experiments, simulations indicated that a major factor affecting the transport of the MnO_4^- front is the quantity of reactive materials existing in an aquifer. Column experiments by Drescher et al. (1998), which used materials from the Tyndall Air Force Base, Florida , showed that over 90% of MnO_4^- was consumed in the oxidation of the aquifer materials. It is therefore very important to implement column experiments to determine the extent of reaction between the aquifer materials and MnO_4^- before implementing a field experiment.

Simulation of A Field-Scale Experiment at a DOE facility

A field-scale experiment of MnO_4^- oxidation of TCE was performed at the Department of Energy Portsmouth Gaseous Diffusion Plant (PORTS) in Ohio by researchers from Oak Ridge National Laboratory (ORNL) (West et al., 1997). The field test involved injecting MnO_4^- in one horizontal well and extracting fluid in other horizontal well about 27 m up-gradient of the injection well (Figure 10). In this experiment, the MnO_4^- was recirculated, with provisions to "top up" MnO_4^- in the treatment fluid before reinjection.

There are four major geological units of interest at the test area at Portsmouth (X701-B). The upper unit, the Minford silt and clay, has an average thickness of 7.5 m. The zone targeted for treatment is the Gallia sand and gravel with an average thickness of 1.5 m. Deeper units include the 4 m thick Sunbury shale, and the 15 m thick Berea Sandstone. Circulation of the injected fluid between the two parallel horizontal wells in the Gallia formation is facilitated by the relatively high hydraulic conductivity. However, the 27 m x 61 m zone between the two horizontal wells is heterogeneous in terms of hydraulic conductivity.

In the experiment, there was preferential flow of the MnO_4^- near the ends of the injection well (Figure 10). There was difficulty in the experiment in maintaining a constant injection/withdrawal rate of 10 gpm for both the injection and extraction wells. The injection rate was reduced to 6 gpm. MnO_4^- was also added through a vertical well at the center of the treatment zone to improve the efficiency of flooding. A total of 10,740 kg of $KMnO_4$ was injected between July 26 and August 27, 1997 through the horizontal well. In addition, 1960 kg of $KMnO_4$ was delivered using the vertical well (74G injected at 2 gpm) between August 20, 1997 and August 28, 1997. There was a significant reduction in the TCE concentration in the ground-water as the experiment continued.

Mahinthakumar and West (1997) simulated the migration front of MnO_4^- for the experiment. However, they did not explicitly consider the various chemical reactions taking place. In this study, simulations were aimed at not only providing the distribution of MnO_4^- but also the reactions among the

different chemical species. We restricted our model to the Gallia formation because the injected fluids moved primarily through this higher permeability unit.

A two-dimensional model of 51x51 nodes was constructed to represent the treatment zone and its vicinity (Figure 11). The simulation grid was designed with relatively small node spacings inside the test region (Δx = 1m, and Δy = 2 m) and relatively large spacings outside (maximum Δx = 6 m, and maximum Δy = 7.5 m). The thickness of the simulation domain is the same as the Gallia formation (Δz = 1.5 m). The flow from the horizontal injection well to the Gallia was not uniformly distributed along the wellbore. As noted by West et al. (1997) and Korte et al. (1997), aquifer heterogeneity near the well, clogging of the well, or a pressure drop along the well screen may have contributed the variable flooding of the zone between the wells. Without additional data, we could not determine the exact cause of this pattern of flooding. To simplify the model setup, we adjusted flow rates along the well to provide the observed pattern of MnO_4^- flooding, while keeping the hydraulic conductivity constant. The MnO_4^- concentration used as input data to the model for the horizontal injection well and the well 74G approximated the actual pattern of loading (Figure 12a). The MnO_4^- concentration was constrained by recorded information on the mass rate of loading provided by a fluid injection rate of 6 gpm in the horizontal well and the 2 gpm in the vertical well. Injection mass in the simulations is specified as that in the field experiment (Figure 12b).

A mean hydraulic conductivity of 35 m/day is assumed in the entire simulation domain. Values of longitudinal and transverse dispersivity are selected as 5.0 and 0.5 m, respectively, to ensure a Peclet number less 2. The mean porosity of the Gallia is 0.2 as reported by Beard and Anderson (1996). A small regional horizontal gradient of 1.43×10^{-6} was imposed in the simulation region to provide for an ambient flow, although no hydraulic head measurements were reported in the test region by West et al. (1997).

The first task of this simulation exercise was to match approximately the observed MnO_4^- distribution through time. We selected three times (7 days, 32 days, and 120 days) following the start of MnO_4^- injection for this comparison. The initial concentration of TCE (Figure 14a) was from West et al. (1997). At time = 7 days, MnO_4^- was localized around the ends of the horizontal injection well (Figure 13a). At time = 32 days, note how the flooded zone expanded, and the center of the test region was flooded by MnO_4^- injected through well 74G (Figure 13b). Following the cessation of injection, unreacted MnO_4^- still remained in the aquifer for a period of time (Figure 13c). This residual MnO_4^- may be helpful for a while in oxidizing TCE in the aqueous phase, which likely was continuing to diffuse into the aquifer from zones above and below.

The simulation indicates that dissolved TCE concentrations were significantly reduced, where the MnO_4^- was delivered, as compared to the initial TCE concentration (Figure 14a). At time = 7 days, the contour line of 0.005 mg/L TCE (drinking water standard) is located near the horizontal injection well (Figure 14b). After 32 days, the zone of 0.005 mg/L or less TCE concentration expanded outward significantly (Figure 14c). After this time (e.g., 120 days; Figure 14d), there is relatively little enlargement of the treated zone because the zone flooded by MnO_4^- didn't expand very much.

A detailed match of simulated and measured MnO_4^- distributions is impossible due to the lack of detailed hydraulic head measurement and the experimental determination of reactions between the MnO_4^- and the oxidizable aquifer materials (mainly organic carbon content). The present simulation

suggests that 172 mg/kg of aquifer materials has been oxidized. Further sensitivity study indicates that the amount of oxidizable aquifer materials in the aquifer may significantly affect the transformation of TCE into non-harmful products (Figure 15). The area within which the TCE concentration is less than 0.005 mg/L is decreased as the amount of oxidizable aquifer materials is increased from 43 mg/kg to 430 mg/kg.

Concluding Remarks

A simulation and design tool was developed to model a remediation scheme that is based on the oxidation of chlorinated compounds by MnO_4^-. The computer code can simulate coupled processes including the dissolution of NAPLs; the chemical reactions among permanganate, dissolved chlorinated compounds, and aquifer materials; and the mass transport in three dimensions. We demonstrated the application of this code to a series of column experiments (Schnarr et al, 1998), one small field experiment (Schnarr et al, 1998), and a larger-scale field demonstration of source zone flushing (West et al., 1998). The success in generally matching this variety of experiments provides some initial confirmation that the code has been able to capture the essential physics and chemistry of the processes involved. The computer simulations, together with column, test cell, and field experiments also suggest that the proper determination of NAPL saturation, aqueous concentration of chlorinated compounds, and the reactivity between aquifer material and MnO_4^- are critical to a successful chemical oxidization design and field operation. This study and previous work also indicate that oxidization of chlorinated compounds is probably most efficient at a low NAPL saturation. The chemical reaction between the chlorinated compounds and MnO_4^- occurs in dissolved phase, but the dissolution of NAPLs is rate-limited. Our group is presently working to devise new approaches to accelerate the rate of oxidation.

Clearly, there is more work to be done in the development of the modeling approach outlined in this paper. For example, the experimental work has showed that the production of $MnO_2(s)$ is significant in the oxidative treatment of chlorinated compounds with permanganate. The $MnO_2(s)$ particles are transported and deposited as colloids during a remediation process. One of our current modeling initiatives is to study the effect of $MnO_2(s)$ on the efficiency of the oxidative scheme.

Acknowledgement

Funding of this study was supported by Department of Energy Environmental Management Science Program under grant #FG07-96ER14735. The data set for the verification of dissolution models was kindly provided by Dr. Paul Imhoff. Critical comments by Libby West, Carl Steefel, an anonymous reviewer, and an associate editor have improved the presentation of the materials in this study.

References

Ball, W.P., Ch. Buehler, T. C. Harmon, D.M. Mackay, and P. V. Roberts. Characterization of a sandy aquifer material at the grain scale. J. Contam. Hydrol., 5, 253-295, 1990.

Bear, J., Dynamics of fluids in porous media, American Elsevier, New York, 764 pp., 1972.

Beard, T. C., and F.J. Anderson, 3-D multiphase modeling of DNAPL TCE at the DOE Portsmouth Gaseous Diffusion Plant, Piketon, Ohio. Proceedings of ModelCARE 96 Poster Papers, International Conference on Calibration and Reliability in Groundwater Modeling. Golden, Colorado USA,

September 24-26, 31-40, 1996.

Callahan, N. W., M. W. Slimak, N. W. Gabel, I. P. May, C. F. Fowler, J. R. Freed, P. Jennings, R. L. Durfee, F. C. Whitmore, B. Maestri, W. R. Mabey, B. R. Holt, and C. Gould, Water-related environmental fate of 129 priority pollutants, U. S. Environmental Protection Agency, Washington, D.C., 1979.

Colthurst, J. M., and P. C. Singer, Removing trihalomethane precursors by permanganate oxidation and manganese dioxide adsorption, Journal AWWA, 74, 78-83, 1982.

Drescher, E., A. Gavaskar, B. M. Sass, L. J. Cumming, M. J. Drescher, and T. K. J. Williamson, Batch and column testing to evaluate chemical oxidization of DNAPL source zones, Proceedings of The First International Conference on Remediation of Chlorinated and Recalcitrant Compounds, Vol. C1-5: Physical, Chemical, Thermal Technologies, Monterey, California, May 18-21, 425-432, 1998.

Freyberg, D. L. A natural gradient experiment on solute transport in a sand aquifer: 2. Spatial moments and the advective and dispersion of nonreactive tracers. Water Resour. Res., 22, 2031-2046, 1986.

Friedly, J., and J. Rubin, Solute transport with multiple equilibrium-controlled or kinetically controlled chemical reactions, Water Resour. Res., 28, 1935-1953, 1992.

Frind, E.O., Simulation of long-term transient density-dependent transport in groundwater, Adv. Water Resources, 5, 73-88, 1983.

Gates, D.D., R. L. Siegrist, and S. R. Cline, Chemical oxidation of volatile and semivolatile organic compounds in soil, Proceedings of 88th annual meeting and exhibition, San Antonio, 1995.

Huyakorn, P.S., and G.F. Pinder, Computational methods in subsurface flow, Academic Press, San Diego, Calif., 1983.

Imhoff, P. T., P. R. Jaffé, and G. F. Pinder, An experimental study of complete dissolution of a nonaqueous phase liquid in saturated porous media, Water Resour. Res., 30, 307-320, 1994.

Korte, N., M. Muck, P. Kearl, R. Siegrist, T. Houk, R. Schlosser, J. Zutman, Field evaluation of a horizontal well recirculation system for groundwater treatment: Field demonstration at X-701B Portsmouth Gaseous Diffusion Plant, Piketon, Ohio, Oak Ridge National Laboratory, Grand Junction, Colorado, 1997.

LaChance, J. C., S. Reisma, D. Mckay, and R. Baker, In situ oxidization of trichloroethene using potassium permanganate, Part 1: Theory and Design, Proceedings of The First International Conference on Remediation of Chlorinated and Recalcitrant Compounds, Vol. C1-5: Physical, Chemical, Thermal

Technologies, Monterey, California, May 18-21, 397-402, 1998.

Letniowski, F. W., and P. A. Forsyth, A control volume finite element method for three-dimensional NAPL groundwater contamination, International Journal For Numerical Methods in Fluids, 13, 955-970, 1991.

Mahinthakumar, G, and O. R. West, High resolution numerical simulations in support of the ISCOR experiment at Portsmouth, Oak Ridge National Laboratory, Oak Ridge, Tennessee, 1997.

Mckay, D., A. Hewitt, S. Reisma, J. LaChance, and R. Baker, In situ oxidization of trichloroethene using potassium permanganate, Part 2: Pilot Study, Proceedings of The First International Conference on Remediation of Chlorinated and Recalcitrant Compounds, Vol. C1-5: Physical, Chemical, Thermal Technologies, Monterey, California, May 18-21, 377-382, 1998.

Miller, C. T., M. M. Poirier-McNeill, and A. S. Mayer, Dissolution of trapped nonaqueous phase liquids: Mass transfer characteristics, Water Resour. Res., 26, 2783-2796, 1990.

O'Hannesin, S. F. Spatial variability of grain-size parameters and hydraulic conductivity at a dispersion test site. Bachelor of environmental studies honors report. University of Waterloo, Waterloo, Ont., 46 p, 1981.

Pfannkuch, H.O., Determination of the Contaminant Source Strength form Mass Exchange Processes at the Petroleum-Ground-Water Interface in Shallow Aquifer Systems, in Petroleum Hydrocarbons and Organic Chemicals in Ground Water, National Water Well Assn., 111-129, 1984.

Powers, S. E., L. M. Abriola, and W. J. Weber, Jr., An experimental investigation of nonaqueous phase liquid dissolution in saturated subsurface systems: Steady state mass transfer rates, Water Resour. Res., 28, 2691-2706, 1992.

Powers, S. E., L. M. Abriola, and W. J. Weber, Jr., An experimental investigation of nonaqueous phase liquid dissolution in saturated subsurface systems: Transient mass transfer rates, Water Resour. Res., 30, 321-332, 1994.

Roberts, P. V., M. N. Goltz, and D. M. Mackay. A natural gradient experiment on solute transport in a sand aquifer: 3.Retardation estimates and mass balances for organic solutes, Water Resour. Res., 22, 2047-2058, 1986.

Schnarr, M., C. Truax, G. Farquhar, E. Hood, T. Gonullu, and B. Stickney, Laboratory and controlled field experiments using potassium permanganate to remediate trichloroethylene and perchloroethylene DNAPLs in porous media, Journal of Contaminant Hydrology, 29, 205-224, 1998.

Sleep, B., and J. Sykes, Modeling the transport of volatile organics in variably saturated media, Water Resour. Res., 25, 81-92, 1989.

Steefel, C. I., and K. T. B. MacQuarrie, Approaches to modeling of reactive transport in porous media, Reviews in Mineralogy, 34, 83-129, 1996.

Steward, R., Oxidation by permanganate, In Oxidation in organic chemistry, Wiberg, K. B., ed., Academic Press, New York, Part A, Chapter 1, 1-68, 1965.

Sudicky, E. A. A natural gradient experiment on solute transport in a sand aquifer: Spatial variability of hydraulic conductivity and its role in the dispersion process, Water Resour. Res., 22, 2069-2082, 1986.

Vella, P.A., and B. Veronda, Oxidation of trichloroethylene: comparison of potassium permanganate and Fenton's reagent, In Chemical oxidation technologies for the nineties, Eckenfelder, W.W., ed., Technomic publishing, Lancaster, Basel, 1992.

Valocchin and Malmstead, Accuracy of operator splitting for advection-dispersion-reaction problems, Water Resour. Res., 28, 1471-1476, 1992.

West, O. R., S. R. Cline, W. L. Holden, F. G. Gardner, B. M. Schlosser, J. E. Thate, D. A. Pickering, T. C. Houk, A full-scale demonstration of in situ chemical oxidation through recirculation at the X-701B site, Oak Ridge National Laboratory, Oak Ridge, TN, ORNL/TM-13556, 101 p., 1997.

Wexler, E.J., Analytical solutions for one-, two-, and three- dimensional solute transport in ground-water systems with uniform flow: U.S. Geological Survey Techniques of Water-Resources Investigations, book 3, chap. B7, 190 p, 1992.

Yan, Y. E., and F. W. Schwartz, Oxidative degradation and kinetics of chlorinated ethylenes by potassium permanganate, Journal of Contaminant Hydrology, 37, 343-365, 1999.

Yan, Y. E., and F. W. Schwartz, Oxidation of chlorinated solvents by permanganate, Proceedings of The First International Conference on Remediation of Chlorinated and Recalcitrant Compounds, Vol. C1-5: Physical, Chemical, Thermal Technologies, Monterey, California, May 18-21, 403-408, 1998.

Yeh, G. T., and V. S. Tripathi, A critical evaluation of recent developments in hydrgeochemical transport models of reactive multichemical components, Water Resour. Res., 25, 93-108, 1989.

Zhang, H., F.W. Schwartz, W.W. Wood, S. P. Garabedian, and D. R. LeBlanc, Simulation of variable-density flow and transport of reactive and nonreactive solutes during a tracer test at Cape Cod, Massachusetts, Water Resources Research, 34, 67-82, 1998.

Zhang, H., Simulations of multi-species contaminant transport in variable-density flow systems, Ph. D. dissertation, The Ohio State University, Columbus, Ohio, 1995.

Zysset, A., F. Stauffer, T. Dracos, Modeling of chemically reactive groundwater transport, Water Resources Research, 30, 2217-2228, 1994.

Table 1. Kinetic rate constants for PCE, TCE, and DCE oxidation by MnO_4^-.

Chlorinated Ethylenes	k ($M^{-1}s^{-1}$)
PCE	0.045
TCE	0.65
Cis-DCE	0.92
Trans-DCE	30
1,1-DCE	2.38
OAM	450

Table 2. Selected dissolution models by different researchers.

Current model	Power's model	Imhoff's model	Miller's model
$a' Re^{b_1'} S_N^{b_2'}$	$4.13 Re^{0.598} d^{0.673} U_i^{0.369} \left(\frac{S_N}{S_{N0}}\right)^{0.5-1.0}$	$340 Re^{0.71} \left(\frac{d_{50}}{X}\right)^{0.31} (nS_N)^{0.87}$	$425 Re^{0.75} (nS_N)^{0.60}$
α'	$\frac{4.13 d^{0.673} U_i^{0.369}}{S_{N0}^{0.5-1.0}}$	$340 \left(\frac{d_{50}}{X}\right)^{0.31} (n)^{0.87}$	$425 (n)^{0.60}$
β_1'	0.598	0.71	0.75
β_2'	0.5-1.0	0.87	0.60

Table 3. Properties of Chemicals

Chemical species	Density (g/cm^3)	MW	$K_{OC}(kg^{-1}/L^{-1})$	Solubility(mg/L)
$KMnO_4$	2.703	118.94		60000
TCE	1.464	131.39	120	1277
PCE	1.623	165.83	468	150-200
CO_2		44.011		
Cl^-		35.457		
$MnO_2(s)$		86.94		
C		12.011		

Table 4. Kinetic reaction rate constants

Column No.	α	$k_f(s^{-1})$	$k_r(s^{-1})$
1	6365	$1x10^{-4}$	$6x10^{-6}$
2	9547	$1x10^{-4}$	$6x10^{-6}$
3	3182	$1x10^{-4}$	$6x10^{-6}$
4	2228	$1x10^{-4}$	$6x10^{-6}$
5	1273	$1x10^{-4}$	$6x10^{-6}$

Figures

1. Test of the coupled transport and dissolution processes using three empirical dissolution models (Miller et al., 1990; Imhoff et al., 1994; and Powers et al, 1994).
2. Verification of the operator-splitting approach using an analytical solution.
3. Model setup for the simulation of MnO_4^- oxidation of PCE in column experiments.
4. Calculated breakthrough curves of MnO_4^- for the column experiments 1 through 4 and the measured breakthrough curve for the column experiment 3.
5. Simulated breakthrough curves for PCE for column experiments 1 through 5.
6. Simulated breakthrough curves for Cl^- for column experiments 1 through 4.
7. Basic setup for a field test cell at the CFB Borden site (Scharr et al, 1998).
8. A three-dimensional model of the injection and extraction system in the Borden test cell.
9. Simulated and measured mass removal rates in terms of Cl^- for the Borden test cell.
10. A field-scale demonstration of MnO_4^- oxidation of TCE at the Department of Energy Portsmouth Gaseous Diffusion Plant (PORTS) (West et al., 1997).
11. A two-dimensional representation (51x51 nodes) of the treatment zone and a surrounding zone at the PORTS experiment site.
12. Injected permanganate mass. (a) Simulated and actual MnO_4^- concentration in the treatment fluid added from the horizontal injection well and the well 74G; (b) Comparison of cumulative mass injected in the simulation and the experiment.
13. Simulated MnO_4^- distribution. (a) Time = 7 days; (b) Time = 32 days; (c) Time = 120 days.
14. Simulated TCE distribution. (a) Time = 0 days; (b) Time = 7 days; (c) Time = 32 days; (d) Time = 120 days.
15. Sensitivity analysis of simulated TCE distribution at 32 days for different amount of oxidizable aquifer materials: (a) 43 mg/kg; (b) 172 mg/kg; (c) 430 mg/kg.